



University
of Glasgow

Sinclair, Gavin (2006) *Experiments using holographic optical tweezers*. PhD thesis.

<http://theses.gla.ac.uk/5894/>

Copyright and moral rights for this thesis are retained by the author

A copy can be downloaded for personal non-commercial research or study, without prior permission or charge

This thesis cannot be reproduced or quoted extensively from without first obtaining permission in writing from the Author

The content must not be changed in any way or sold commercially in any format or medium without the formal permission of the Author

When referring to this work, full bibliographic details including the author, title, awarding institution and date of the thesis must be given

*Experiments Using Holographic
Optical Tweezers*

Gavin Sinclair

Department of Physics and Astronomy
University of Glasgow

Presented for the degree of
Doctor of Philosophy
at the University of Glasgow
June 2006

© Gavin Sinclair 2006

Declaration

This thesis has been composed by the undersigned. It has not been accepted in any previous application for a degree. The work of which it is a record has been done by myself, unless indicated otherwise in the text. I further state that no part of this has already been or is being concurrently submitted for any such degree or qualification at any other university.

Gavin Sinclair.

Acknowledgements

I would like to thank my supervisors Prof. Miles Padgett and Dr. Johannes Courtial for their guidance and help over the last 3 years. A special thanks is given to Miles for giving me the chance to study and carry out my research with his group. A big thanks is given to Jonathan Leach and Pamela Jordan for their help carrying out some of the many experiments I have completed over the last 3 years. Many collaborators have to be thanked for their input to various aspects of my research. Most notably Dr. Zsolt Laczik (Dept. Engineering Science, University of Oxford) is thanked for making some of my more exciting experiments possible. The other collaborators were Prof. Jon Cooper, Norbert Klauke and Paul Monaghan (Dept. Electronics and Electrical Engineering, University of Glasgow), Dr. John Girkin and Dr. Gail McConnell (Centre of Biophotonics, University of Strathclyde) and finally Prof. Ewen Smith, Francis Docherty, Rachael Littleford and Graeme McNay (Dept. Pure and Applied Chemistry, University of Strathclyde). Last but not least are the other members of the optics group, past, present and temporary, who have my time in the optics group very enjoyable; Steve Monk, Valerie Nadeau, Ben Van Well, Graham Gibson, Ken Skeldon, Martin O'Dwyer, Eric Yao, Graeme Whyte, Claire Patterson, Laura Thompson, Kevin O'Holleran, Lesley McMillan, Kurt Wulff, Ethan Schonbrun and Kayode.

Abstract

This thesis mainly describes experiments carried out to advance the techniques of manipulating dielectric particles trapped using holographic optical tweezers. Holographic optical tweezers are a relatively recent advancement in optical trapping, using a spatial light modulator to display holograms that are used to shape the trapping laser beam. In my work, most experiments involved dielectric particles trapped using Gaussian beams to form simple to complex patterns. To allow complex patterns of particles to be trapped, the limits of the spatial light modulator were initially defined to allow a workable trapping volume to be specified. The working volume was defined by determining the efficiency of an optical trap in a pre-defined three dimensional coordinate system, using Stokes drag to find the force exerted by the trap. The working volume was found to be $40\ \mu\text{m}$ by $40\ \mu\text{m}$ by $50\ \mu\text{m}$, centered around the zeroth diffraction order. Initially complex patterns of particles were trapped in structures resembling cubic and diamond unit cells, using precalculated static holograms. In the cubic unit cell example, the structure could be rotated and its size controlled using cursor controls. The diamond unit cells was difficult to trap using a static hologram and this prompted the manipulation of particles initially trapped in simple two dimensional patterns, then manipulated into more complex two and three dimensional patterns.

An important aspect of the above experimental work was feedback to the developers of the two main algorithms used to design the holograms I used. The two different algorithms used to design these holograms were a direct binary search algorithm developed by Dr. Zsolt Laczik and a modified Gerchberg-Saxton algorithm developed by Dr. Johannes Courtial. The feedback helped to refine the hologram design process and helped the Glasgow group to develop a suite of tools for hologram design.

A major part of my research has been to design, build and commission optical tweezers systems for collaborators. I have been involved in three collaborations over the last 3 years, supplying optical tweezers to the three groups of collaborators. The first was to supply an optical tweezers system to Dr. John Girkin for an experiment to investigate the angular momentum carried by light and its interactions with dielectric particles. The second collaboration with Prof. Ewen Smith involved combining surface enhanced Raman scattering spectroscopy with optical tweezers. This involved designing optical tweezers around a conventional upright microscope attached to a commercial Raman spectrometer. The third collaboration with Prof. Jon Cooper involved designing optical tweezers systems around a commercial inverted microscope to allow functionalised particles to be trapped and manipulated within microfluidic devices, as well as allowing spectrometry measurements to be made.

Publications

Journal Publications Arising in Whole or in Part From Research Covered by this Thesis

1. Klauke, N., Monaghan, P., Sinclair, G., Padgett, M., Cooper, J. 2006. Characterisation of spatial and temporal changes in pH gradients in microfluidic channels using optically trapped fluorescent sensors. *Lab On a Chip* 6, 788-793.
2. Leach, L., Wulff, K., Sinclair, G., Jordan, J., Courtial, J., Thomson, L., Gibson, G., Karunwi, K., Cooper, J., Laczik, Z. J., Padgett M. 2006. Interactive approach to optical tweezers control. *Appl. Opt.* 45, 897-903.
3. Jordan, P., Cooper, J., McNay, G., Docherty, F. T., Graham, D., Smith, W. E., Sinclair, G., Padgett, M.J. 2005. Surface-enhanced resonance Raman scattering in optical tweezers using co-axial second harmonic generation. *Opt. Exp.* 13, 4148-4153.
4. Jordan, P., Cooper, J. M., McNay, G., Docherty, F. T., Smith, E. W., Sinclair, G., Padgett, M. 2004. Three-dimensional optical trapping of partially silvered silica microparticles. *Opt. Lett.* 29, 2488-2490.
5. Sinclair, G., Jordan, P., Courtial, J., Padgett, M. J., Cooper, J. Laczik, Z. J. 2004. Assembly of 3-dimensional structures using programmable holographic optical tweezers. *Opt. Exp.* 12, 5475-5480.
6. Sinclair, G., Leach, J., Jordan, P., Gibson, G., Yao, E., Laczik, Z. J., Padgett, M. J., Courtial, J. 2004. Interactive application in holographic optical tweezers of a

multi-plane Gerchberg-Saxton algorithm for three-dimensional light shaping. *Opt. Exp.* 12, 1665-1670.

7. Leach, J., Sinclair, G., Leach, J., Jordan, P., Courtial, J., Padgett, M. J., Cooper, J., Laczik, Z. J. 2004. 3D manipulation of particles into crystal structures using holographic optical tweezers. *Opt. Exp.* 12, 220-226.
8. McNay, G., Docherty, F. T., Graham, D., Smith, E. W., Jordan, P., Padgett, M., Leach, J., Sinclair, G., Monaghan, P. B., Cooper, J. M. 2004. Visual observations of SERRS from single silver-coated silica microparticles within optical tweezers. *Angew. Chem. Int. Ed.* 43, 2512 -2514.
9. Sinclair, G., Jordan, P., Leach, J., Padgett., M. J., Cooper, J. 2004. Defining the trapping limits of holographical optical tweezers. *J. Mod. Opt.* 51, 409-414.

Conference Presentations

1. Sinclair, G., Jordan, P., Courtial, J., Padgett, M., Cooper, J., Laczik, Z. Pre-programmed microassemblies in holographic optical tweezers. *Proc. Prep* 2005, 116-117.
2. Sinclair, G., Klauke, N., Monaghan, P., Padgett, M., Cooper, J. 2005. pH Microprobe manipulated in microchannels using optical tweezers. *Proc. SPIE*, 5736, 66-72.
3. Sinclair, G., Leach, J., Jordan, P., Laczik, Z. J., Courtial, J., Padgett, M. J., 2004. 3-D Manipulation of particles in holographic optical tweezers: Assembly of crystal-like structures. *Proc. Photon04*.
4. Sinclair, G., Leach, J., Jordan, P., Laczik, Z. J., Courtial, J., Padgett, M. J., 2004. Semi-automated 3-dimensional assembly of multiple objects using holographic optical tweezers. *Proc. SPIE*, 5514, 137-142.
5. Sinclair, G., Leach, J., Jordan, P., Courtial, J., Padgett, M. J., Cooper, J., Laczik, Z. J., 2004. Crystal-like structures in holographic optical tweezers. *Proc. Prep* 2004, 49-50.

Contents

Declaration	i
Acknowledgements	ii
Abstract	iii
Publications	v
Table of Contents	vii
1 Introduction	1
1.1 Introduction	1
1.2 Aims and Objectives	2
1.2.1 Aims	2
1.2.2 Objectives	2
1.3 Previous Work	3
1.3.1 Introduction	3
1.3.2 Biological Optical Tweezing	5
1.3.3 Trapping Multiple Objects	11
1.3.4 Scattering Particles and Shaped Particles	13
1.3.5 Microfluidics and Optical Tweezers	17

1.3.6	Holographic Optical Tweezers	19
1.3.7	Colloidal and Crystal Research	23
1.3.8	Summary	24
2	The Workings of Optical Tweezers	26
2.1	Introduction	26
2.2	Optical Tweezers	26
2.3	Forces in Optical Tweezers	27
2.3.1	Other Forces	29
2.3.2	Mie and Rayleigh Scattering	30
2.3.3	Optical Trap Efficiency	31
2.4	Holographic Optical Tweezers	33
2.5	Hologram Design Algorithms	35
2.5.1	Direct-Binary Search Algorithm	36
2.5.2	Modified Gerchberg-Saxton Algorithm	39
2.6	Spatial Light Modulators	41
2.6.1	Liquid Crystals	42
2.6.2	How An SLM Works	45
2.6.3	Hamamatsu PAL-SLM X7665	45
2.6.4	Holoeye LC-R 2500	46
3	Trapping Limits of Holographic Optical Tweezers	48
3.1	Introduction	48
3.2	Theory	49
3.3	Experimental Arrangement and Procedure	50
3.3.1	Calibration of Trap Displacement Using SLM	51

3.4	Results	53
3.4.1	Force Results	53
3.4.2	Efficiency of the Trap	53
3.5	Discussion	55
3.6	Conclusions	58
4	Hologram Design Algorithm Development	60
4.1	Introduction	60
4.2	Direct-Binary search Algorithm	61
4.3	Modified Gerchberg-Saxton Algorithm	63
4.4	Hologram Offset	64
4.5	Summary	64
5	Two and Three Dimensional Arrays Trapped Using Holographic Optical Tweezers	66
5.1	Introduction	66
5.2	Hologram Design Algorithms	67
5.2.1	Anti-blazing Holograms	67
5.2.2	Generation and Display of Hologram Sequences	68
5.2.3	Experimental Arrangement and Procedure	70
5.3	Results	72
5.3.1	Crystal-Like Structures	72
5.3.2	Two Dimensional Manipulation	73
5.3.3	Three Dimensional Manipulation	77
5.4	Discussion	80
5.4.1	Crystal-Like Structures	80

5.4.2	Automated Manipulation	81
5.5	Conclusions	83
6	Optical Trap Quality	85
6.1	Introduction	85
6.2	Experimental Arrangement and Procedure	86
6.3	Hologram Design	86
6.4	Results	88
6.5	Discussion	90
6.6	Conclusions	92
7	Optical Tweezers Systems	93
7.1	Introduction	93
7.2	Optical Tweezers and SERRS	93
7.2.1	Raman Scattering	94
7.2.2	SERRS Theory	97
7.2.3	Sample Preparation	99
7.2.4	Summary of SERRS Experiments	100
7.3	Optical Tweezers For Trapping Functionalised Particles	102
7.4	Abraham-Minkowski Experiment	105
7.5	Summary	109
8	pH Microprobe Calibration	112
8.1	Introduction	112
8.2	Sample Preparation	113
8.3	Microfluidic Device Fabrication and Operation	114

8.4	Experimental Procedure	117
8.5	Results	118
8.6	Conclusions	121
9	Conclusions and Future Work	123
9.1	Introduction	123
9.2	Conclusions	123
9.3	Future Work	124
9.3.1	Update on Current Research	125

Chapter 1

Introduction

1.1 Introduction

Holographic optical tweezers are a new and exciting research area of optical trapping, recently exemplified by the work of Grier and co-workers (for example the work presented in [1, 2]). Optical trapping dates back to 1970 [3] and was the precursor to the development of optical tweezers [4]. Holographic optical tweezers are a progressive step in the development of optical tweezers. They have incorporated developments in display technology (spatial light modulators) and advances in computer-generated holography, to give a powerful micromanipulation tool. The main limitations of the application of holographic optical tweezers are speed and resolution of spatial light modulators and desktop computer processing power.

Writing this chapter, my aim and objectives are listed followed by a summary of the history of development and uses of optical tweezers and holographic optical tweezers. This section is not an exhaustive summary, but highlights the major uses and advances made over the last 30 years in optical trapping research.

1.2 Aims and Objectives

This section lists the aims and objectives of my research reported in this thesis. Many of these will have been achieved in full and will be part of continuing work in the optics group and with its collaborators.

1.2.1 Aims

The aims of my Ph.D are as follows:

1. describe experiments using holographic optical tweezers that will lead to advances in optical tweezing techniques;
2. supply enough information to allow the reader to construct optical tweezers and holographic optical tweezers with a spatial light modulator in the Fourier plane;
3. give a clear and concise record of research carried out by myself;
4. detail various collaborative projects and the outcome of these projects;
5. describe applications of holographic optical tweezers to new areas of research and develop new applications of the tool (e.g. biological research and photonic crystal fabrication).

1.2.2 Objectives

The objectives of my experiments were set on a 3-4 monthly period. As an experiment was nearing completion, a new experiment was put together, which built upon the results of the previous experiment(s). The objectives set over the period of my doctoral degree are listed below:

1. build optical tweezer systems for my own experiments and for those of collaborators;

2. determine the trapping limits of holographic optical tweezers;
3. trap complex patterns of particles in two- and three-dimensional geometries;
4. automate trapping of particles to reduce user interaction with the experimental apparatus;
5. apply optical tweezers to biological studies as preliminary work to applying holographic optical tweezers to similar studies;
6. trap nano-size particles with holographic optical tweezers;
7. determine how close two trapped particles can be positioned to each other using holographic optical tweezers.

The nature of my research meant that experiments were completed from start to end in 3-4 months, usually concluding with the submission of a manuscript to a journal. This approach worked well for me and allowed ample time for background reading to become familiar with the new physics required for the experimental work.

1.3 Previous Work

The following section contains a summary of the development of optical tweezing techniques and numerous examples of previous work. The examples are presented in small subsections to give the reader a feel of the different applications of optical tweezers and an understanding for developing different trapping techniques using optical tweezers. The aim is to highlight a selection of previous work, showing that the uses of optical tweezers are diverse and varied.

1.3.1 Introduction

Optical trapping was first shown to work for dielectric particles by Ashkin [3]. Early developments in optical trapping enabled micron-sized particles to be trapped by two

opposing focused laser beams (Figure 1.1) and accelerated by a single focused laser beam. All the trapped particles were of a higher refractive index than the medium in which they were suspended, for example the oil droplet and polystyrene particle [5] shown in figure 1.2.

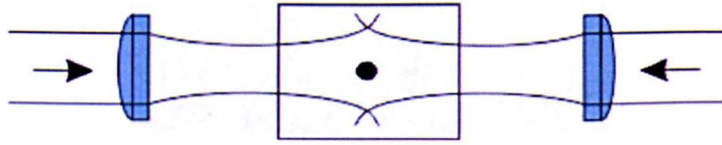


Figure 1.1: *A particle trapped by two counter propagating beams.*

Optical levitation was achieved using a single focussed laser beam in an inverted microscope optical arrangement, by balancing the scattering force with gravity to hold a particle in air [6]. This was the first configuration to move a trapped particle with single laser beam. These single beam optical levitation traps could also trap oil droplets [7]. Ashkin et al. [4] first demonstrated optical tweezers as a single-beam optical trap to hold dielectric particles ranging from 25 nm to 10 μm in diameter and particles up to 140 μm in size have been trapped [8]. Optical tweezers were realized by tightly focusing the laser beam so that the gradient force becomes large enough to overcome the scattering force. However, the concepts behind the first optical tweezers were developed for trapping atoms by suppressing their Brownian motion [9]. Common to all these early experiments was the use of visible wavelengths of light in the trapping laser beam [10].

A typical optical tweezers experiment traps particles suspended in water. Water offers both cooling and damping of harmonic oscillatory motion. Other liquids can be used to suspend particles, such as alcohols and buffer solutions [5]. In a conventional optical tweezers configuration, the trapping distance in the axial direction is limited by the working distance of the oil immersion objective. The working distance can be increased by using a microscope objective in an arrangement such that is not limited by a coverslip. This can be achieved by using a water immersion objective in a conventional microscope arrangement, in which the objective can be placed directly in contact with the suspension liquid. Dry objectives are used to trap particles in air, thus removing the use of both coverslip and a liquid [11]. Particles with a lower refractive index than the surrounding medium (e.g. hollow glass spheres) are repelled from the focal point of a Gaussian light

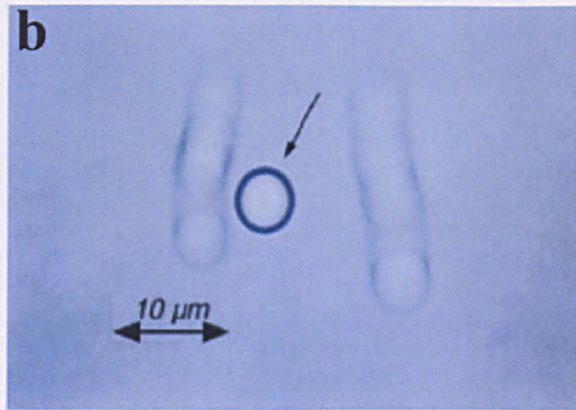
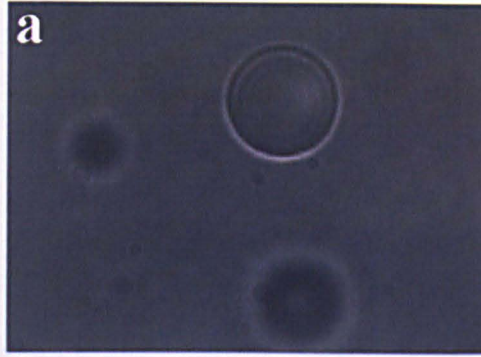


Figure 1.2: *Examples of different types of particles that can be trapped using optical tweezers: a) an oil droplet and b) a polystyrene sphere, with an arrow showing the direction of manipulation.*

beam, but were trapped in the center of an optical vortex [12].

1.3.2 Biological Optical Tweezing

The use of visible laser beams in optical tweezers for practical applications, limits trapping to non-biological dielectric particles. Although living biological specimens can be trapped with visible light, these wavelengths eventually kill trapped living samples, a process termed optocution [13]. The ability to trap and manipulate living samples without killing them is of interest because optical tweezers are non-invasive and offer an entirely sterile environment. Biological samples include whole cells, DNA, components of cells, viruses

and bacteria. Ashkin et al. [14] overcame the problem of killing trapped living samples by using an infrared wavelength laser (1064 nm which is not absorbed as much as visible wavelengths) to trap and manipulate living samples. These living samples included *E.coli* bacteria that reproduced while being trapped; conclusive evidence that living biological samples could be trapped and manipulated. Recently, arrays of living bacterial cells were trapped (Figure 1.3) by scanning the trapping laser beam and the cells were adhered to the surface of a glass coverslip [15].

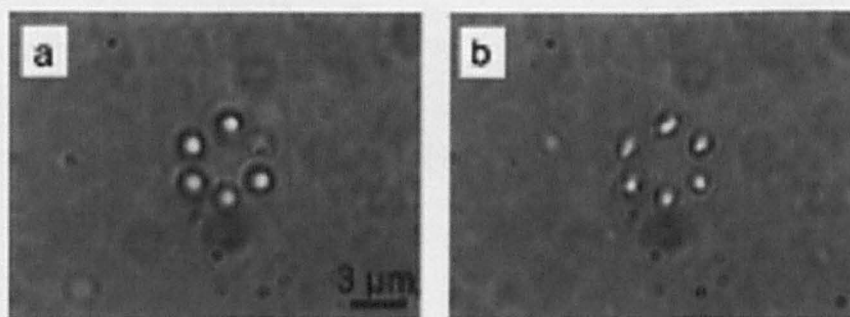


Figure 1.3: *Two photos showing a) six bacterial cells trapped in a hexagonal pattern and b) the same six cells stuck to the glass coverslip.*

For trapping inorganic particles (e.g. glass spheres), laser power is not as important as for trapping biological (organic) samples. However, biological specimens can be killed by heating them when too much power is supplied from an infrared laser, typically killing a bacterium within a minute [16]. The heat supplied from the trapping laser beam can be used for good uses: one early experiment used optical tweezers to take advantage of heating from an infrared laser, to relate organelle movement reactions in plant cells to temperature changes [17].

In addition to heating trapped particles, optical tweezers exert small forces on trapped particles, typically in the range of tens of piconewtons to a few nanonewtons, from laser powers ranging from tens to a few hundreds of milliwatts. Typically, a trap containing 10-20 milliwatts of power is required for optical tweezers experiments. An experiment on biological samples was the first to measure and calibrate forces exerted by optical tweezers. It measured the compliance of individual bacterial tails tethered to the surface of a coverslip. The bacterial tail's compliance was measured by trapping the tail with the optical

tweezers and moving it in a circular motion to unwind it. Then the tail was released and it returned to its original state, with the compliance taken to be directly related to the force in the optical trap [18]. The ability to carry out measurements on individual bacteria was an advance on previous studies, which relied on testing bulk samples of specimens [19]. This allowed forces related to biological samples to be quantitatively measured, aiding biologists to a better understanding of fundamental processes in biological systems. For example, Ashkin et al. [20] measured biological motor forces by trapping fast moving mitochondrion and reducing the power in the trapping laser beam until they were released. Others measured the forces required to stretch and break DNA strands by sticking one end of the DNA strand to a coverslip and pulling on a glass sphere attached to the other end of the DNA, with the optical trap. Movements of the trapped glass spheres were detected using an interferometer [21]. Sometimes it is necessary to make measurements on cells and biological molecules that are tens of nanometers in size (as with the DNA above), too small to trap in an optical tweezers. These problems can be resolved by attaching the biological sample to a dielectric sphere (termed a handle, Figure 1.4 [10]). It can be envisaged that a large object (several tens of microns in diameter) could be manipulated using several handles attached to its surface.

In many of the force measurement studies above, the trapped particle was moved several microns with the optical tweezers. However, studies involving biological samples often require small movements of the optical trap, on the scale of a few nanometers to a micron. Problems associated with making very accurate measurements with optical tweezers is the stiffness of the trap and the detection of small movements. Trap stiffness is characterised by the vibration of the trapped particle within the trap, typically around a few tens of nanometers at frequencies ranging from a few tens of Hertz to several kilohertz [19]. Trap stiffness can be measured by dampening with actuators that move the sample at the same frequency as the trap frequency. These small movements of trapped particles can be hard to detect and can be detected using position-sensitive photodetectors [22], often in the form of quadrant detectors [23]. In the work of Smith et al. [22], two latex spheres were attached to the ends of a DNA strand, one of the spheres held with the optical trap and the other was held with a micropipette acting as a force transducer, calibrated against the viscous drag of the bead it held (Figure 1.5). The DNA was extended by pulling on

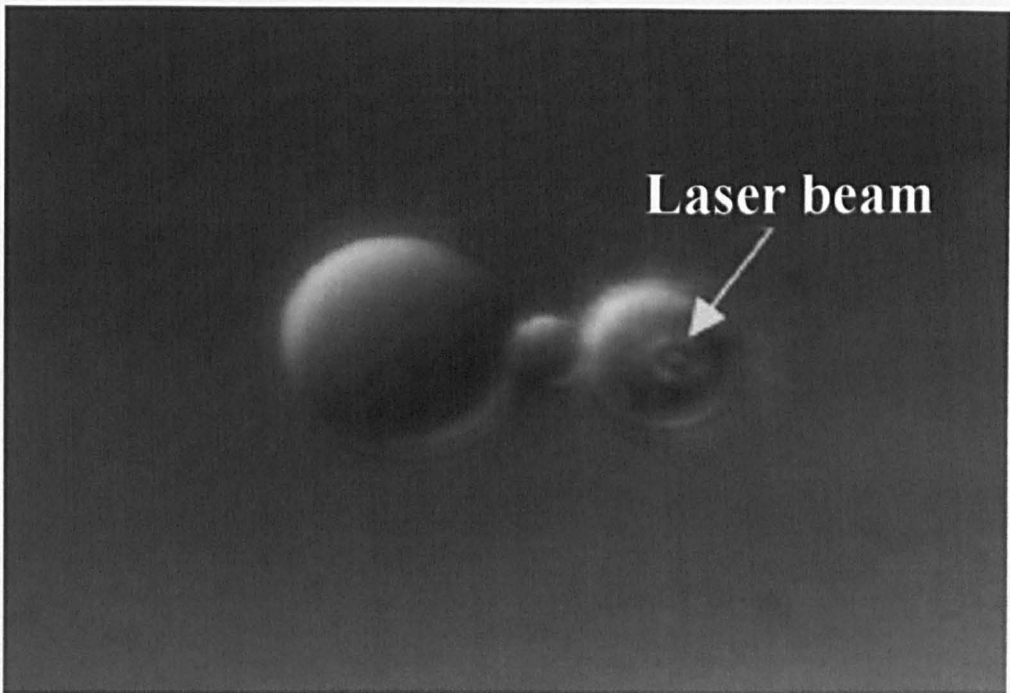


Figure 1.4: *Stretching of a single collagen molecule. The collagen molecule is between the two dielectric spheres. The larger sphere is trapped between the glass slide and coverslip. The molecule is stretched by pulling the smaller sphere with the optical tweezers.*

the micropipette until the sphere held in the optical trap was released (e.g. DNA was fully extended) and movement of the sphere held by the optical trap was detected by the position-sensitive photodetectors as a deflection of the laser beam. The extension of the DNA was measured from images recorded by a CCD video camera.

So far I have mentioned force measurements, detection of small movements of trapped particles and heating of particles, in relation to biological studies. Some purely biological applications of optical tweezers are optical scalpels and optical scissors, which both use optical tweezers and an additional laser. Optical scalpels can be used in conjunction with an optical tweezers to perform microsurgery on cells [24]. Figure 1.6 shows a series of images of optical tweezers and an optical scalpel being used to dissect a chromosome fragment [24]. The ability to hold the chromosome fragment with the optical trap makes it easier to not only dissect the fragment, but also to remove it from the cell. Optical scissors and optical tweezers were also used to trap and dissect chromosomes from newt

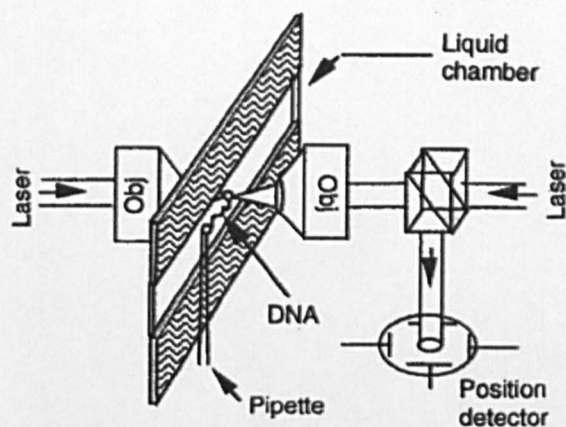


Figure 1.5: *The experimental arrangement used to detect movement of a trapped particle using photodetectors.*

lung cells [25]. Although optical scalpels and scissors are invasive, the cell wall can repair itself (depending on how much damage it has received), leaving the cell alive [26].

Many biologists are more interested in the biochemistry of living systems. Research with optical tweezers is not limited to the manipulation of a single particle with a chemically inert surface. Specific types of particles can carry out customized tasks, although restricted to specific tasks, allow optical tweezers to be extended to other areas of biological research. Spheres can have functionalized surfaces to allow materials/biomolecules to adhere to their surfaces, allowing specific chemical reactions [5] and fluorescence to be studied [27]. Biochemical reactions were induced by colliding particles to measure their probability of adhesion. One particle was a silica sphere coated with an influenza virus and the other a chicken red blood cell, both controlled with dual-trap optical tweezers. The force required to separate the adhered particles was measured from the power in the trapping beam required to pull the two particles apart [28]. Fluorescence is a powerful tool allowing specific aspects of molecular mechanics to be studied. An example is the visualization of DNA molecules being stretched (Figure 1.7). The DNA was attached to a single bead and stretched by holding the bead with optical tweezers and passing fluid through the sample cell at a fast enough flow to extend the DNA. The DNA was stained with a fluorescent dye which was excited by the trapping laser and allowed the stretching of the DNA to be observed [29].

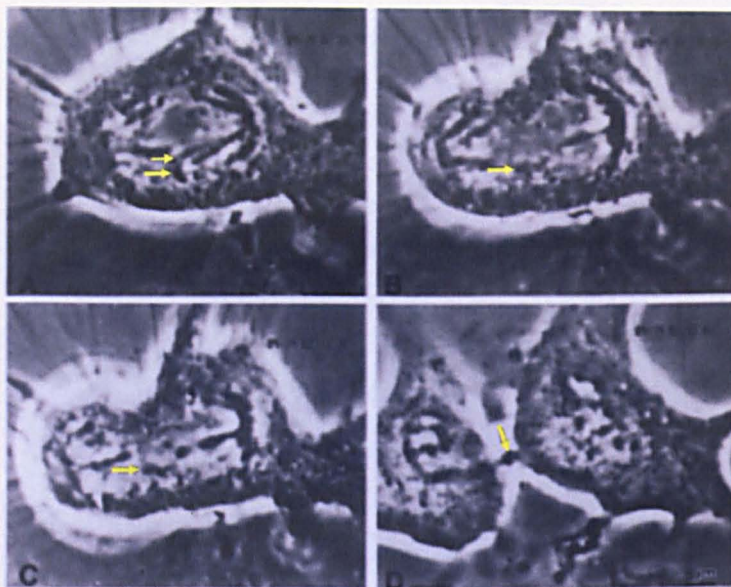


Figure 1.6: *An optical scalpel being used to dissect a chromosome fragment (indicated by the longer arrow in A) held by an optical trap. The dissections are indicated by the arrows in frames B and C. The dissected fragment is seen held by the optical trap in D.*

Fluorescence has also been used to measure the heating of cells while trapped using an infrared laser. The cells were heated in one chamber with a heating coil and another chamber contained a thermocouple to record the temperature change. The two chambers were separated with an ultrathin glass coverslip [30]. In these two examples, the fluorescence of the cells was observed. Combining two-photon excitation fluorescence and optical trapping of human sperm cells, tagged with a pH sensitive fluorescent label, allowed researchers to determine if the trapped cells were alive or dead [31]. The advantage of using two-photon excitation fluorescence is the excitation source is the trapping laser beam, thus utilising the tight focus required for the optical trap. Fluorescence can be used as a form of spectroscopy, with the fluorescence emitting wavelengths of light specific to chemical changes. Other methods of spectroscopy are used in optical tweezers, including Raman spectroscopy, absorption and emission spectroscopy and surface enhanced resonance Raman scattering (SERRS), to name a few. These methods usually involve coating or impregnating the trapping particle with a dye, which is excited either by the trapping laser beam or a secondary light source. Raman spectroscopy was first used in optical tweezers to study morphology-dependent resonances in trapped microdroplets of

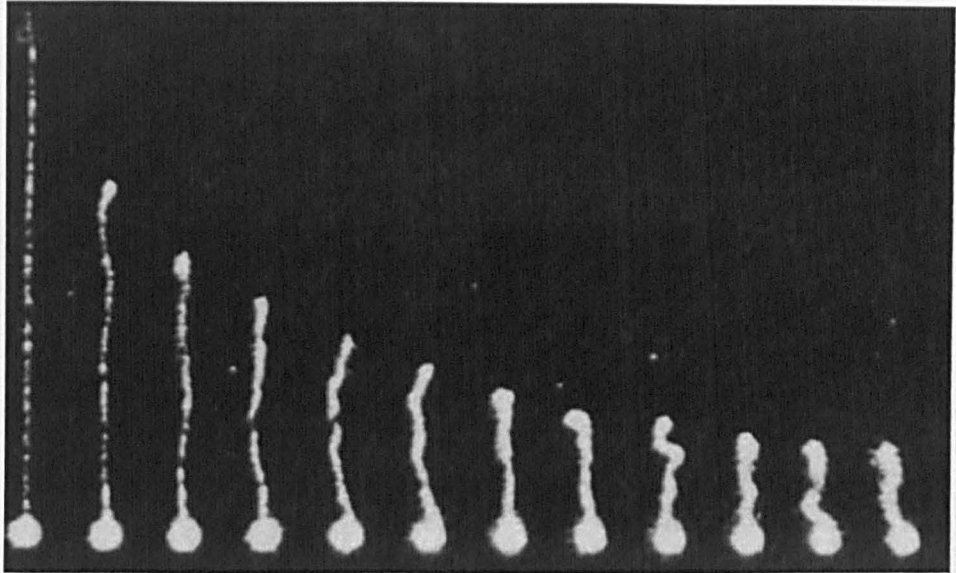


Figure 1.7: *A sequence of images (from right to left) showing the fluorescence of DNA as it is stretched.*

water-glycerol mixtures [32]. Since this study, Raman spectroscopy studies using optical tweezers have become varied and many (see [5] and references within). Another form of Raman spectroscopy, SERRS, was used in various studies in the last few years because it gives a stronger, more distinct signal than Raman spectroscopy [33].

The flexibility of optical tweezers in combination with the various types of spectroscopy mentioned above, allows chemical reactions inside and on the surface of cells to be studied. The above mentioned examples are just a few of the applications of optical tweezers in the biosciences and the number of applications is rising. The demand to understand biological systems and processes continues to drive the development of new applications of optical tweezers.

1.3.3 Trapping Multiple Objects

The previous section introduced the trapping of single and multiple particles for biological studies. This section introduces the development of trapping techniques for multiple objects. Many early applications of optical tweezers used a single optical trap to hold

and manipulate a single particle. The limitation of one optical trap holding only one particle was overcome by the development of several trapping techniques which allow more than one particle to be trapped. The trapping of multiple particles allows patterns of trapped particles to be created and force measurements to be made (see previous section for examples).

The simplest way to trap multiple particles is time-sharing of a single optical trap. Time-sharing an optical trap involves scanning the trap at a frequency that allows multiple particles to be held long enough to maintain their position in the specified pattern. Time-sharing of traps with a single laser beam can be achieved by using servo-controlled scanning mirrors [34, 35] and galvo-mirrors [36] (Figure 1.8). In addition to trapping multiple particles, scanning mirrors can also be used to manipulate trapped particles. However, two-dimensional and three-dimensional patterns of particles can be trapped and manipulated by time-sharing optical traps.

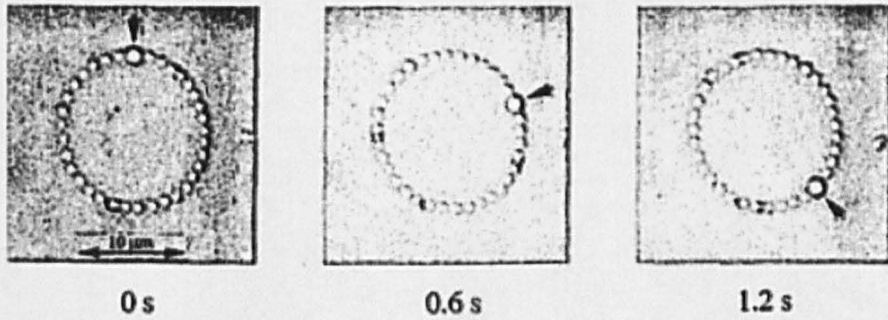


Figure 1.8: *An example of a two-dimensional configuration trapped by time-sharing an optical trap. The arrow indicates the position of a sphere as it is moved around the circle.*

The trapping of multiple particles is not restricted to time-sharing of a single trap. Another technique used to trap more than one particle is splitting the trapping laser beam into two or more beams and recombining the beams before entering the back aperture of the microscope objective, allowing multiple particles to be trapped [37]. Using a multiple-beam arrangement, the position of the optical traps can be manipulated independently of each other either manually using beam-steering mirrors or by programming computers to control the mirrors. These manipulation techniques produce two-dimensional manipulation of trapped particles. A multitude of papers has been published in which multiple-

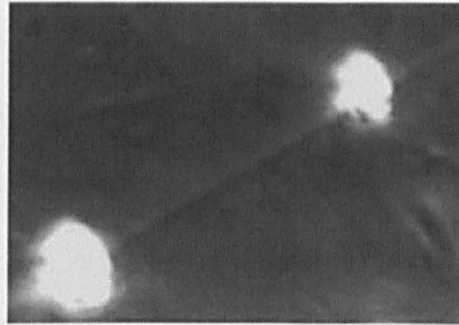
traps were created to trap two or more objects. One novel application of multiple-trap optical tweezers, which shows two trapped particles being manipulated independently of each other, was the measurement of the mechanical properties of microtubules [38]. The stiffness of microtubules were measured by attaching spheres to the ends of the microtubules, trapping the spheres with the optical traps and moving the traps towards each other to bend the microtubule (Figure 1.9).

The strength of controlling the position of multiple traps with mirrors is that each trap can be controlled independently. The ability of controlling multiple optical traps independently has many applications, mainly in biophysics. Spheres can be attached to both ends of a fibre and they can pull on both ends until it reaches breaking point (similar to Figure 1.4).

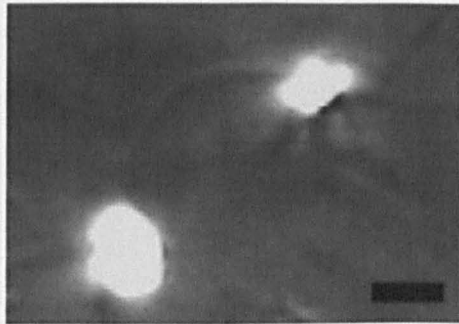
Although the use of mirrors is used extensively in the trapping of multiple objects with optical tweezers, other techniques do exist. An example is the creation of a 3 by 3 array of traps with an array of vertical cavity surface emitting cavity lasers (VCSELs, [39]). Such an array of traps was used for trapping and manipulating of yeast cells (Figure 1.10). The VCSELs were arranged in the 3 by 3 array and focused through the same optics in the optical tweezers arrangement, thus allowing more than one particle to be trapped. Another advantage of the VCSELs was the output of a Laguerre-Gaussian mode, allowing low refractive index cells to be trapped. These Laguerre-Gaussian modes are advantageous to trapping low refractive index particles compared to Gaussian modes, which do not trap low refractive particles well.

1.3.4 Scattering Particles and Shaped Particles

Biological samples, glass and most polymer spheres can be regarded as non-birefringent and transparent (non-absorbing) particles. The ability to trap different types of particles with optical tweezers has not been restricted to these dielectric particles. Birefringent and absorbing particles have been trapped and manipulated by optical tweezers. Common to these particles is a strong scattering force, making them difficult to trap. Metal particles are one type of strongly scattering particles and were trapped to investigate movements of



(a)



(b)

Figure 1.9: *Photographs showing a) two polystyrene spheres at the ends of a microtubule held with dual-trap optical tweezers and b) the optical traps moved closer to produce a buckling in the microtubule. Scale bar is 2 μm .*

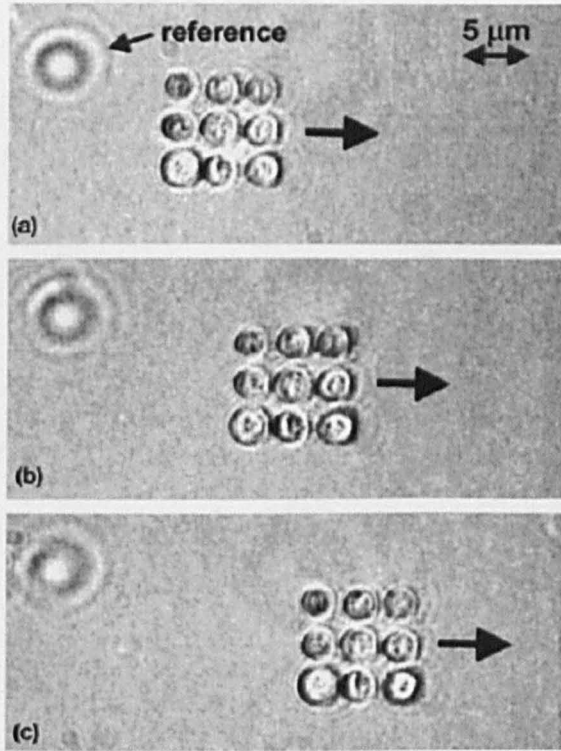


Figure 1.10: A sequence of frames showing nine yeast cells, arranged in a 3 by 3 array, being moved from left to right.

membrane proteins [40]. The movements were investigated by tagging the membrane with gold particles and dragging the particles through the membrane with optical tweezers. Edinin et al. [40] showed that absorbing Rayleigh particles could be trapped with a Gaussian beam, using the same principles that allow Mie particles to be trapped [4]. Another early technique used to trap scattering particles was a scanning beam, which was scanned around metallic particles fast enough to confine and manipulate the particle [41].

Absorbing particles were first trapped with a Laguerre-Gaussian beam to investigate the effects of light's angular momentum [42]. The absorbing particle was held in the dark region of the beam, where the scattering forces balance gravity and other forces. Related to the angular momentum of light, is the rotation of particles using optical tweezers. Particles can be rotated using Hermite-Gaussian laser modes. Such beams were used to rotate red blood cells [43]. Helical wavefronts (optical vortices) in Laguerre-Gaussian beam rotate birefringent particles and were used to investigate torques on calcite particles [44, 45], as shown in figure 1.11. Arrays of these vortices (Figure 1.12) can behave like a pump and were used to induce a flow of particles [46]. The flow was induced by the vortices rotating in opposite directions.

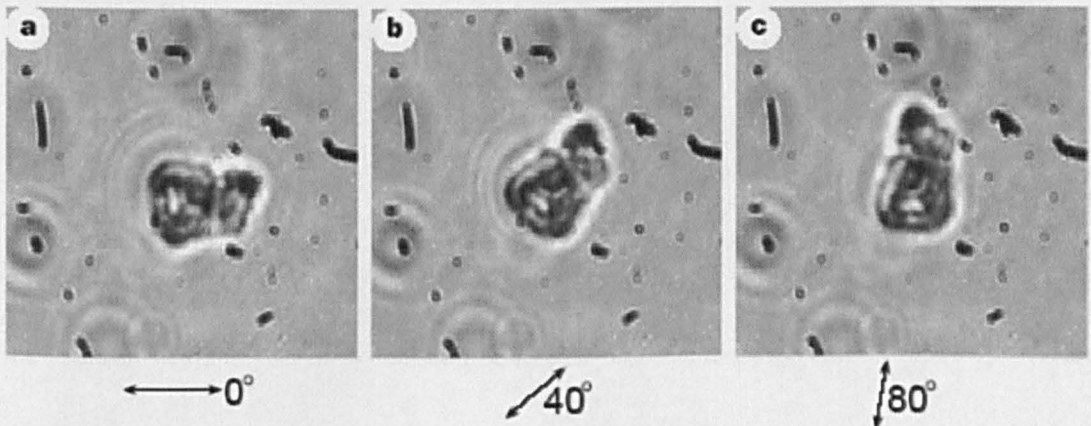


Figure 1.11: *An example of a calcite particle (several microns in diameter) being rotated, with the rotation controlled by rotating a half-wave plate.*

So far, the trapping and manipulation of mainly spherical, micron sized dielectric particles has been discussed. Many researchers have foreseen the use of optical tweezers as a way

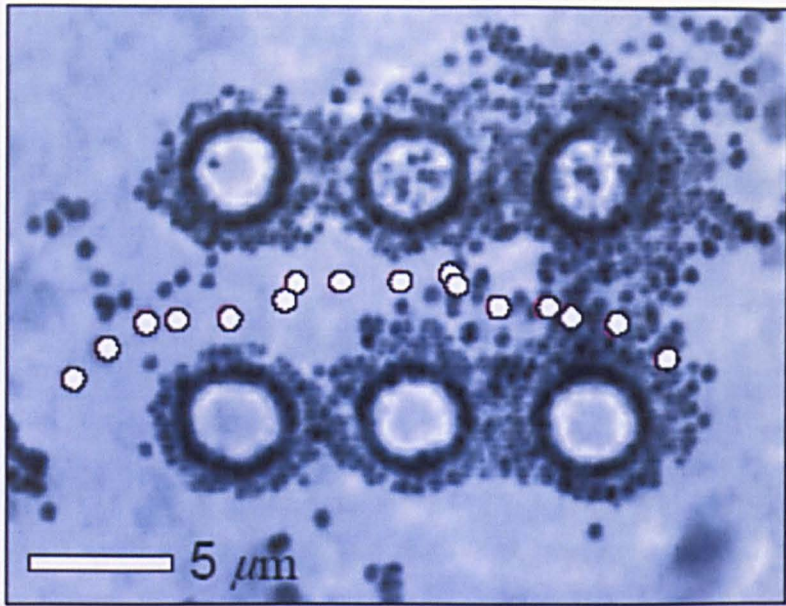


Figure 1.12: *Two lines of optical vortices, whereby the top three vortices rotate in the opposite direction compared to the bottom three vortices. The opposite directions of rotation creates a flow or optical pump in the region between the vortices, indicated by the trajectory of a particle moving from right to left.*

of powering micromachines. Micromachines are basically mechanical devices which use micron sized moving components. Optical pumps mentioned previously can be regarded as micromachines. Preliminary work initially concentrated on producing and optically trapping micron sized components, for example the rotation of asymmetrical particles and light driven cogs (Figure 1.13). Trapped particles such as these can be manipulated, rotated and reoriented [47].

1.3.5 Microfluidics and Optical Tweezers

The previous section introduced micromachines. This section introduces micromachines and optical tweezers combined with microfluidics. One type of micromachine, optical vortices can be arranged to produce an optical pump [46]. The first optical pumps were achieved in a microfluidic device by Terray et al. [48]. These optical pumps used piezo-controlled scanning mirrors to rotate several particles in a lobe-shaped cavity to produce

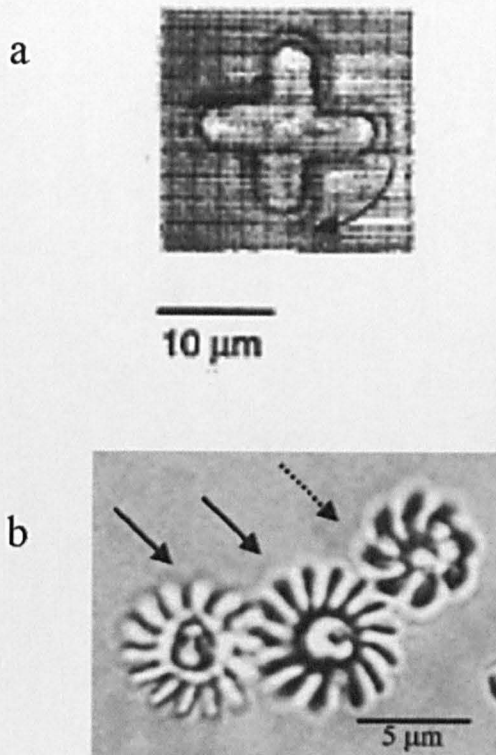


Figure 1.13: *Examples of custom-manufactured micron-sized components: a) a rotating cross shaped glass cog (arrow indicating direction of rotation) ; b) two cogs (indicated by solid arrows) driven by the cog held by an optical trap (indicated by dashed arrow).*

pumping (Figure 1.14a); a second pump used lines of particles as a peristaltic pump (Figure 1.14b). Additionally, Terray et al. made a valve device from a line of spheres (Figure 1.14c).

The use of optical tweezers with microfluidic devices is a relatively new application of optical tweezers, with one of the first applications involving the sequencing of DNA [49]. One simple use of optical tweezers with a microfluidic device is directing a particle along a specific channel (Figure 1.15), which could be described as a simple sorting device [50].

A recent sorting device that combines microfluidics with optical tweezers sorts biological cells and different types of particles (Figure 1.16). Cells can be sorted by simply diverting the direction of their flow with a single laser beam [51] or by passing a flow of mixed cells through a three dimensional interference lattice [52]. Cell sorting devices are of great

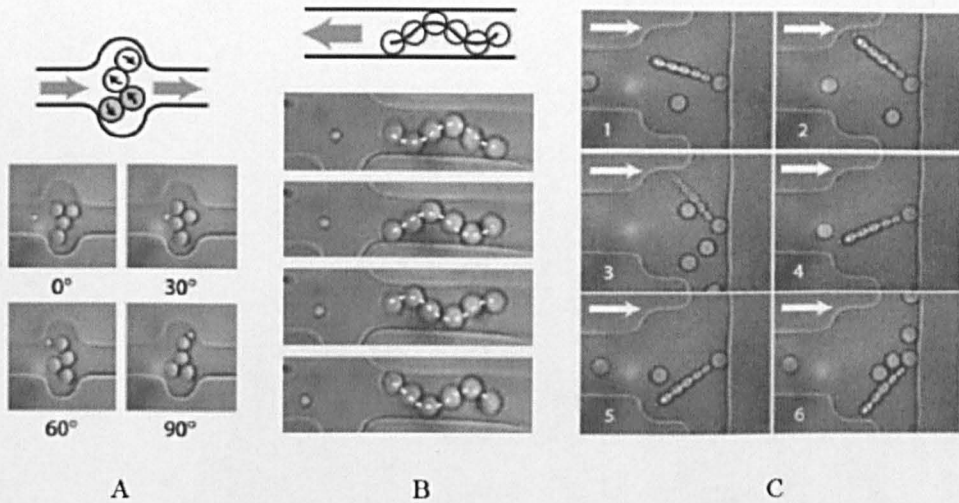


Figure 1.14: *Examples of microfluidic devices: a) pump designed on lobe movement, b) peristaltic pump and c) a two-way colloidal valve.*

interest to both industry and the bio-sciences because the microfluidic devices can be designed for a specific purpose and mass produced.

1.3.6 Holographic Optical Tweezers

By the late 1990s a number of techniques were developed to create multiple optical traps and to shape the trapping laser beam. No single technique of shaping the trapping beam could perform all of these in a single optical tweezers configuration. One technique uses diffractive optical elements and revolutionized optical tweezers. By displaying the correctly calculated computer-generated holograms in liquid crystal displays, the trapping laser beam can be shaped into the desired array of optical beams. Each of these beams can independently trap an object in a lateral plane [53]. The use of computer-generated hologram patterns displayed in liquid crystal displays (LCDs), to shape the trapping laser beam, has advantages over fixed holographic plates. Holograms displayed in LCDs can be calculated in less than a second to a few minutes and do not require the toxic chemicals used to manufacture holographic plates.

The first holograms (recorded on holographic plates) used in optical tweezers shaped a

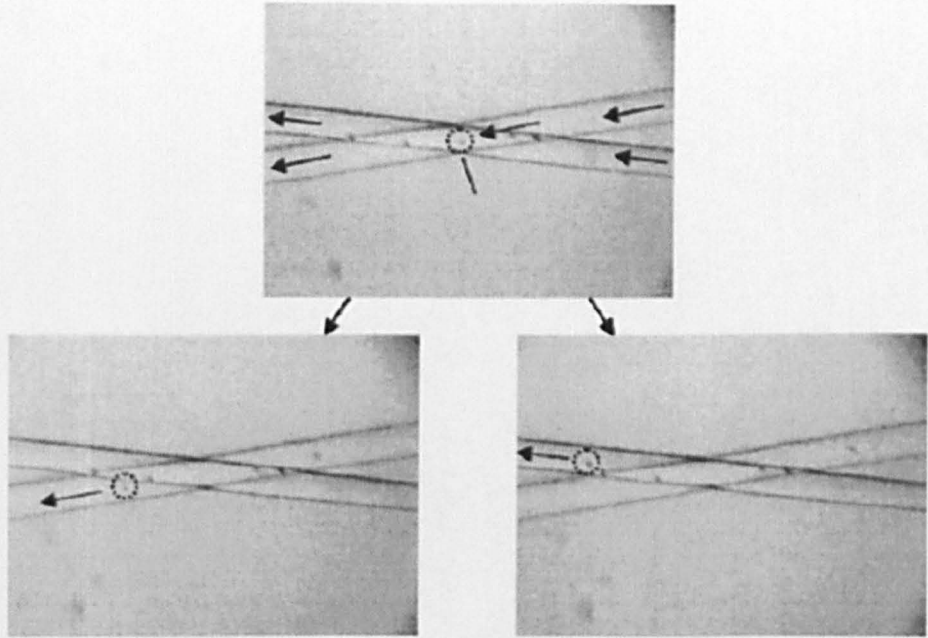


Figure 1.15: A $5\ \mu\text{m}$ particle moving along a channel. Optical tweezers are used to push the particle into a different channel or leave the particle to continue on its starting trajectory.

Gaussian laser beam into a Laguerre-Gaussian beam for the trapping of reflective and absorptive particles [42]. Reicherter et al. [53] replaced the holographic plate with a liquid crystal display. The first fully three dimensional experiments (Figure 1.17) using holographic optical tweezers were demonstrated by lifting a trapped particle over and around a stationary particle [54].

By replacing the LCDs with computer-addressed liquid crystal spatial light modulators (SLMs) [53, 54], large numbers of traps can be generated and introduced the ability to control them interactively in three dimensions (Figure 1.18). Hence, the term holographic optical tweezers (HOTs) was introduced.

HOTs require a hologram design algorithm that can efficiently shape the trapping laser beam, into the desired intensity distribution in the plane of the microscope objective. Many algorithms have been used over the last 5 years and several of these will be explained in more detail in Chapter 2. Examples of hologram design algorithms are the Gerchberg-Saxton algorithm [55] and its variations [53, 1]. Although not a holographic technique,

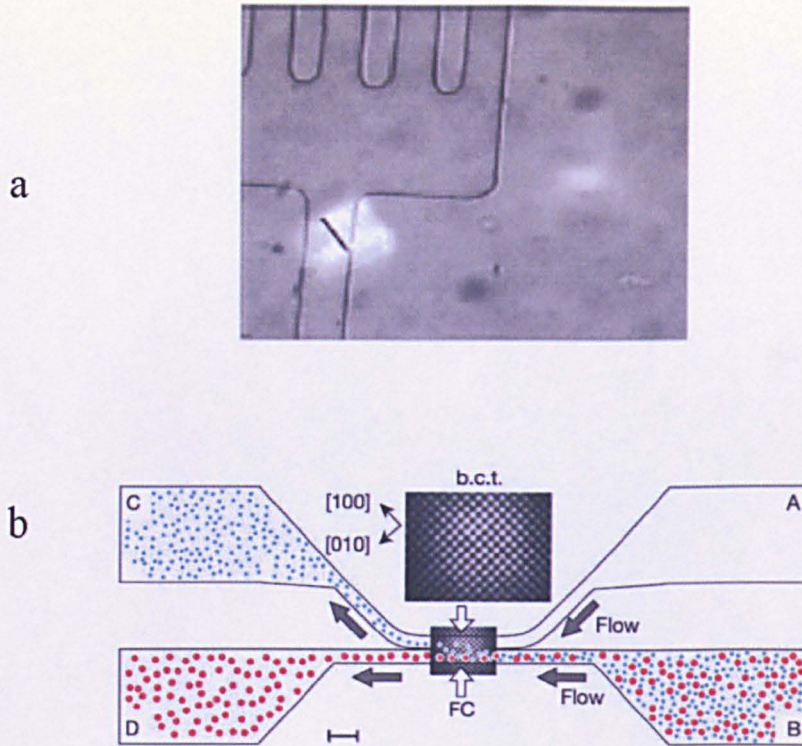


Figure 1.16: *Examples of cell sorting devices: a) using optical tweezers to divert particles to channels and b) particles sorted by size using a 3-dimensional interference lattice.*

the generalized phase contrast (GPC) method offers fast and reliable two dimensional manipulation of particles and limited three dimensional manipulation [56]. The GPC method, unlike most holographic trapping methods, can manipulate particles in real-time. However, HOTs using a ferroelectric SLM can manipulate particles just as fast as the GPC method [57]. An example is shown in figure 1.19 of two particles moving in a circular path in real-time.

The type of hologram used in HOTs is dependant on the liquid crystal used in the SLM. Commonly, nematic liquid crystal SLMs are used in HOTs and details of such devices are given in Chapter 2. These SLMs have typical display rates of 20-60 Hz and are used to display phase holograms [19]. Ferroelectric liquid crystal SLMs have faster display rates, typically between 100 Hz and 1000 Hz, allowing holograms to be displayed at faster rates, giving real-time manipulation of trapped particles [57]. A limitation of ferroelectric SLMs is their binary-phase modulation, which gives low diffraction efficiencies in the 1st

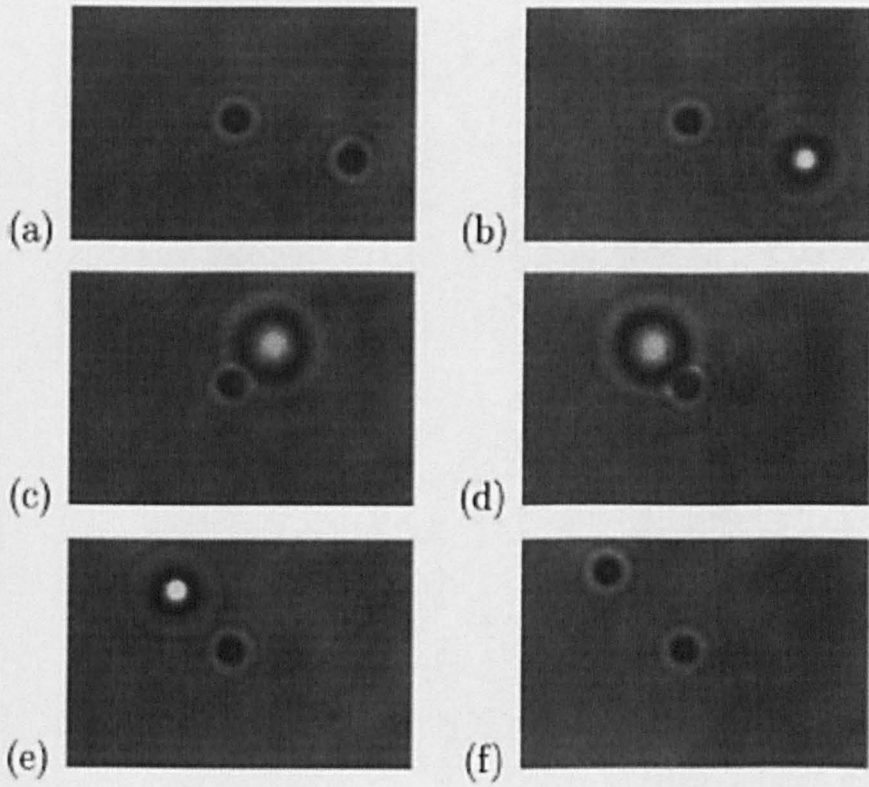


Figure 1.17: *A series of six frames showing the first example of fully three dimensional manipulation of trapped particles using HOTs.*

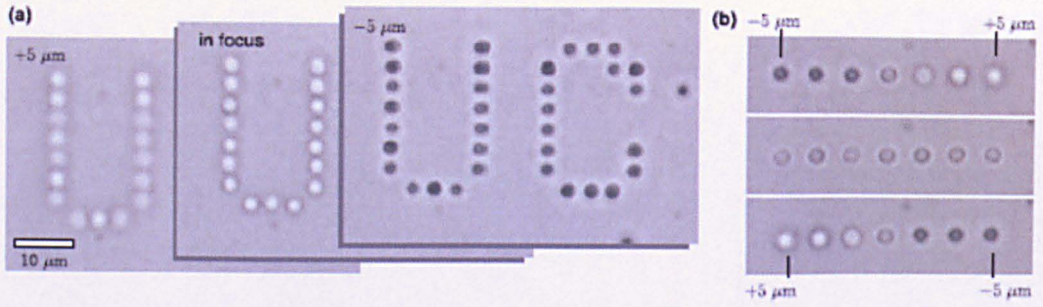


Figure 1.18: *Three dimensional trapping of 0.99 μm silica spheres: a) in a three plane pattern and b) a line of seven spheres moved independently of each other.*

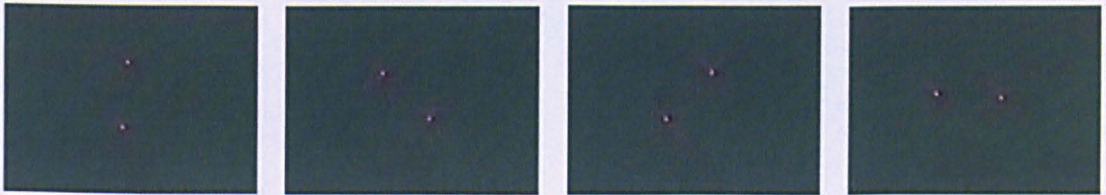


Figure 1.19: *A sequence of frames showing two traps rotating two beads in a 10.5 μm circle at a speed of 35 μms^{-1} .*

diffraction order, which is used for trapping.

1.3.7 Colloidal and Crystal Research

Two of the most recent and exciting applications of both optical tweezers and holographical optical tweezers, colloidal and crystal research, have been left to the end. The ability to trap and manipulate particles ranging from the nano-scale to micron-scale makes optical tweezers highly suited to these two research areas. The term colloids is defined as systems in which there are two or more phases, with one (the dispersed phase) distributed in the other (the continuous phase). Colloids include emulsions, gels, foams and aerosols.

Optical tweezers were used to grow and seed the growth of biocrystals [58] and to pattern colloidal crystals [59]. By repositioning colloidal spheres, dislocations can be introduced into colloidal crystals or removed (Figure 1.20). Colloidal crystals have also been formed

by annealing patterns of colloidal particles [60].

Colloidal crystals and substances cover many areas of both physical and biological sciences. They are of interest in many industries, including pharmaceutical, food and drinks, chemical and petrochemicals. Therefore, research in this area of optical tweezers is likely to be very active for some time.

Recently optical tweezers were proposed as a tool to aid the manufacture of photonic crystals [61]. Zhou *et al.* used optical trapping techniques as part of the process to make void-based diamond-lattice photonic crystals. This was achieved by trapping micron-sized spherical voids in a diamond lattice arrangement with a femtosecond laser [62].

1.3.8 Summary

This section has shown the main developments and the various uses optical tweezers over the last 30 years. Optical tweezers have evolved from a single optical trap to become a widely used tool across a range of sciences and engineering. These include measurements of forces and fluorescence, investigations into the properties of light and trapping multiple particles. Optical tweezing still continues to progress and in recent years holographic optical tweezers have revolutionised the field. Novel applications continue to be developed, for example combining optical tweezers with microfluidic devices. New research using optical tweezers is not restricted to applications and fundamental scientific experiments still continue, for example in the areas of angular momentum and optical vortices. In short, optical tweezers have been a successful area of scientific research and look set to continue to expand over the next few years.

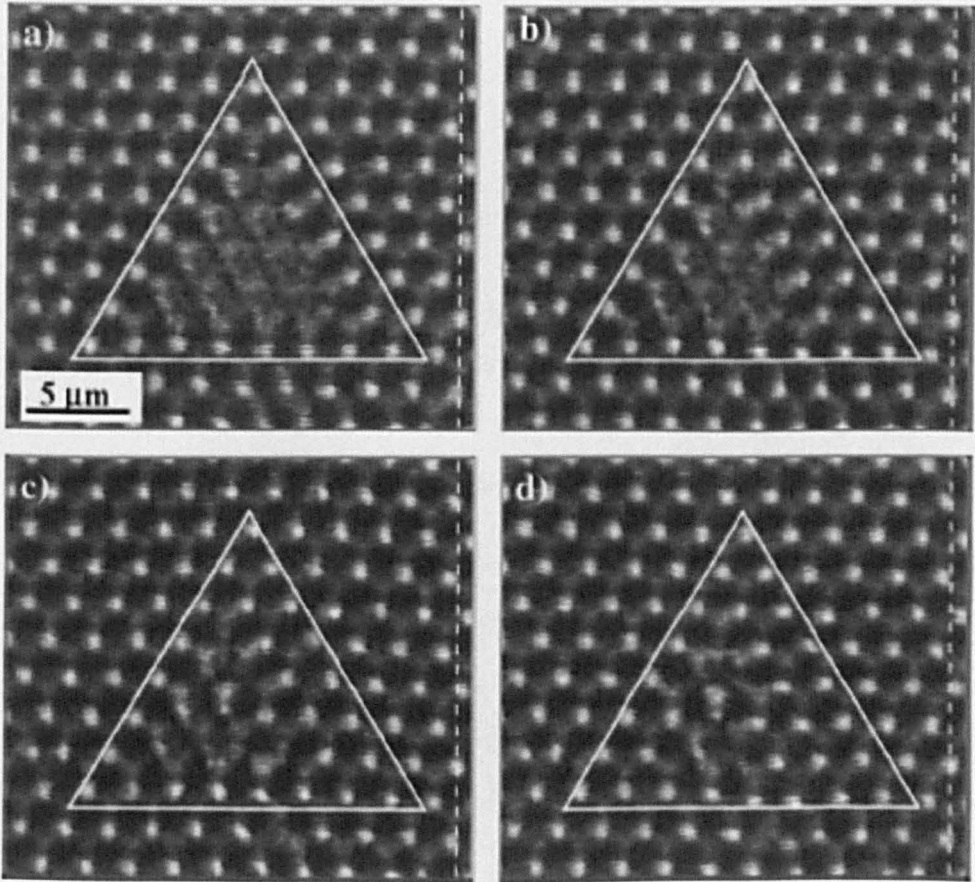


Figure 1.20: *Annealing of a triangular stacking fault, using local shearing. After 120 scans the defect (a) has been eliminated (d).*

Chapter 2

The Workings of Optical Tweezers

2.1 Introduction

The following chapter describes the basic principles on which optical tweezers, including holographic optical tweezers, are based. A section outlining the hologram design algorithms used for my experimental work is given to highlight the advantages and disadvantages of the computer-generated holograms used in experiments carried out over the last three years. Lastly a summary of the different spatial light modulators used in various incarnations of the holographic optical tweezers is given.

2.2 Optical Tweezers

To obtain an optical trap, a collimated beam of coherent light is tightly focused through an objective lens with a large magnification and high numerical aperture . Usually optical tweezers are built around a microscope, which also makes it possible to view the trapped particles while they are being manipulated. Figure 2.1 shows a basic arrangement for optical tweezers.

Optical tweezers use a tightly focussed laser beam to generate an intensity gradient capa-

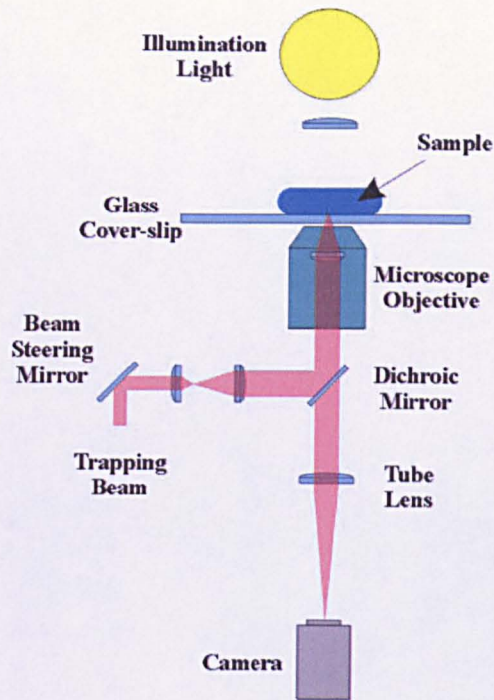


Figure 2.1: *Schematic representation of an optical tweezers arrangement.*

ble of trapping objects in three dimensions. The size of particles that have been trapped ranges from tens of nanometers to over a hundred micrometers in diameter. In the basic setup shown in figure 2.1, the position of the optical trap (focus) is controlled with the beam-steering mirror, with an angular movement of the mirror producing a lateral movement of the optical trap (Figure 2.2). Axial movement of optical traps can be achieved using deformable mirrors, but is technologically limited to a few microns [63].

2.3 Forces in Optical Tweezers

Many forces (e.g. gradient, scattering, gravity) act on trapped particles. The net effect of such forces acting on a particle is to hold it within the tight focus of the light beam. The dominant force acting on particles trapped using optical tweezers is the gradient force, given as [4]

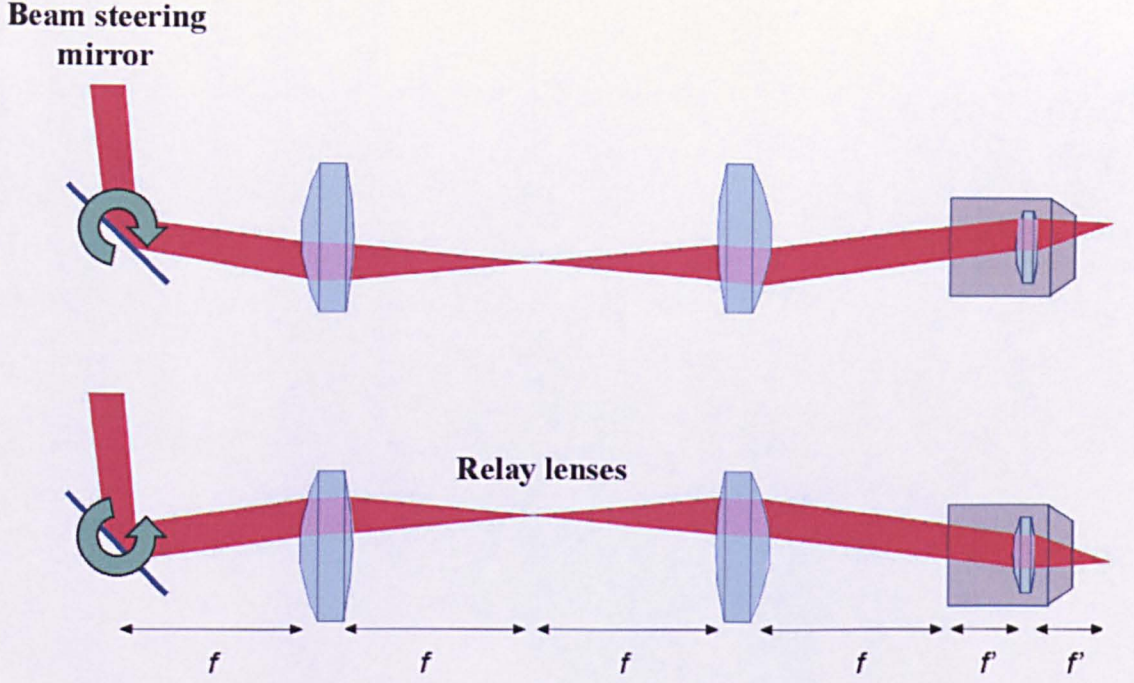


Figure 2.2: Diagrammatic representation of movement of an optical trap using the beam-steering mirror

$$\vec{F}_{grad} = -\frac{n^3 r^3}{2} \left(\frac{N^2 - 1}{N^2 + 2} \right) \vec{\nabla}(|E|^2), \quad (2.1)$$

where n is the refractive index of the surrounding medium, r is the radius of the particle, N is the ratio of the refractive indices of the particle and the surrounding medium and E is the electric field if the refractive index of the particle is less greater than the refractive index of the surrounding medium. The gradient force acts towards the area of highest intensity, where particles are trapped. Another significant force acting on trapped particles is the scattering force and its magnitude is [4]

$$F_{scat} = \frac{I_o}{c} \frac{128\pi^5 r^6}{3\lambda^4} \left(\frac{N^2 - 1}{N^2 + 2} \right)^2 n, \quad (2.2)$$

where I_o is the intensity of the laser beam and λ the wavelength of the laser beam. The scattering force acts along the direction of laser beam propagation. The scattering force acts on different sized (Mie particles and Rayleigh) particles in different ways. Mie and

Rayleigh scattering are explained later.

In most of my experimental work, the trapped particles were non-birefringent, non-absorbing dielectric particles, where the gradient force is much greater than the scattering force. The other types of particles trapped were calcite and diamond particles (see Abraham-Minkowski experiment in Chapter 7), two types of birefringent, absorbing particles, which were trapped using the scattering force with a Laguerre-Gaussian beam.

2.3.1 Other Forces

In addition to the gradient and scattering forces, gravitational, buoyancy and Stokes drag forces act on trapped particles. These forces are shown acting on moving particles in figure 2.3.

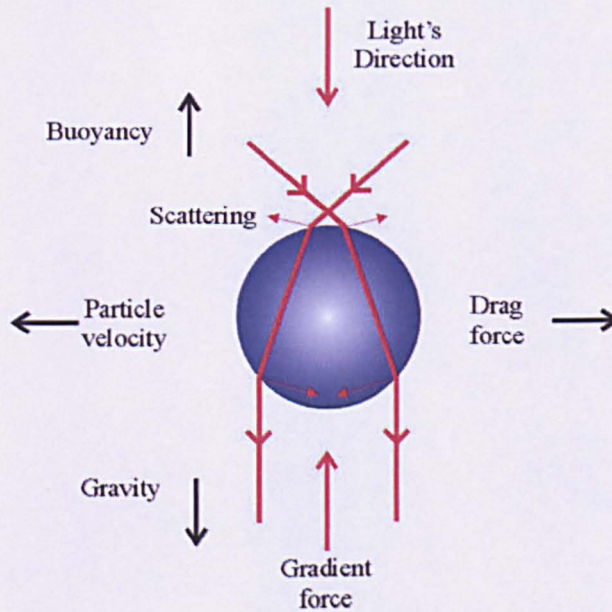


Figure 2.3: *Additional forces acting on a trapped sphere. The light is propagating from the top to bottom and light scattered from the trapped sphere indicated.*

The magnitude of the gravitational force allowing for buoyancy effects, acting on a trapped particle is given as

$$F_{grav} = V_s g (\rho_s - \rho_l), \quad (2.3)$$

where V_s is the volume of the solid, g is gravity, ρ_s is the density of the solid and ρ_l is the density of the liquid. In an inverted microscope geometry, the buoyancy force can help to stop a particle being pulled to the bottom of the sample cell. However, if strong enough, the gravitational force (which includes the buoyancy force) can cause a particle to be dislodged from the optical trap. When a trapped particle is moved through the suspension liquid, the liquid behaves as if in a laminar flow regime and a drag force is exerted on the particle, due to viscosity of the suspension fluid acting like a friction on the particle's surface. For a moving sphere, the magnitude of the drag force acting on it was calculated by Stokes and is given by

$$F_{drag} = 6\pi\eta r v, \quad (2.4)$$

where η is the coefficient of viscosity, r is the radius of the trapped particle and v the speed of travel of the particle.

2.3.2 Mie and Rayleigh Scattering

Mie and Rayleigh scattering depends on the ratio of particle size to the wavelength of incident light. Mie scattering occurs when the diameter of the particle is larger than the wavelength of the incident light. Rayleigh scattering occurs when the diameter of the particle is much smaller than the wavelength of the incident light (Figure 2.4).

Mie scattering occurs when two criteria are met, the incident light has a wavelength a tenth the diameter of the particle and there is a difference between the refractive indices of the medium through which the light passes and the particle it scatters off. Ray optics apply to Mie scattering because the wavelength of the incident light is small compared to the diameter of the particle, therefore scattering is not wavelength dependent. As light is scattered, momentum is transferred to the particle, thus scattering is inelastic.

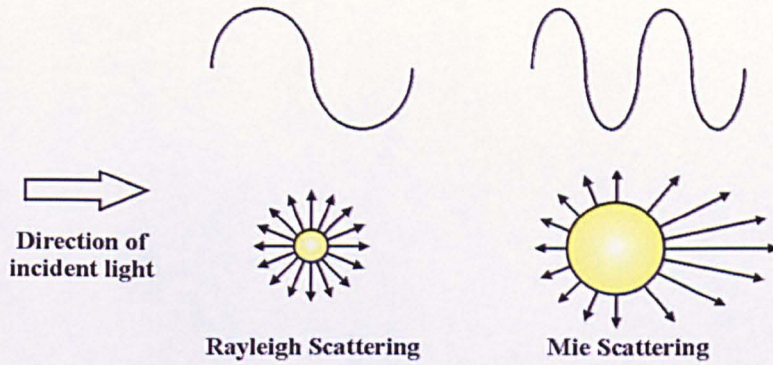


Figure 2.4: *Rayleigh and Mie scattering regimes.*

Ray optics does not apply to Rayleigh scattering because the wavelength of the incident light is much greater (more than ten times) than the diameter of the particle. The light incident on the particle and the light scattered contain the same energy; scattering is elastic. Unlike Mie scattering, Rayleigh scattering is wavelength dependent ($\sim \lambda^{-4}$) and is greater at shorter wavelengths.

2.3.3 Optical Trap Efficiency

As an alternative to considering the trapping forces in the terms of equations 2.1 - 2.3, a useful insight to the optical trapping mechanism is given by ray optics. An optical trap exerts a force on a trapped particle by momentum transfer. The momentum transfer is produced by a change in the direction of light propagation as the trapping laser beam is refracted and reflected (Figure 2.5).

The light beam exerts of force on the particle related to the power in the beam. The magnitude of the force is given as

$$F = Pn/c, \tag{2.5}$$

where P is the power in the light beam, n is the refractive index of the particle and c is the speed of light in a vacuum. The total force acting on a particle ranges from a few picoNewtons to a few nanoNewtons.

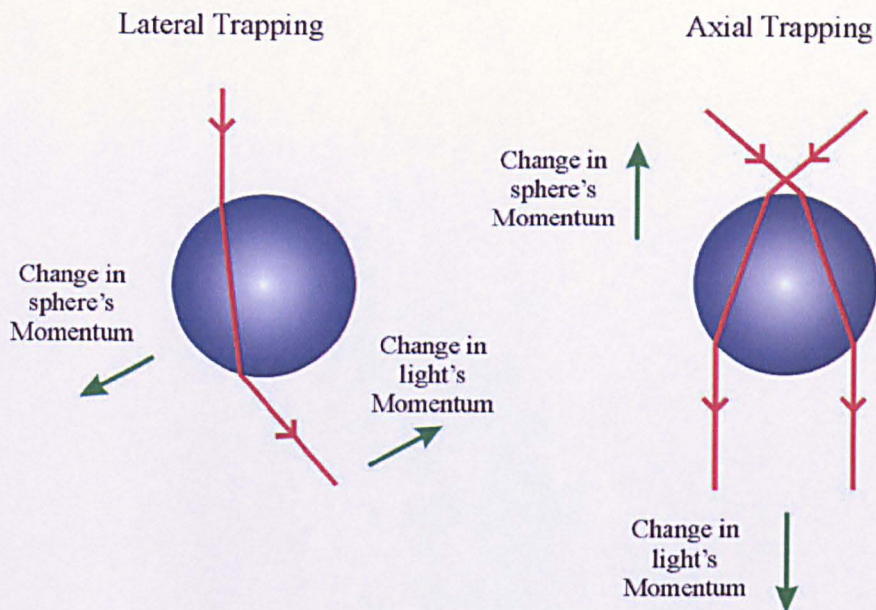


Figure 2.5: Ray optical representations of light refracted as it passes through a dielectric sphere, showing the direction of momentum change in the light and the equal and opposite momentum change of the sphere, resulting in a reaction force.

The trapping of particles in optical tweezers relies on the transfer of momentum from the trapping laser beam to the trapped particle. The amount of momentum transferred is termed the optical trap efficiency, measured as a dimensionless quantity Q , defined as

$$Q = \frac{Fc}{nP}. \quad (2.6)$$

The greater the Q value, the more efficient the trap. The Q value is 1 when all the momentum of the trapping light is transferred to the trapped particle. The efficiency of the trap is influenced by the difference between the refractive indices of the particle and surrounding medium. The larger the difference in the refractive indices, the more the incident light is refracted and the stronger the trap. Other influences are the degree of focusing and the extent of aberrations in the optics, most importantly the objective lens. Typical values of Q for dielectric and metal particles trapped with optical tweezers are between 0.03 and 0.1 [19].

2.4 Holographic Optical Tweezers

Holographic optical tweezers (HOTs) are optical tweezers in which computer-generated holograms are used to shape the trapping laser beam. In HOTs, the beam-steering mirror is replaced with a diffractive optical element, typically a phase-only spatial light modulator (Figure 2.6). Alternatively the plane of the spatial light modulator (SLM) can be imaged on to the beam-steering mirror. Other diffractive optical elements (DOEs) used are holographic films [42] and liquid crystal displays [53].

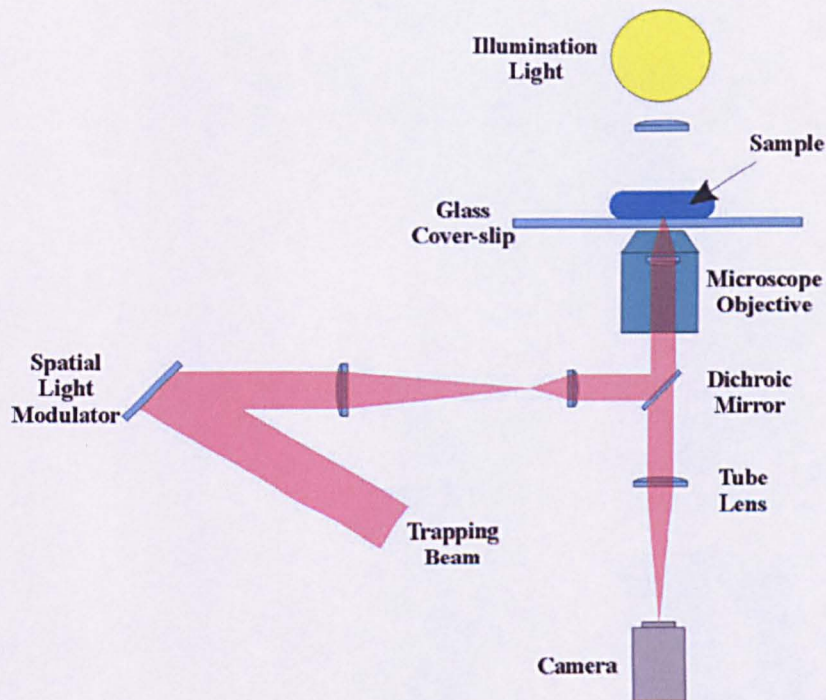


Figure 2.6: *Schematic representation of an holographic optical tweezers arrangement.*

SLMs (used to display computer-generated holograms), from which the trapping laser beam is reflected off. In the experimental arrangement shown in figure 2.6 the computer-generated hologram displayed on the SLM is imaged in to the objective lens. The focal plane of the objective lens is effectively the Fourier plane of the SLM. The computer-generated holograms act as diffraction gratings, modifying the laser beam to give the intended intensity distribution. In the terms of applications to HOTs the desired intensity distribution is an arbitrary pattern of spots of light. As the laser beam interacts with the computer-generated hologram, the phase of the beam is changed. In its simplest form,

a computer-generated hologram displayed in a SLM changes the phase of the incident light to maximise as much light into a single trap. This is achieved by displaying a blazed wedge, which in principle places all the light into the first diffractive order. This changes the phase and amplitude of the trapping laser such that its focus can be offset arbitrarily in the x and y directions. Simple extensions allow the focus to be offset in the z direction and to be split in to multiple foci and transformed in to different types of beams (Figure 2.7). An offset of the trapping beam in the lateral plane is produced by a phase hologram representing a prism. Focussing the trapping beam is achieved by displaying a phase hologram of a lens. Splitting a beam into multiple beams is achieved through a combination of lens and wedge holograms. Calculating the correct hologram that gives the desired intensity distribution (optical trap pattern) in the trapping plane(s) requires an algorithm capable of designing arbitrary intensity patterns.

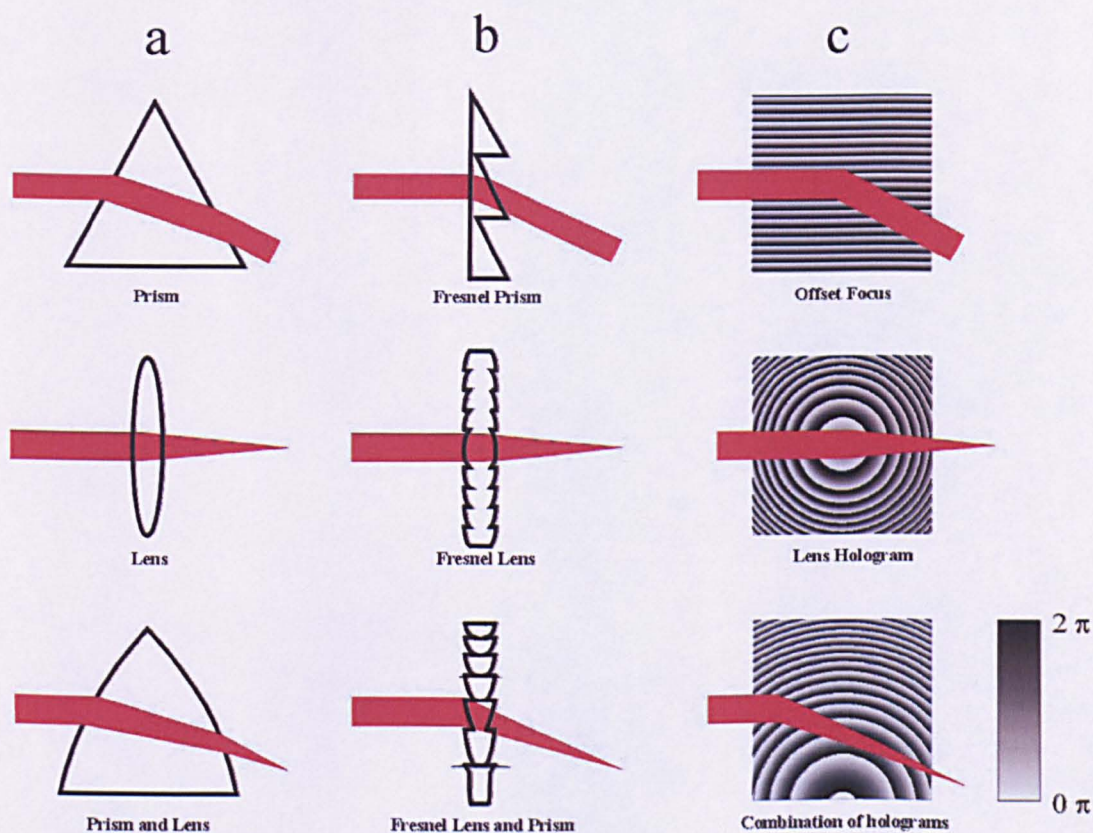


Figure 2.7: *Examples of phase holograms displayed in a spatial light modulator, shown as: a) optical component, b) Fresnel component and c) greyscale representations of the phase holograms.*

Two types of phase holograms were displayed in the SLM for my experiments, static/precalculated holograms and reconfigurable holograms. Static holograms are one-off holograms producing either single or multiple traps. Reconfigurable holograms can be calculated quickly enough to be displayed at video frame rates in the SLM, allowing interactive movement of the optical traps.

2.5 Hologram Design Algorithms

Holograms come in two forms: phase holograms and intensity holograms. For use in HOTs, the hologram should maximise the power in the optical traps. Phase holograms are preferred over intensity holograms. Phase holograms are preferred because they shape light more efficiently, placing more power into the optical traps. Intensity holograms modulate the intensity and this leads to loss of power in optical traps.

Holograms used in HOTs can be recorded on holographic film or displayed on a SLM. Computer-generated holograms are used in both of these techniques. Recording holograms onto holographic film is a time-consuming process, involving the use of toxic chemicals and this technique of hologram fabrication was not used in my experiments. Displaying holograms on a SLM is the favored technique and has many advantages over holograms recorded on holographic film. SLMs display computer-generated holograms quicker because they are loaded directly from the computer calculating them. In the case of the SLMs I have used, the holograms can be loaded at video-frame rates.

HOTs display a hologram in the plane of the SLM and the trapping laser beam is reflected off this plane. The far-field of the reflected laser beam is imaged on to the focal plane of the objective lens. The hologram changes the phase of the laser beam and shapes it in to the desired intensity pattern in the far-field. The hologram achieves the shaping of the laser beam because it can be programmed to act as diffraction gratings resembling wedges, lenses, apertures etc. The desired intensity patterns required for experiments using HOTs can often be very complex and these are best designed using computers. Computers are capable of quickly calculating complex holograms and assessing the performance of the holograms via simulations.

Complex computer-generated holograms usually require an iterative algorithm for their design. Iterative algorithms calculate the hologram required to produce a specified pattern in the target plane. Many iterative algorithms converge on a solution in which the error between the intensities of the hologram plane and target plane is reduced to a specified level, set by a figure of merit.

Many iterative hologram design algorithms are used to design holograms for use with HOTs [55, 53, 1, 64]. In the main, these algorithms were written to shape light for uses other than HOTs. For example, one of the most commonly used algorithms, the Gerchberg-Saxton algorithm, was developed to find the phase of an electron beam from its intensities in two planes [55].

In my research two algorithms were used to design most of the holograms. Another algorithm, using a combination of wedge and lens holograms, termed the anti-blazing technique is explained in detail in chapter 5. The two most widely used algorithms are a modified Gerchberg-Saxton algorithm (GS) [65] and a direct-binary search algorithm (DBS) [66]. These two different algorithms were used because they have different strengths and weaknesses, making the algorithms suited to some applications of HOTs, but not all applications. Both the GS and DBS algorithms are iterative and produce phase holograms. These phase holograms are usually calculated to a 512×512 pixel resolution using the GS algorithm and at 256×256 pixel resolution using the DBS algorithm. The phase of the holograms is represented as a 256 level grey-scale, equivalent to $0 - 2\pi$ phase modulation. A black pixel corresponds to 0 radians and a white pixel corresponds to 2π radians. More details of each algorithm are described below.

2.5.1 Direct-Binary Search Algorithm

The original direct-binary search algorithm was derived to design binary computer-generated holograms that efficiently utilize the holograms resolution [64]. The DBS algorithm used in my research [66] allows an intensity pattern to be specified within a fully three dimensional volume by specifying the positions of light spots as x,y,z coordinates.

The DBS algorithm flow diagram used is shown in Figure 2.8. DBS is based on making

random changes to the pixel pattern of the hologram to produce the specified intensity distribution in the target plane. The user assumes a Gaussian intensity distribution is reflecting off the hologram. The target plane intensity distribution is a pattern of bright spots (Figure 2.8). The DBS algorithm calculates a hologram that will produce the desired spot pattern in the plane of the objective lens. A defined figure of merit measures the holograms performance at meeting these criteria. Thus, the figure of merit is basically a measure of the error between the intensity distributions in the plane of the SLM and the pupil of the objective lens. A common figure of merit (ε) is the mean square error

$$\varepsilon = \sum_k (I_{t,k} - I_{a,k})^2, \quad (2.7)$$

where $I_{t,k}$ are the target and $I_{a,k}$ the predicted intensity in pixel number k . This figure of merit is a good measure for most target specifications.

A pixel change is either kept or discarded depending on whether or not it improves the match between the resulting beam and the target intensity distribution, after a number of successive iterations have not produced an increase in the error. The hologram is then repeatedly changed randomly until an acceptable solution is calculated. DBS requires many iterations and is therefore slow. The calculation time scales linearly with the number of pixels specified. Therefore, a hologram with a 256×256 pixel resolution takes longer to calculate than a hologram with a 128×128 pixel resolution, for the same target intensity distribution.

The time taken for the DBS algorithm to converge can be optimised by setting certain limits on the calculation. The user can specify the number of grey-scale phase levels and how many times each pixel is changed. By monitoring the reduction in error with the number of iterations, the number of iterations can be set to a given number after which a reduction in error only gives a slight improvement to the hologram.

Holograms calculated using the DBS algorithm are saved as bitmap files, which are displayed on the SLM in our HOTs arrangement. The convergence time of the algorithm is too slow to allow real-time manipulation of trapped particles. However, by loading sequences of bitmap files, particles can be manipulated through predetermined trajectories.

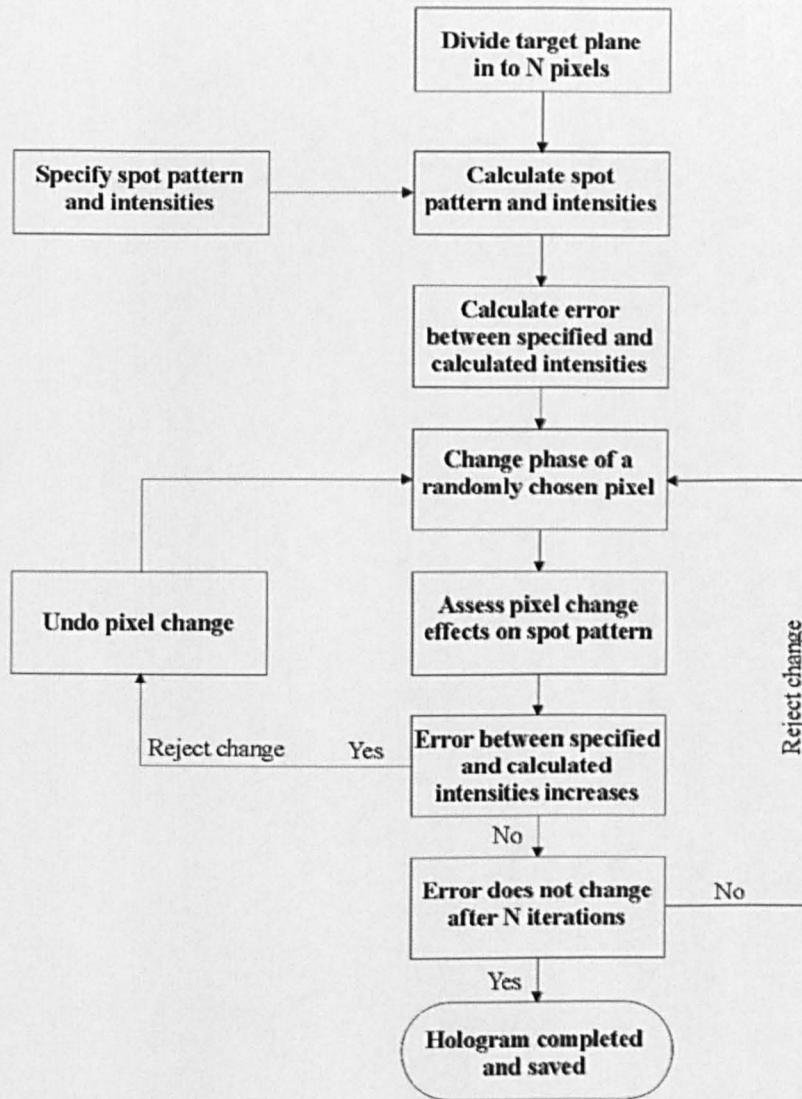


Figure 2.8: Schematic diagram of the direct-binary search algorithm.

The trajectories of the optical traps is calculated by specifying trap positions in a spread sheet.

2.5.2 Modified Gerchberg-Saxton Algorithm

Two variations of the original Gerchberg-Saxton algorithm were used in my research. These two variations of the Gerchberg-Saxton algorithms are shown in Figure 2.9. In its simplest form the GS algorithm allows spots of light to be specified in a two dimensional plane. In more advanced forms of the algorithm, light can be shaped in multiple-planes [67, 65] and in a fully three dimensional volume [68, 69].

The GS algorithm infers the phase distribution ϕ_h in the hologram plane from the intensity distribution I_h in the illumination laser beam in the plane of the hologram and the intensity distribution I_t in the target plane. The algorithm achieves this by starting with a beam of intensity I_h in the hologram plane and Fourier transforms the beam to target plane. The intensity I_h is often not that required in the target plane and is replaced with the correct intensity I_t , while the phase distribution ϕ_h is kept. The beam is inversely Fourier transformed back to hologram plane, where the new intensity I_t no longer fits the required intensity and is changed to fit I_h , while keeping the changed phase ϕ_t . This process is repeated until the intensity in the hologram plane I_h is a good approximation of the desired intensity distribution I_t in target plane. The convergence time of the algorithm is less than a second for simple 2-D patterns of bright spots. The mechanism that produces the required intensities in the near and far fields is an error reduction between the intensities of the two planes, thus the GS algorithm is also known as an error reduction algorithm [70].

The fast convergence of the GS algorithm makes it very useful for designing holograms that can be used to manipulate trapped particles using HOTs. To speed up the hologram calculations, each successive hologram is calculated from the spot patterns calculated for the previous hologram. However, in some circumstances is not always possible to calculate holograms in real-time and this is described below.

In the case of a 3D hologram, the far field intensities are specified in unrelated multiple

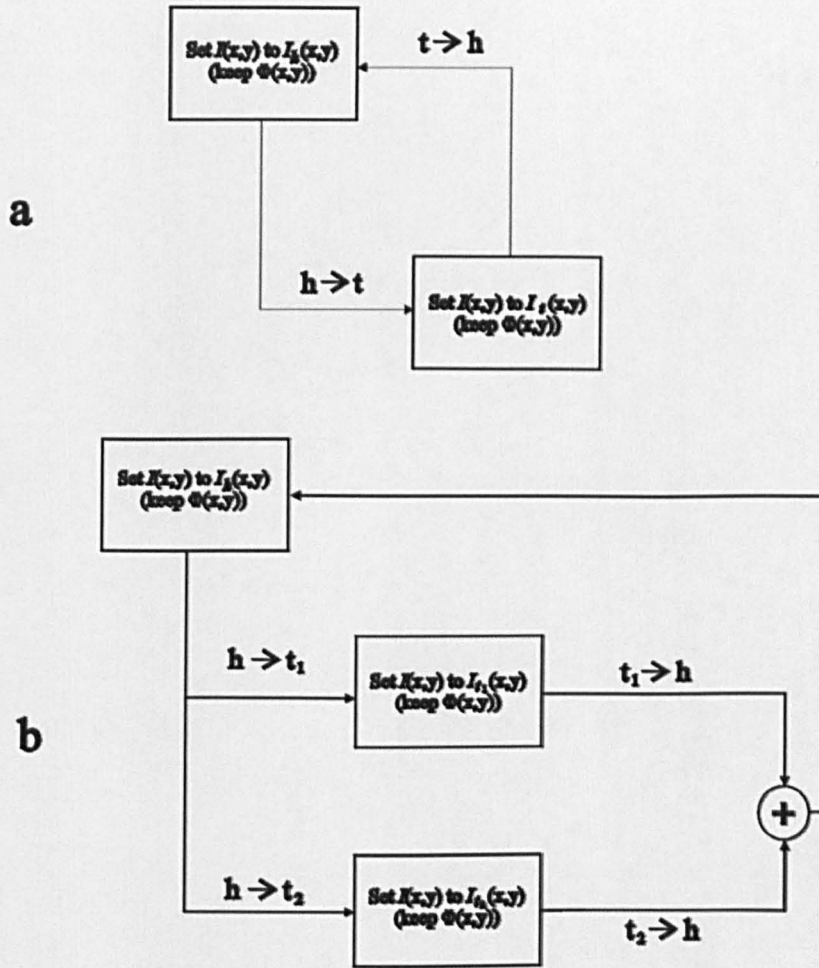


Figure 2.9: Schematic diagram of the Gerchberg-Saxton algorithm for a) single plane (2-D) geometries and b) multiple-plane (3-D) geometries. h is the plane of the hologram and t the target plane(s).

planes (t_1, t_2 , etc.). The intensities in different planes are unrelated and are combined before the inverse Fourier transformation of the beam back to hologram plane. As more bright spots are defined at different focal positions, and a greater number of planes are defined in the far field, the longer the algorithm takes to generate a hologram. When the convergence time of the algorithm becomes too slow to allow real-time manipulation of the spot patterns, the holograms can be saved as bitmap files. These bitmaps can be displayed in sequences, in the same manner the DBS hologram sequences are displayed by the SLM. Similarly to the DBS algorithm, the trajectories of the trap positions are specified in a spreadsheet file.

2.6 Spatial Light Modulators

SLMs are devices that can convert an electrical signal into a spatially modulated coherent optical signal [71]. SLMs are used to modulate the phase of the trapping laser beam, but can also be used to modulate amplitude or polarisation of light waves. SLMs have many uses (see reference [71] and references within), but in my work they are basically used to shape light beams, in particular laser beams. The reason I have used SLMs to modulate the phase of the trapping beam is the speed at which they work, allowing computer generated holograms to be displayed at video frame rates (20-60 Hz).

Many companies and academic institutes are now marketing SLMs to the communication industry (e.g. Boulder Nonlinear Systems, Holoeye Photonics AG, Hamamatsu Photonics (UK) Ltd). The two main types of SLM used are ferroelectric liquid crystal display devices and nematic liquid crystal devices, the latter was used in my research.

This section will explain the functionality of the different types of SLMs, highlighting the different materials and their properties used in the crystal displays, how SLMs work and details of the two makes of SLM I used in my research. Firstly, liquid crystals are described because they are an integral part of the SLMs used in my research.

2.6.1 Liquid Crystals

Liquid crystals are materials that can change their refractive index by controlling the orientation of their molecules [71]. Liquid crystals are birefringent, but do not have a fixed crystalline structure (Figure 2.10). The materials in the liquid crystal's phase are neither liquids nor solids, but something in between and the molecules comprising the crystals are free to move. It is this freedom in movement of the molecules that allows their refractive index to be controlled.

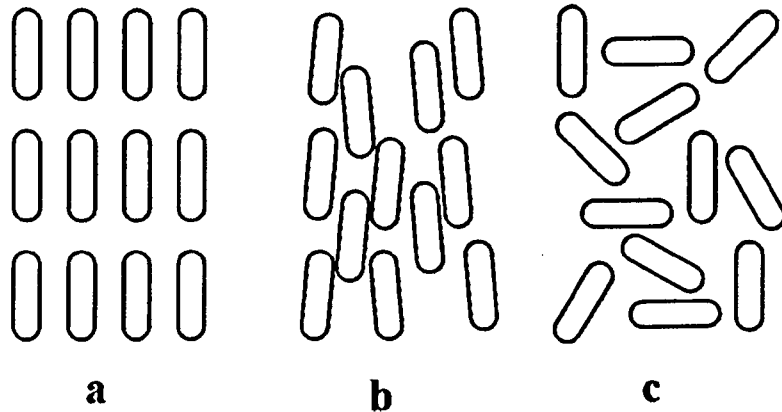


Figure 2.10: *Differences between the phases of a) solids, b) liquid crystals and c) liquids. The shapes indicate the orientations of the needle-like molecules.*

There are three types of liquid crystal used to make SLMs nematic, smectic and cholesteric liquid crystals (Figure 2.11). Here I represent the molecules as rod-like in structure, but disc-like molecules are also found in liquid crystal displays. The exact shape of the molecules is controlled by their molecular structure; most commonly being long-chained aromatic compounds, such as benzene, which gives the molecules their rod-like shapes. The benzene rings are connected by a linkage group and have terminal and side chains attached to them [72]. An example of a molecule chain is shown in figure 2.12.

Smectic liquid crystals form planar structured crystals and the molecules within each layer have the same alignment. This allows the crystals to have parallel orientated layers. Smectic liquid crystals have different compositions related to their chemical composition. The chemical composition of the smectic liquid crystals controls the properties of the liquid crystal. Smectic-C phase liquid crystal, referred to as ferroelectric liquid crystals

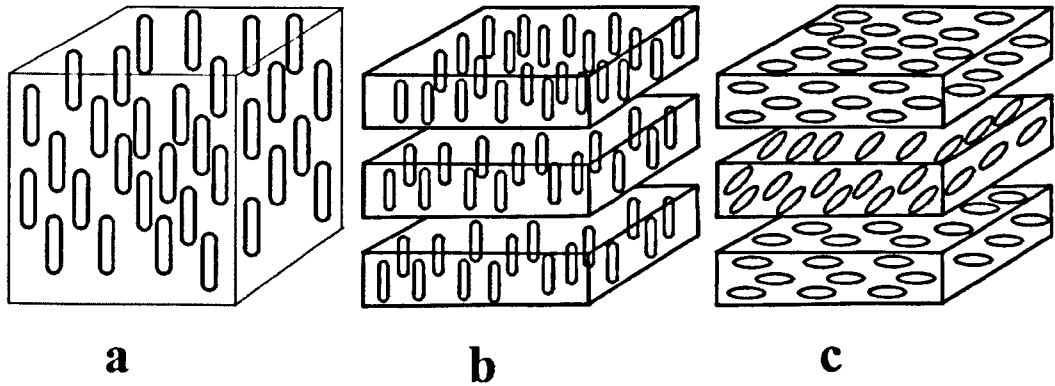


Figure 2.11: *Schematic representations of the alignment of molecules in a) nematic liquid crystals, b) smectic liquid crystals and c) cholesteric liquid crystals. The spacings between the layers for smectic and cholesteric crystals are exaggerated for clarity.*

are the most common type of smectic liquid crystal used in SLMs. Cholesteric liquid crystals are similar to both nematic and smectic liquid crystals. Early cholesteric liquid crystals were composed of cholesterol derivatives. Like smectic liquid crystals, they have layers and similar to nematic liquid crystals the molecules in each layer can rotate, but only by a fixed amount (Figure 2.11c). Nematic liquid crystals are the favored liquid crystal for SLMs. The nematic liquid crystal phase is characterized by molecules that have no positional order but tend to point in the same direction (Figure 2.11a).

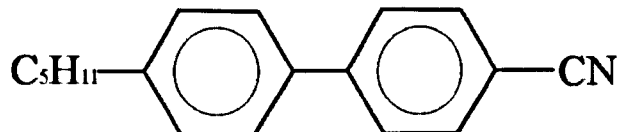


Figure 2.12: *An example of a molecule (5CB p-n-pentyl-p'-cyanobiphenyl) used in liquid crystal displays.*

To change the refractive index of a liquid crystal, its molecules have to be rotated. Rotation of the molecules is achieved by applying an electric field to the liquid crystal (Figure 2.13). The electric field is applied through conducting layers coating the inside faces of the cover glass/cell wall. Between the conducting layer and liquid crystal is a polished alignment layer, which serves the purpose of aligning the molecules in the correct orientation (Figure 2.13). An electric field interacts with permanent dipole molecules (e.g.

smectic liquid crystals) to align them along the direction of the field and induces a dipole in dielectric molecules (e.g. nematic liquid crystals). The orientation of smectic liquid crystals are controlled by a DC current and have only two orientation states possible for their molecules. Nematic liquid crystal cells are controlled by an AC current to prevent permanent changes to the liquid crystal material.

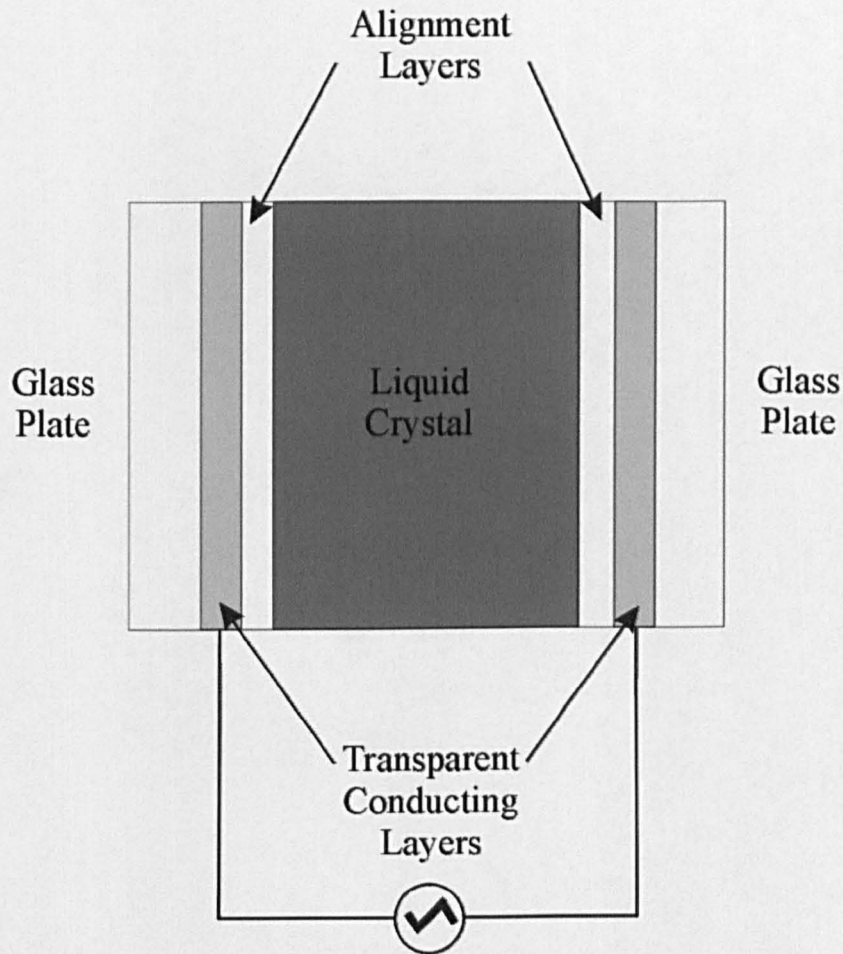


Figure 2.13: *Schematic representation of how a liquid crystal cell is controlled electrically.*

In my work all SLMs were reflective. When a light beam reflects off the SLM its phase is modified as it passes through the liquid crystal. By controlling the rotation of the molecules in the liquid crystal, its refractive index is changed and it is these changes that allow the phase of the light to be modulated. The phase modulation is proportional to the applied electric field [72].

2.6.2 How An SLM Works

In my research, only nematic liquid crystal SLMs were used. The two devices are described in the following two sections of this chapter. By changing the orientation of the needle-like molecules comprising the liquid crystal, the refractive index of the liquid crystal is changed. The change in refractive index occurs due to the birefringence of the molecules. The orientation of the molecules is controlled by the electric field applied across the liquid crystal.

2.6.3 Hamamatsu PAL-SLM X7665

The Hamamatsu PAL-SLM X7665 used is an optically addressed, non-pixelated, nematic liquid crystal device with an effective area of 20 mm by 20 mm on its front end. The front panel has a reflectivity of over 90 %. The photo of the unit used in my research is shown in Figure 2.14. The write light is projected (as a pixelated pattern with a resolution of approximately 700 by 800 pixels) on to the rear of the LCD unit, where it hits a photosensitive layer which controls the electric field across the liquid crystal layer, reorienting the liquid crystal molecules. This produces a change in the refractive index of the LCD and imparts a phase change in the laser light reflecting off the front face of the LCD.

This device is good for use in HOTs because the LCD is optimized for visible wavelengths (400 nm - 700 nm) and has a diffraction efficiency of over 40 % for the 1st diffraction order. Additionally, the unit connects to a computer through a standard VGA connection and acts as a second monitor to the computer, it can withstand in the order of 1 Watts of laser power per cm^2 , offers up to 2π phase modulation, displays images at video frame rates (in my use these are mainly 256 grey scale bitmaps of computer generated holograms) and is fully compatible with LabVIEW.

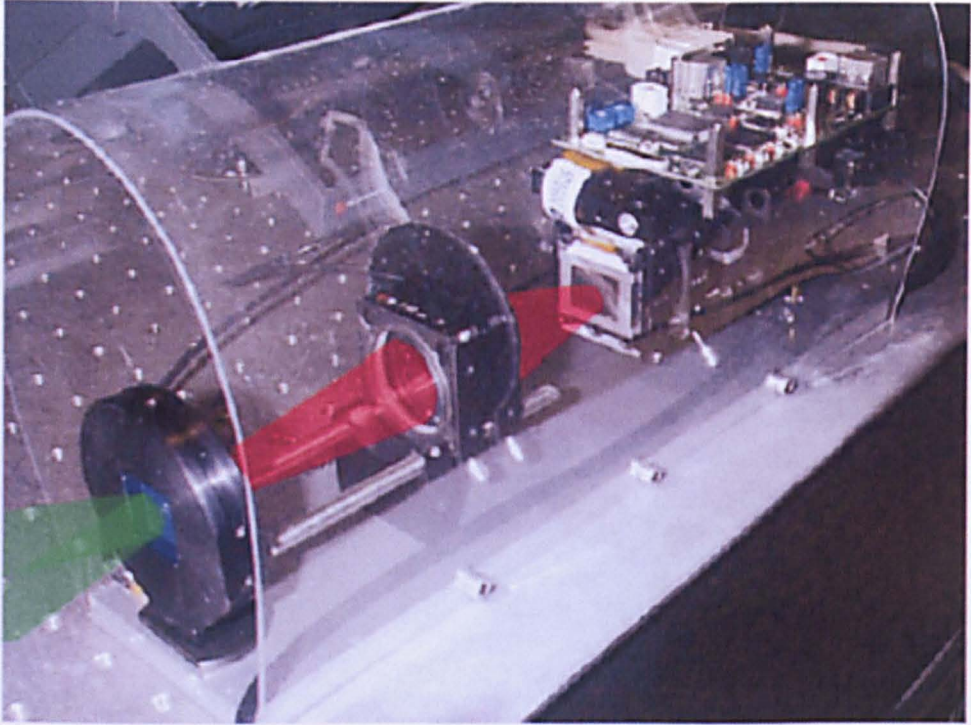


Figure 2.14: *Photo of the SLM based on the Hamamatsu PAL-SLM X7665 used in my research. The red beam represents the illumination of the back plane of the front end and the green beam represents the trapping laser beam.*

2.6.4 Holoeye LC-R 2500

The Holoeye LC-R 2500 SLM is an electrically addressed, pixellated device, with a resolution of 1024 by 768 pixels on an panel size of 19.5 mm by 14.6 mm. Unlike the PAL-SLM X7665 device, the LC-R 2500 does not have an optimized LCD and has varying efficiency values for the 1st diffraction order, for wavelengths of 400 nm - 700 nm. For our trapping wavelength of 532 nm, the efficiency was consistently over 40 %. An image of a unit is shown in figure 2.15. A limiting factor in the use of the LC-R 2500 in HOTs is the amount of power used in the trapping beam, which is limited to around 1 Watt per cm².

Similar to the PAL-SLM X7665 device, the LC-R 2500 gives 2π phase modulation, displays images at video frame rates, has a reflectivity greater than 90 %, is easily connected to a computer using DVI to display images at the 1024 by 768 pixel resolution, allows images

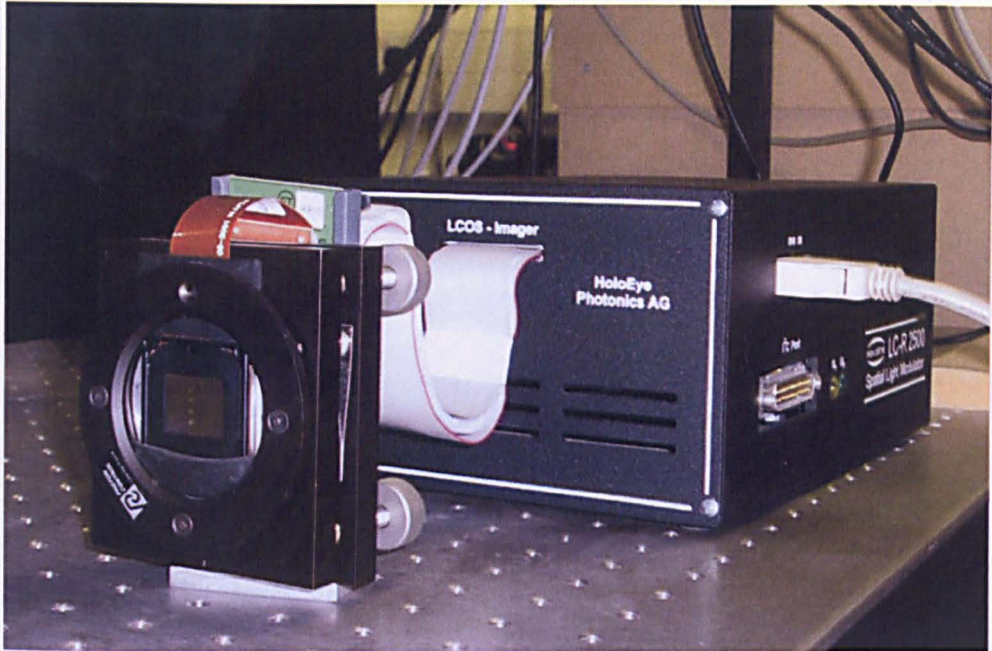


Figure 2.15: A photo of a LC-R 2500 unit, with the liquid crystal display held in an adjustable mirror mount.

to be displayed as 256 grey scale bitmaps and can easily be interfaced with LabVIEW. The greater display resolution of the LC-R 2500 gives a slightly larger trapping volume in HOTs compared to the PAL-SLM X7665 device and additionally, it can display images at a faster speed than the later.

Chapter 3

Trapping Limits of Holographic Optical Tweezers

3.1 Introduction

Holographic optical tweezers (HOTs) have revolutionized the field of application of optical tweezers [2]. By splitting a single laser beam into either a two-dimensional [53] or three-dimensional [1] arrangement of multiple optical traps, multiple objects can be trapped and manipulated. A spatial light modulator (SLM) makes the splitting of a single laser beam into many optical traps possible. Other techniques based on optical tweezers that can trap multiple particles exist [36, 73] and large numbers of particles can be trapped using a lensless optical trapping technique [74].

The ability to trap large arrays of particles is of interest to the optical tweezers community, especially HOTs users. In my case, I am interested in the size of arrays that can be trapped with HOTs. In reality, the limitations of the SLM and objective lens in the HOTs should limit the field of trapping to a finite volume. This chapter presents an experiment that was carried out to determine this volume. This experiment is a precursor to work described in later chapters, where patterns of trapped particles are presented.

3.2 Theory

In order to define a trapping volume for HOTs, the force an optical trap exerts on a trapped silica sphere was measured at a number of pre-defined positions within a volume. In addition, the dimensionless efficiency factor Q , was measured. The maximum possible force exerted on an object, based on the momentum flow of a light beam of power P is

$$F = Q Pn/c, \quad (3.1)$$

where n is the refractive index of the particle, c is the speed of light in a vacuum and Q is the dimensionless efficiency ratio between the measured force exerted on a trapped particle and the maximum possible force exerted on the particle [75, 76, 77]. Increasing the laser power will increase the strength of the optical trap. However, the magnitude of Q depends not only on the shape of the trapping beam; which is given by such factors as the degree of focussing and the extent of any aberrations in the optical components, but also the particle trapped (e.g. refractive index and size).

The method used to find the strength of the trap, was to measure the maximum velocity at which a trapped object can be translated in the optical trap before escaping [75]. This is the vectorial sum of the Stokes drag force (F_{drag}) and the force due to gravity (F_{grav}). The velocity of a moving sphere is used to find the force acting on the particle using the magnitude of the Stokes drag force,

$$F_{drag} = 6\pi\eta r v, \quad (3.2)$$

where η is the coefficient of viscosity, r is the radius of the trapped particle and v the speed of travel of the particle. The magnitude of the force due to gravity, also including the buoyancy, is

$$F_{grav} = V_s g(\rho_s - \rho_l), \quad (3.3)$$

where V_s is the volume of the solid, g is the acceleration due to gravity, ρ_s is the density of the particle and ρ_l is the density of the liquid.

3.3 Experimental Arrangement and Procedure

The experimental arrangement was based on a NA 1.3, $\times 100$, Zeiss Plan Neofluar oil immersion microscope objective used in an inverted geometry (Figure 3.1). The sample cell was mounted on a 3-axis PZT stage to control its spatial position. The trapping laser was a Casix frequency-doubled Nd:YVO₄ laser, supplying a 100mW beam with a wavelength of 532nm. Prior to entering the microscope, the laser beam was expanded and reflected off a computer-controlled SLM based on a Hamamatsu PAL-SLM X7665. The SLM is an optically addressed nematic liquid crystal with VGA resolution, a diffraction efficiency in the region of 40% and near video update rate. The plane of the SLM was imaged to the plane of the objective lens with a magnification of 0.44, such that the aperture of the modulator slightly overfilled the back aperture of the objective lens.

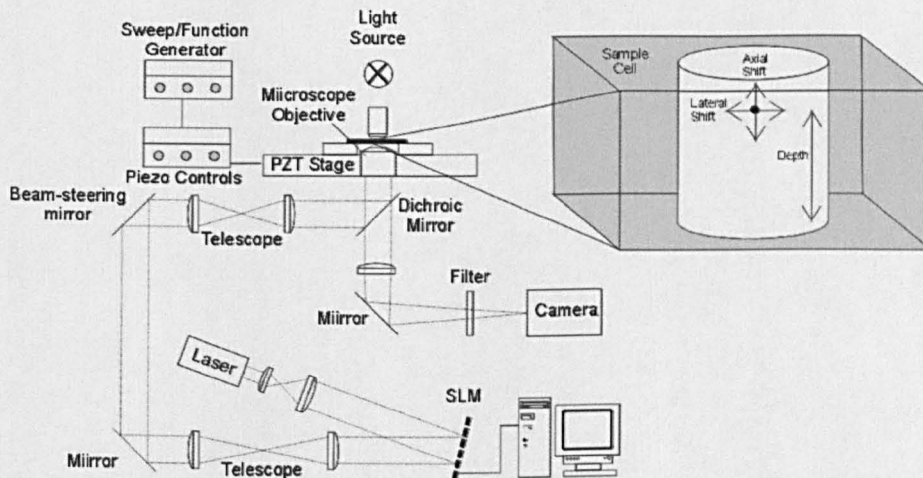


Figure 3.1: Schematic diagram of the experimental arrangement, with a close-up of the the sample cell details.

For this experiment, 2 μm diameter silica spheres were trapped in deionised water, 80 μm above the coverslip to minimise sample cell wall effects. The PZT stage was scanned back and forth with increasing frequency and the velocity at which the sphere escaped

was recorded. The frequency of the oscillations was controlled with a function generator, which input a triangular wave signal that controlled the PZT stage. The same sphere was then trapped at different lateral and axial displacements which defined a volume. Lateral displacements were controlled with the SLM and axial displacements controlled with both the z-axis of the PZT stage (z_1) and the SLM (z_2) (Figure 3.2). The measurement set was repeated several times with different spheres and the average trap forces and efficiencies were calculated.

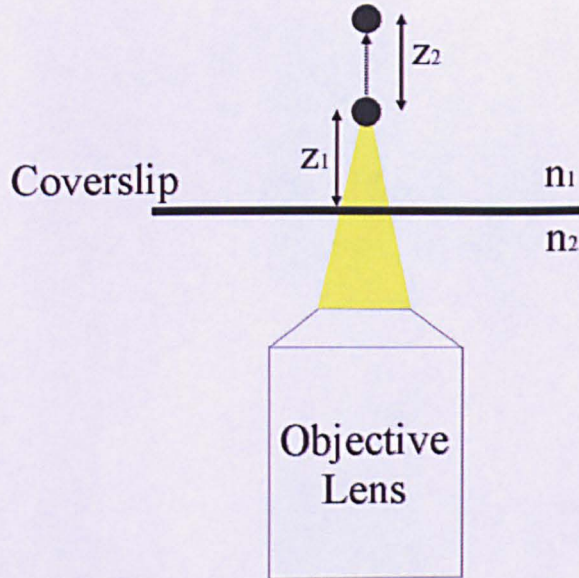


Figure 3.2: Schematic diagram of an objective lens and sample-cell, showing axial displacements introduced by the PZT stage (z_1) and the SLM ($n_1 z_1 + n_2 z_2$). n_1 is the refractive index of the immersion oil and n_2 the refractive index of the suspension liquid.

3.3.1 Calibration of Trap Displacement Using SLM

To ensure that the position of the trapped sphere was known accurately, the displacement of the trap in relation to the computer-generated hologram designed to give the desired displacement had to be calibrated. Three examples of holograms used to displace a trap are shown in figure 3.3.

To calibrate the trap displacement the number of lines per micron of movement was

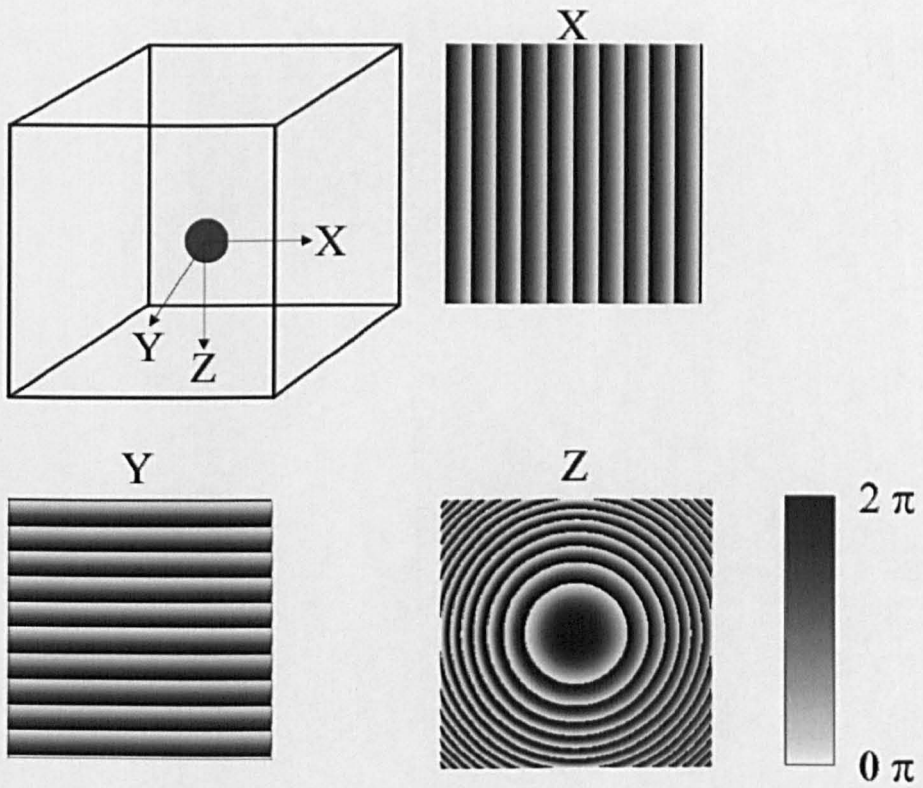


Figure 3.3: Schematic diagram showing three holograms used to move a trapped sphere to the correct positions in the pre-defined grid. The phase is represented as a greyscale.

determined to be 4 lines/ μm of trap displacement. This was then verified by noting the starting position of a trapped 2 μm sphere and then displacing it laterally or axially using a hologram and checking the movement with the PZT stage.

3.4 Results

The results are presented in two sections, respectively describing the force on the sphere and the efficiency of the trap. The results were collected by myself, with help from Pamela Jordan and Jonathan Leach.

3.4.1 Force Results

As a trapped sphere is moved, the total force acting on it is a vectorial sum of the Stoke's drag force and the gravitational force. The total force on spheres at the moment of escape, as a function of both the lateral and axial displacements of the trap positions, are shown in figure 3.4. These show the force of the trap is strongest nearer to the cover slip, where only small displacements of the optical trap (z_2) were introduced.

3.4.2 Efficiency of the Trap

The efficiency of the optical trap was measured over the same lateral and axial ranges of displacements, as shown in figure 3.4. Figure 3.5 shows the measured diffraction efficiency of the SLM; the ratio of the maximum power that can be placed in the +1st diffraction order and the power in the trapping beam measured at an intermediate beam waist prior to incidence with the SLM's front end. Losses in efficiency occur due to the beam reflecting off mirrors, transmission through lenses and the objective lens. The results of figure 3.4 and figure 3.5 are combined to give the efficiency, Q , of the tweezers trap (Figure 3.6). A 50% reduction in trap efficiency (Q value) defines an operating volume corresponding to a lateral range of $\pm 20 \mu\text{m}$ and an axial range of $\pm 25 \mu\text{m}$. Although an increase in laser power will produce a stronger trap, it will not improve the efficiency.

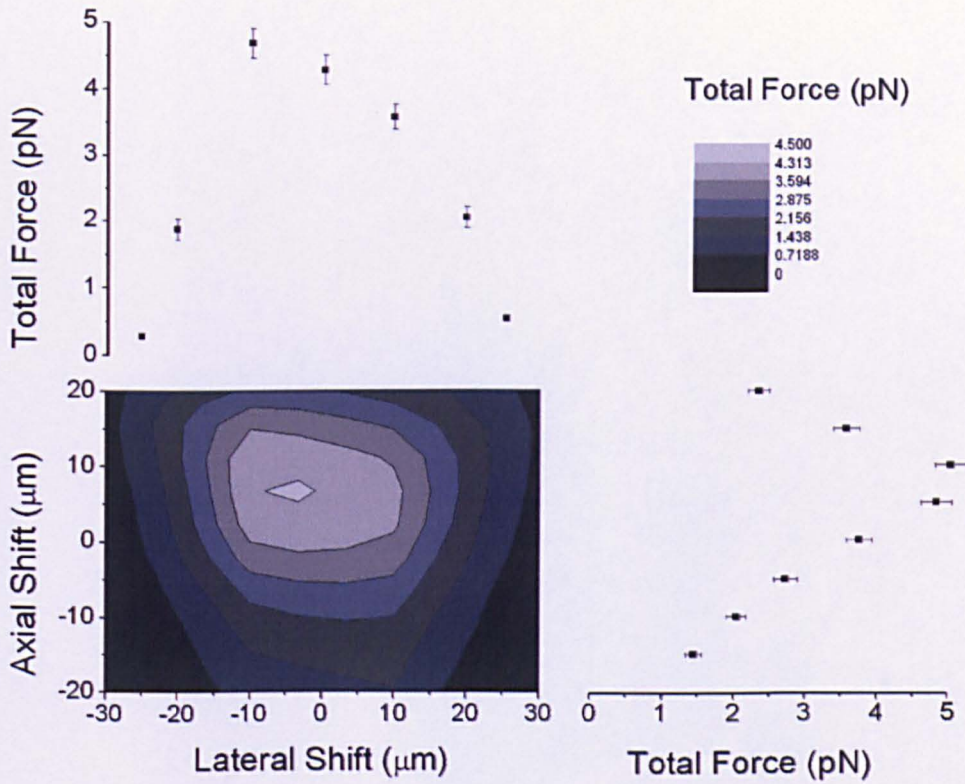


Figure 3.4: Total force acting on the trapped spheres for axial displacements (z_2) and lateral displacements introduced by the SLM. The starting position of the experiment was lifting the particle $80 \mu\text{m}$ above the coverslip. The cross-sections for a lateral shift of $-10 \mu\text{m}$ and an axial shift of $10 \mu\text{m}$ are shown.

The trapping of an object at different heights above the cover-slip can be achieved using combinations of piezo-settings and axial trap displacement. This results in varying trapping efficiencies. We note that in figure 3.6, the highest trapping efficiency occurs for a slightly positive axial displacement of the trap position, i.e. a displacement bringing the trap position back towards the cover-slip. This relationship was investigated by measuring the trap efficiency for a range of axial displacements introduced by the PZT stage and SLM at a fixed lateral displacement (Figure 3.7). For trapping about $5 \mu\text{m}$ above the cover-slip, optimum performance is achieved for zero axial displacement (z_1), i.e. the microscope objective lens is used at its design conjugates. As the trap position is moved deeper into the sample cell, where imaging aberrations are more significant, optimum trap

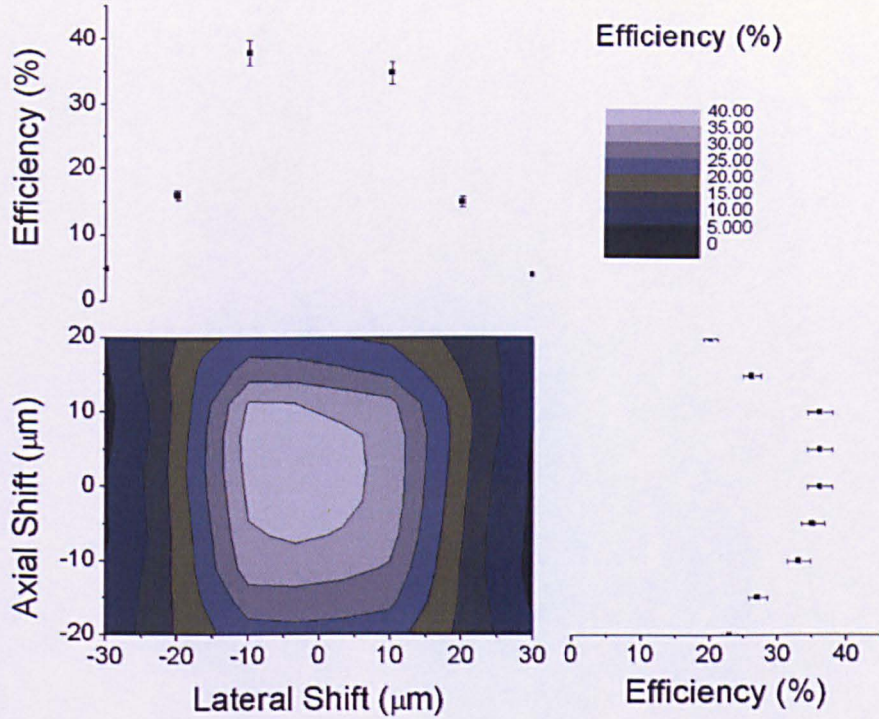


Figure 3.5: *Efficiency of the optical trap expressed as a ratio of the power in the trap to the total power in the trapping beam.*

performance is obtained by increasingly larger axial shifts introduced by the SLM (z_2). For example, if the aim is to trap an object $80\ \mu\text{m}$ above the cover slip, optimum trap performance is achieved using a piezo-setting of $92\ \mu\text{m}$ and a $12\ \mu\text{m}$ axial displacement back towards the cover slip introduced by the SLM.

3.5 Discussion

Lateral displacements of the optical trap were produced by displaying a linear phase ramp across the aperture of the SLM. When expressed as modulo 2π , this is a simple diffraction grating, blazed to maximize the power in the first diffraction order. Larger displacements require a higher spatial frequency on the modulator, displaying each grating period across

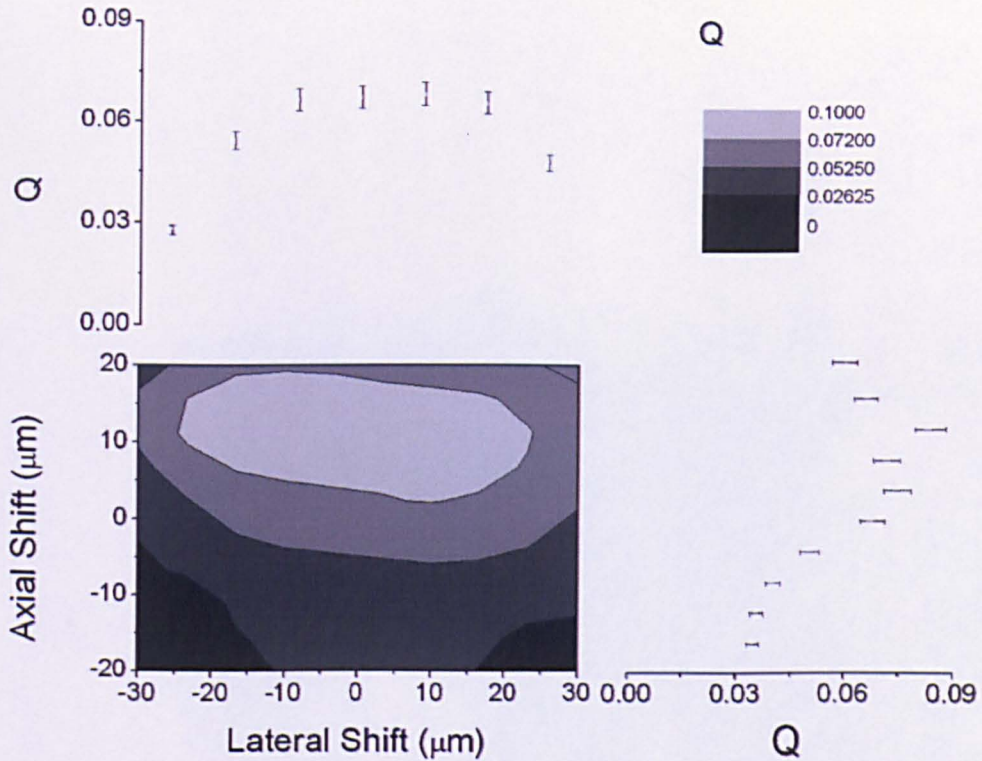


Figure 3.6: The trap efficiency (Q) plotted as a ratio between the measured escape force and the maximum possible force plotted against the lateral and axial displacements introduced with the SLM.

fewer pixels, giving reduced contrast and hence lower diffraction efficiency. Larger displacements maybe be achieved with future developments in SLM technology, such as a higher spatial resolution capable of utilizing the full field of view of a microscope objective. Higher resolution in an SLM could be more pixels, smaller pixels or a combination of these two. Changing the size of pixel would also have an influence on the efficiency of the optical trap. A decrease in pixel size would give an increase in trap efficiency over a larger area.

The other part of the experiment expanded trapping displacements in the axial plane. In the axial plane a reduction in efficiency was observed for displacements where the SLM efficiency is still high. This indicates axial displacement limits are not controlled by the

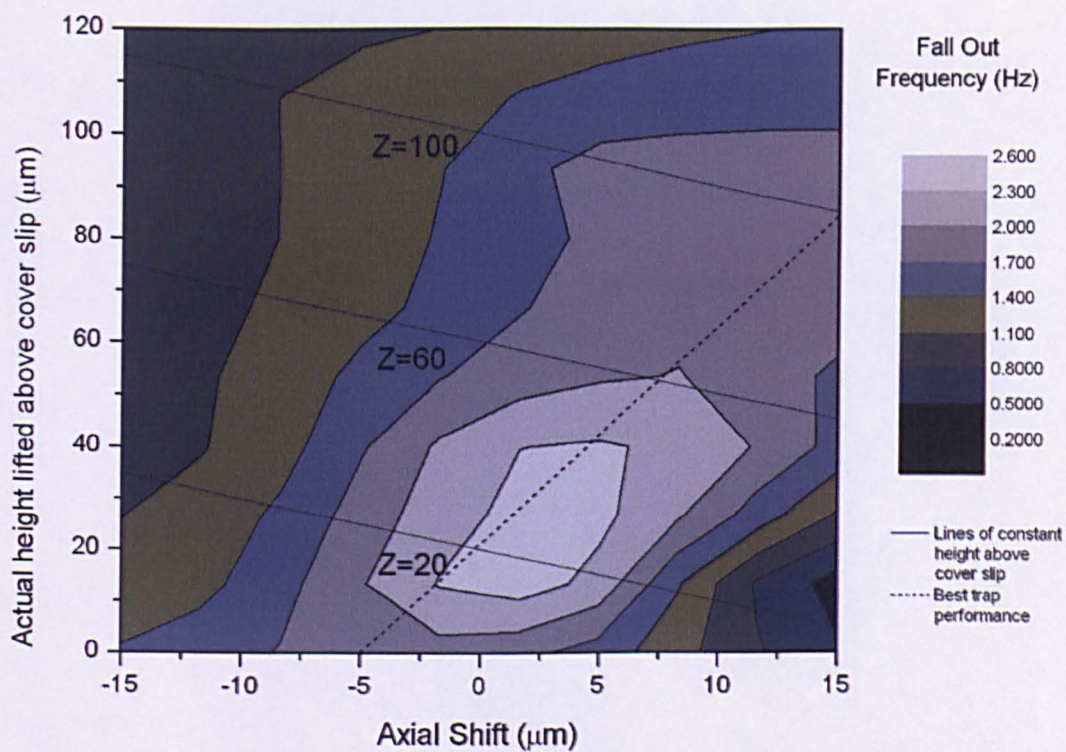


Figure 3.7: Frequencies at which spheres escaped the optical trap plotted against axial displacements introduced by both the PZT stage (y -axis) and SLM (x -axis).

SLM, but by the objective lens being used away from its designed conjugates. An axial displacement of the optical trap requires a Fresnel lens hologram displayed on the SLM, to change the trapping beam's wavefront curvature; again larger displacements require larger spatial frequencies, hence a lower diffraction efficiency. At even higher spatial frequencies, aliasing may result in the generation of additional foci and corresponding traps away from the beam axis [78]. Aliasing occurs when a pattern is displayed at too low a resolution. In the case of the phase hologram of a wedge, it changes the wedge angle. In the case of the phase hologram of a lens it creates an array of lenses (Figure 3.8).

Importantly, within the experimental configuration, the infinity corrected objective lens is used away from its design conjugates and degradation in both the imaging and trapping performance is observed. Techniques used to correct aberrations introduced by an objective lens include the use of deformable membrane mirrors [63, 79]. However, these techniques only have a limited range for wavefront correction. Potentially, the use of SLMs may correct for these aberrations, increasing the maximum range of axial displacement. Additionally, SLM technology has advanced since this experiment and with higher resolution units now available, better corrections of aberrations could be attained.

3.6 Conclusions

A range of lateral and axial displacements have been characterised for a Hamamatsu PAL-SLM X7665. It is shown that the maximum lateral displacement of the +1st diffraction order is $40\ \mu\text{m}$, limited by the spatial resolution of the SLM. In contrast, the maximum axial displacement of $50\ \mu\text{m}$ is limited by the performance of the microscope objective lens when it is used away from its design conjugates. In addition, we have shown that the performance of an optical tweezers for trapping objects deep within a sample cell may be improved by using an SLM to compensate for spherical aberrations. To correct for aberrations more precisely, further work needs to be carried out to gain better constraints of aberrations in the optics used in optical tweezers, including SLMs (e.g. curvature in planes of the liquid crystal displays).

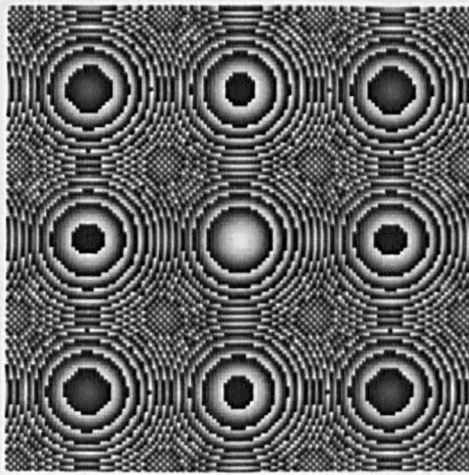


Figure 3.8: *An example of aliasing in an under-sampled lens hologram.*

Chapter 4

Hologram Design Algorithm Development

4.1 Introduction

Several different methods were used to design the computer generated holograms used in my experiments. Computer generated holograms have been in use for some time to shape light and continue to be used in novel experiments [80, 81]. In this work, computer generated holograms were used to split a single laser beam into many laser beams to allow multiple optical traps to be created. The different hologram design methods used to generate holograms used in these experiments are shown in figure 4.1. The different hologram design techniques were used because they are better at generating a specific type of pattern than other methods, for example the anti-blazing hologram design is very fast at designing symmetrical patterns of optical traps. In my research the direct-binary search (DBS) and modified Gerchberg-Saxton (GS) algorithms were mainly used to design holograms. However, common to all hologram design methods is placing as much of the light into the desired target plane spot pattern and minimizing the amount of light placed into unwanted orders which can weaken the optical traps.

The development of the hologram design algorithms was a two way process between the programmers (Dr. Johannes Courtial, Jonathan Leach and Dr. John Laczik) and the

experimentalists. My role in this process was the experimentalist, putting the hologram design algorithms into practice in the holographic optical tweezers (HOTs). This involved feedback to the programmers on problems encountered with the algorithms and suggestions for improving the algorithms. The following sections detail my role in the development of the DBS and GS algorithms, the two main algorithms used in my research.

4.2 Direct-Binary search Algorithm

The DBS algorithm was used to design the more complex holograms used in experiments detailed in chapters 5. The programming was carried out by Dr. John Laczik (Department of Engineering Science, University of Oxford), who has developed the algorithm over the last 5 years.

Initial trapping using holograms designed using the DBS algorithm was of a diamond structure. These holograms were static, the hologram produced a fixed array of optical traps in multiple layers (see chapter 5). The main problems in using a fixed hologram to trap multiple layer patterns of objects is filling each optical trap with one particle and filling the traps in order. To overcome these difficulties, it was proposed that a multiple layer structure be trapped starting from an initial simple geometry of trapped particles and manipulate them into their final position using a sequence of holograms. In the case of the DBS algorithm, the holograms used in a sequence have to be pre-generated before being displayed in a spatial light modulator (SLM). Designing the correct sequence of holograms was often a case of trial and error. When a sequence of holograms was unsuccessful, it was often due to traps being too close to each other or a trap being stronger than adjacent traps. Feedback allowed the correct sequence of holograms to be designed and the size of the structure to be optimized.

Inherent to the DBS algorithm is the number of iterations required to optimize the hologram design to produce the desired intensity pattern. The number of iterations controls the speed of hologram design. To speed up the process of hologram design, the number of iterations were limited to a given number, at which improvements in the hologram design were minimal. These small, but crucial, steps typically led to several hours of calculation

Hologram Design Algorithms	Advantages	Limitations	Work Done
Direct Binary Search	Widest range of patterns and planes	Many iterations Too slow to use interactively	Static diamond unit-cell and rotation of unit-cell
Modified Gerchberg-Saxton Algorithm	Few iterations allowing real-time dynamic holograms	Slows with number of planes and number of traps	Manual and automated manipulation of particles into complex geometries
Anti-blazing	Non-iterative and produces holograms quickly	Symmetrical patterns	Rotating and expanding cube

Figure 4.1: *Methods used to design the holograms used in my experiments.*

time being saved for a sequence of several hundred holograms.

4.3 Modified Gerchberg-Saxton Algorithm

Most experiments carried out in this work have involved the use of the modified GS algorithm to design holograms. The modified GS algorithm requires fewer iterations than the DBS algorithm and is therefore faster at converging to the desired hologram. This makes the modified GS algorithm more suitable for generating sequences of holograms in real-time.

Initially the modified GS algorithm was applied in our HOTs to design simple holograms, that allowed particles to be trapped in two dimensional patterns and was then extended to three dimensional patterns. The speed of the algorithm was found to be very high, converging in less than a second. The speed of convergence allowed trap positions to be controlled interactively and cursor controls were introduced, giving keyboard input control of trap position, while particles were trapped. This gave both two and three dimensional control over trap positions. However, manipulating particles using keyboard inputs was limited by the calculation speed of the algorithm, which could not cope with more than 3 inputs a second. When more than 3 inputs were entered, the movement of the trap was jerky and trapped particles were easily lost. The solution was to remove keyboard inputs from the manipulation process. This was achieved in two ways, firstly by pre-generating hologram sequences (that achieved manipulation of trapped particles in two and three dimensions) and displaying the saved holograms in a similar way to the DBS hologram sequences. Secondly, by specifying trap locations in a spreadsheet file and importing the file into the modified GS algorithm interface, sequences of holograms were generated in real-time. The latter was suitable for many applications. By extending the spreadsheet to a three dimensional coordinate system, it was possible to generate fully three dimensional patterns of particles, by manipulating them from initial two dimensional patterns. The time taken to complete these manipulation sequences was a few minutes. The time taken to obtain the correct trajectories of traps in the sequences (e.g. traps did not collide or move too close to each other), using a spreadsheet file was on average a day.

4.4 Hologram Offset

Common to all holograms designed with the DBS and modified GS algorithms is the zeroth diffraction order. Typically the diffraction efficiency of the SLMs used in these experiments is around 40 percent, meaning 40 percent of the trapping laser power is diffracted into the +1st diffraction order. This leaves up to 50 percent of the laser power in the zeroth diffraction order and the remaining 10 percent in other orders. To remove the influence of the zeroth diffraction order, a hologram that offset the +1st diffraction order from the zeroth diffraction order, was added to the holograms used to trap patterns of particles. This allowed the patterns of trapped particles to be removed from any influence of the zeroth diffraction order.

Often a pattern of trapped particles was difficult to visualise because several particles were on top of each other or in layers within a multiple layer geometry. To aid visualisation, an axial offset could be introduced to the structure by adding a Fresnel lens hologram to the SLM.

Related to the hologram offset is the reduction in trap efficiency as the distance between the traps and the zeroth diffraction order is increased. Although this is only a trivial problem for relatively simple two dimensional patterns of trapped particles, it is a significant problem associated with trapping large patterns of particles. This highlights that the hologram offset is limited by the trap strength and also by the trapping volume specified in chapter 3.

4.5 Summary

In summary, the development of the modified GS algorithm and to a lesser extent DBS algorithm, were advanced as a result of the feedback from experiments. Most significantly, reduction in the time to design holograms was achieved. Also, by experimenting with different paths to manipulate particles into patterns, the development of the modified GS algorithm was aided, transforming its application from initially designing static holograms

to generating hologram sequences capable of manipulating particles into three dimensional patterns. Additionally, the experimentation and development of algorithms has aided the optics group's understanding of computer-generated holograms, leading to constructive talks with other researchers, for example Dr. Jennifer Curtis, University of Heidelberg, Germany.

Chapter 5

Two and Three Dimensional Arrays Trapped Using Holographic Optical Tweezers

5.1 Introduction

The ability to trap multiple objects with optical tweezers is not new to holographic optical tweezers (HOTs). Many workers have used various trapping techniques to create arrays of particles, ranging from a few to several hundred particles. Scanning a single beam rapidly can trap multiple objects by time sharing the trap [36, 60]. This technique is simple, but limited by the scanning speed and the range to which the scanning mirror can divert the trap. A commonly used technique in recent years to create multiple traps is shaping the trapping beam with a hologram. Holograms are used to split a single laser beam into many laser beams, each capable of trapping an object [1]. HOTs have many advantages over the other trapping techniques mentioned above. HOTs in theory can create an unlimited number of traps within the spatial limits of the spatial light modulator (SLM) used in the HOTs, not only in a two dimensional array, but also in three dimensional arrays.

Being able to trap objects in two and three dimensional static patterns is one applica-

tion of optical tweezers. Another application of optical tweezers is the manipulation of trapped objects. Early techniques for manipulation of particles with optical tweezers involved beam-steering mirrors, scanning mirrors [34] and galvo-mirrors [36]. These early techniques were limited to manipulating trapped particles in a two dimensional plane, the object plane of the microscope objective lens. Trapping and manipulation of particles in a fully three dimensional volume was realised with the use of deformable mirrors [63] and HOTs [54], both of which can shape the wavefront curvature of the trapping laser beam.

The ability to trap objects in a three dimensional array or pattern is of great interest. Early experiments conducted during my research created several three dimensional patterns of trapped objects, resembling crystal geometries. Another set of results built upon the results from the static holograms and showed the evolution of the automated manipulation of particles, mainly using the DBS and GS algorithms. In the case of the GS algorithm, the aim was to produce holograms in real-time to manipulate particles along specified trajectories. The DBS algorithm was used to calculate sequences of holograms to manipulate particles. These results are presented in this chapter, along with the different hologram design methods used to generate the holograms.

5.2 Hologram Design Algorithms

The holograms used to create the patterns of optical traps required to trap objects were designed using three techniques. The first two (direct-binary-search and modified Gerchberg-Saxton algorithms) are discussed in detail in the previous chapters. The third method used to design holograms was designed by Dr. Johannes Courtial and uses a combination of blazed grating and Fresnel lens holograms, referred to as the anti-blazing hologram design technique in chapter 4. This is discussed below.

5.2.1 Anti-blazing Holograms

The anti-blazing hologram design technique was used to generate an array of eight traps. The first step splits a single beam in two by introducing a blazed wedge hologram (binary

hologram), producing a trap in both the +1st and -1st diffraction orders. A second binary hologram splits these two traps in two, producing four traps, each at the corner of a square in a single plane. Finally, each trap in the square is split in two by introducing another binary hologram, resulting in eight traps positioned at the corners of a cube (Figure 5.1). The calculation period for these symmetrical patterns of traps is less than a second, for holograms with a 256 by 256 pixel resolution, allowing the holograms to be calculated in real-time. In addition to the speed of the hologram design, the whole structure can be rotated around any arbitrary axis. The overall actual efficiency is high using this hologram design method because the power in both the +ve and -ve first diffraction orders is used. This has an advantage over the DBS and GS algorithms, which use only the power in the +1 diffraction order.

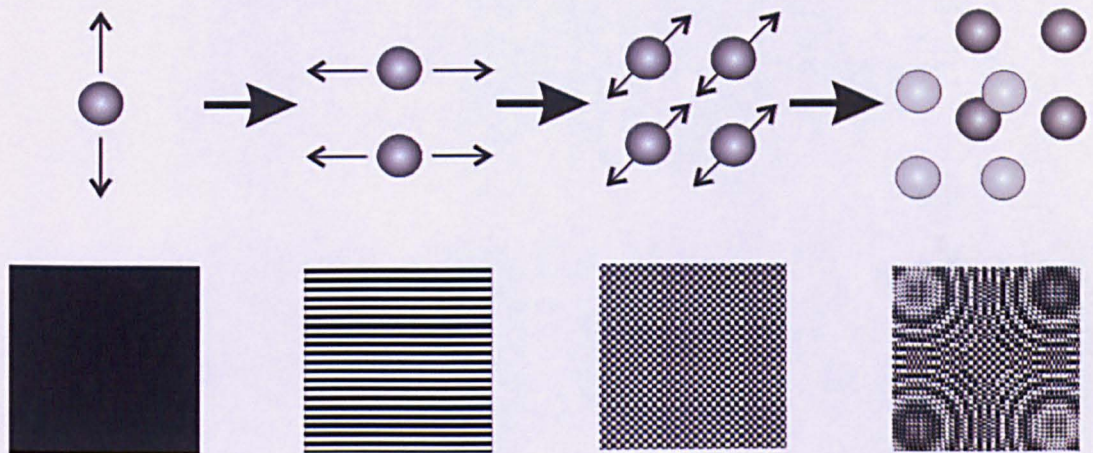


Figure 5.1: *Schematic representation of the formation of a cube structure. The spheres represent the positions in which the trapped particles are held and the bitmaps are of the corresponding holograms required to produce the trap arrangements above.*

5.2.2 Generation and Display of Hologram Sequences

Hologram sequences used to manipulate particles were designed using both the DBS and modified GS algorithms and in real-time using the modified GS algorithm. Initially, the modified GS algorithm was used to pre-generate sequences of holograms, which was a time consuming process because the coordinates of the optical traps were input manually for each hologram. The DBS algorithm has to pre-generate hologram sequences because

of the slow speed of the algorithm design. The DBS algorithm uses a spreadsheet to specify the initial, intermediate and final trap positions. These hologram sequences were displayed in the SLM using a LabVIEW interface (Figure 5.2).

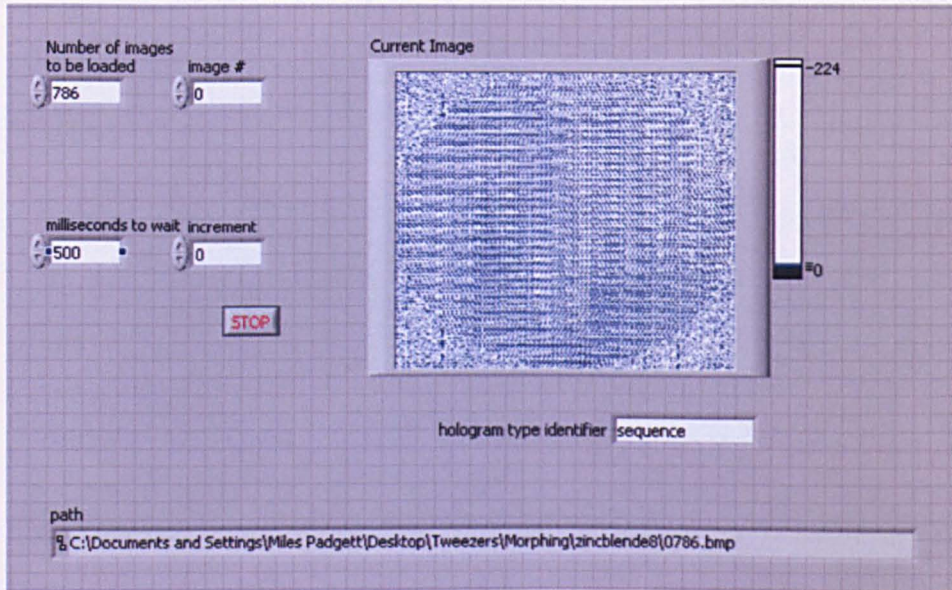


Figure 5.2: *The LabVIEW interface into which bitmap files were imported and displayed as sequences. The holograms were designed with both DBS and GS algorithms. The bitmap displayed is an example of a hologram designed using the DBS algorithm.*

To reduce the time taken to design sequences of holograms using the modified GS algorithm, a spreadsheet facility similar to the DBS algorithm, was incorporated into the hologram design process (Figure 5.3). The coordinates of the trap positions and time taken to move from one trap position to another are specified in a spreadsheet file, which is imported into a LabVIEW interface (Figure 5.4). The program calculates a sequence of holograms using the initial, interpolated intermediate and final trap positions (i.e. predefined trajectories) over a specified number of time steps. The user defines the rate at which holograms are displayed on the SLM. In addition to the above features of the program, a linear scaling factor is included to reduce or increase the separation of trap positions during or prior to generating the hologram sequence.

Name	time	x	y	z	stationary?
Bead 1	0	-8	8	0	TRUE
Bead 1	50	-5	5	0	TRUE
Bead 1	100	-3	-3	0	TRUE
Bead 1	150	5	-5	0	TRUE
Bead 1	200	8	-8	0	TRUE
Bead 1	250	5	-5	0	TRUE
Bead 1	300	3	3	0	TRUE
Bead 4	200	-8	8	0	TRUE
Bead 4	250	5	5	0	TRUE
Bead 4	300	-3	-3	0	TRUE

Figure 5.3: An example of a spreadsheet file used to specify trap positions.

5.2.3 Experimental Arrangement and Procedure

A typical experimental arrangement is shown in figure 5.5, similar to that described in Chapter 3. The trapping beam is focused tightly through a NA 1.3, 100, Zeiss Plan Neofluar oil immersion microscope objective used in an inverted geometry. Initial experiments involving the cube structure (see results section) were carried out using a 100mW 532 nm trapping laser beam and a computer-controlled SLM based on a Hamamatsu PAL-SLM X7665.

The experimental arrangement was then changed to include a 1.5W 532 nm trapping laser beam and an electronically addressed Holoeye LC-R 2500 SLM. The increased laser power was required to increase the number of trapped particles and allowed more than 8 particles to be trapped. All holograms generated with the modified GS and DBS algorithms were displayed with the optical traps displaced in relation to the zeroth order, to remove the influence of the zeroth diffraction order.

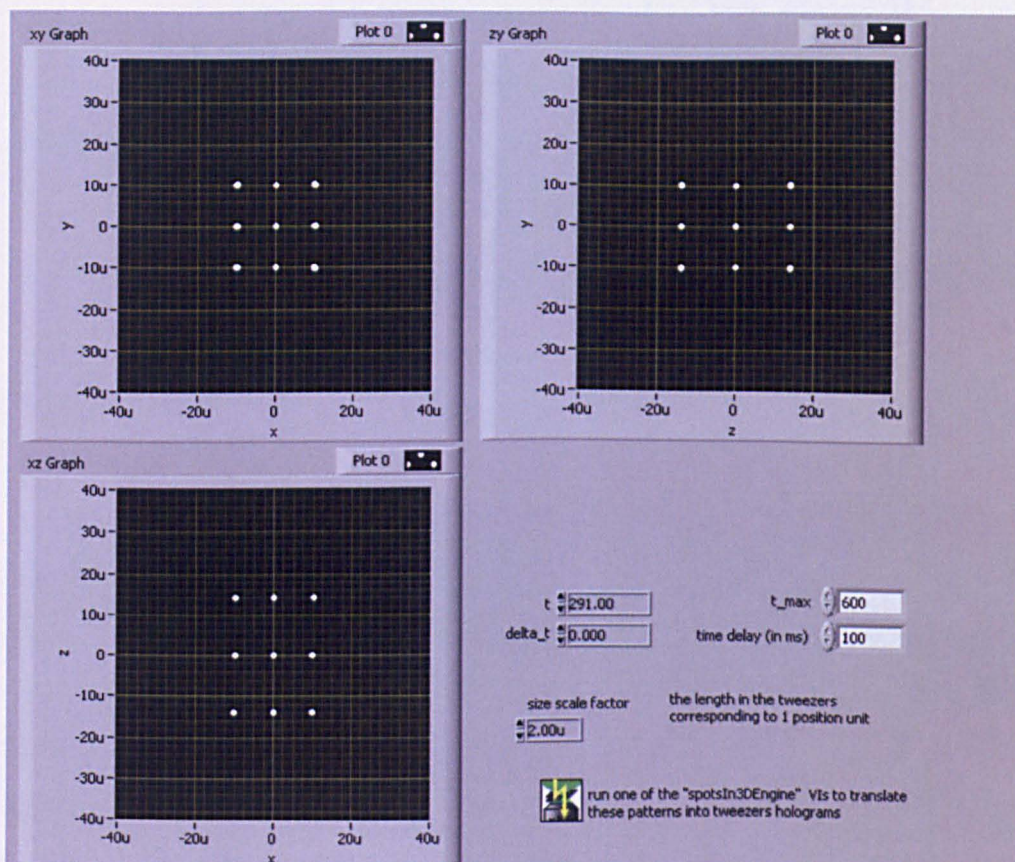


Figure 5.4: The LabVIEW interface into which spreadsheet files were imported and hologram sequences designed with the GS algorithm. The figure shows 27 trap positions in 3 separate planes (see figure 5.12 for a full explanation of the trapped structure).

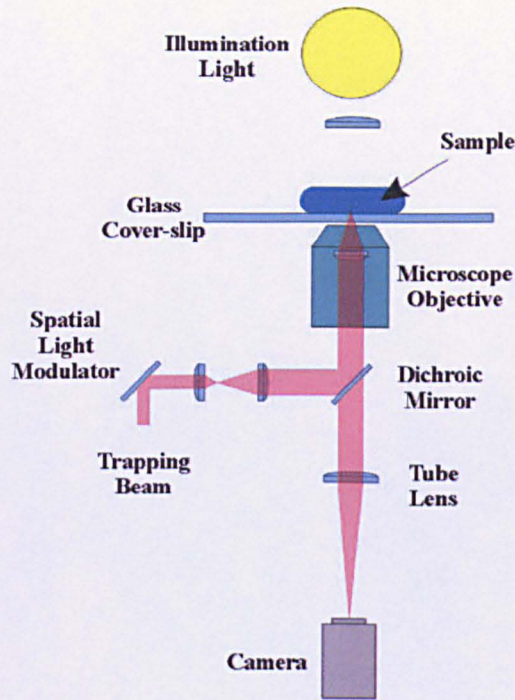


Figure 5.5: *Schematic representation of an holographic optical tweezers arrangement.*

5.3 Results

The results presented here are representative of the the various structures I created, using holograms designed by myself and by Dr. Laczik. The results are split into three sections; crystal-like structures, two dimensional manipulation and three dimensional manipulation.

5.3.1 Crystal-Like Structures

Two results of crystal-like structures are presented in this section. Other crystal-like structures were trapped and presented in [82]. The first result is termed the “dancing cube”, formed by trapping eight $2\ \mu\text{m}$ diameter silica spheres. The dancing cube result is shown as two separate sequences (Figure 5.6), firstly as a cube rotating around its three principle axes and secondly as an expanding cube. Although shown as two separate results (Figure 5.6), the cube can be rotated and changed in size at the same time. Rotation is shown around the principle axes of the cube (Figure 5.6). However, in theory, the rotation

axes can be completely arbitrary. The images shown in Figure 5.6 were obtained using a 100 mW 532 nm trapping laser and a SLM based on a Hamamatsu PAL-SLM X7665.

The size of the cube unit cell is limited by three factors; the size of the spheres, power of the trapping laser and the resolution of the SLM. For the cube structure, the maximum size of a cube obtained was a 20 μm unit cells, using a 1.5 Watt 532 nm trapping laser and Holoeye LC-R 2500 SLM. With the increased laser power and higher resolution of the Holoeye LC-R 2500 SLM, the maximum size of the cube unit cell was increased by 5 μm , compared to the previous experimental arrangement.

Another result, obtained from a hologram designed by Dr. Lazcik using his DBS algorithm, is a diamond unit cell (Figure 5.7). However, the experiment using this hologram was performed by myself. This crystal structure is more complicated and contains elements of many crystal systems (e.g. cubic, body-centered, face-centered). In addition to the more complicated crystal structure, the diamond contains eighteen 2 μm diameter silica spheres trapped in five different layers, to form a unit cell. The unit cell size of 12 μm was the smallest size trapped. Unit cells less than 12 μm in size could not be trapped because trapped spheres were pulled into the layer above as the structure was filled. To eliminate the influence of the zeroth diffraction order, the whole structure was offset in the lateral plane. The layers of the unit cell were imaged by introducing an axial offset, allowing each layer to be imaged in the plane of the objective lens.

5.3.2 Two Dimensional Manipulation

The trapping of complex structures of particles in two dimensional patterns can be time consuming. To make the trapping of complex patterns easier particles were trapped in simple arrays and manipulated into the desired pattern. The first example used a pre-calculated sequence of holograms to manipulate four traps to form a square (Figure 5.8) shows that this is a viable manipulation technique. For each hologram, the position of each trap was input manually. This technique was used to generate both 2-D (Figure 5.8) and 3-D morphing sequences (see later).

The sequence shown in Figure 5.8 contains 66 individual holograms. With a display rate

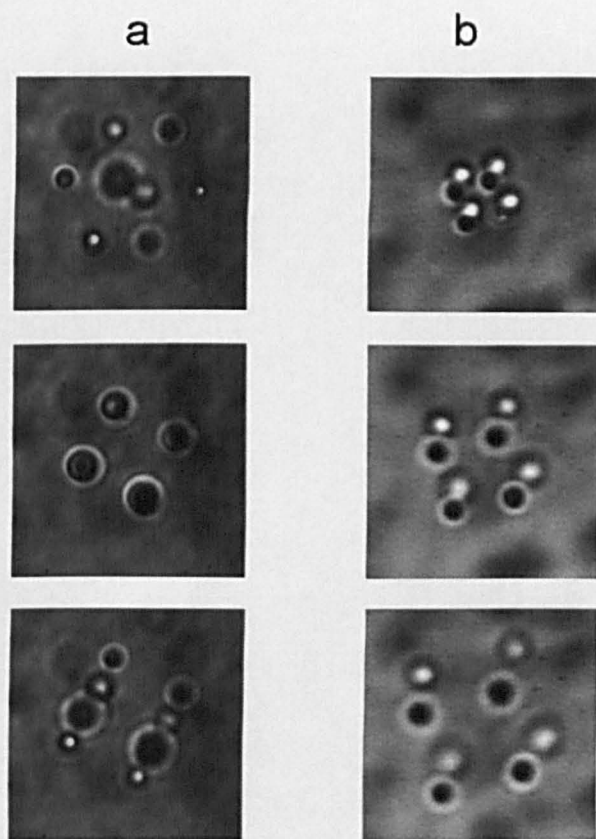


Figure 5.6: *Two sequences of frames showing the versatility of the anti-blazing technique; a) a rotating 8 μm cubic unit cell formed from eight 2 μm diameter silica spheres and b) the same cube structure being expanded from a unit cell size of 5 μm to a unit cell size of 10 μm .*

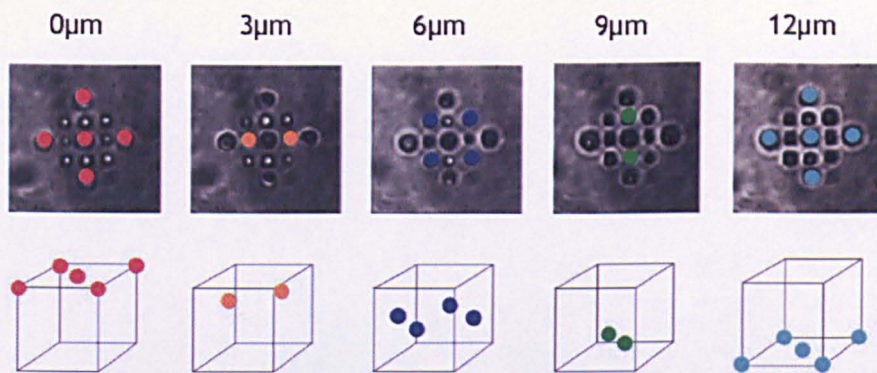


Figure 5.7: Frames showing eighteen $2\ \mu\text{m}$ diameter silica spheres trapped in the different planes of a $12\ \mu\text{m}$ diamond unit cells.



Figure 5.8: An example of a pre-generated hologram sequence designed with the GS algorithm, that manipulates four $2\ \mu\text{m}$ diameter silica spheres morphed from a line into a square.

of up to 5 holograms a second, this sequences took about 10-12 seconds to complete one morphing cycle. The number of holograms required for a morphing sequence depends upon the distance a trapped particle is manipulated and the diameter of the particle. To prevent spheres being lost from an optical trap, the distance a trapped object was moved between two successive holograms was limited to a sphere's radius (e.g. $1\ \mu\text{m}$ in the example shown). Movement of more than a sphere's radius produced jerks and spheres regularly dropped out of their traps.

Pre-generating the holograms is a slow process. To speed up the hologram calculation a facility was introduced to the modified GS algorithm in LabVIEW by Dr. Courtial allowing the x and y coordinates of each trap to be specified as starting, intermediate and final positions. One result, of many, obtained by myself from this trapping technique is a representation of a Scottish dance called Strip-the-Willow (Figure 5.9).

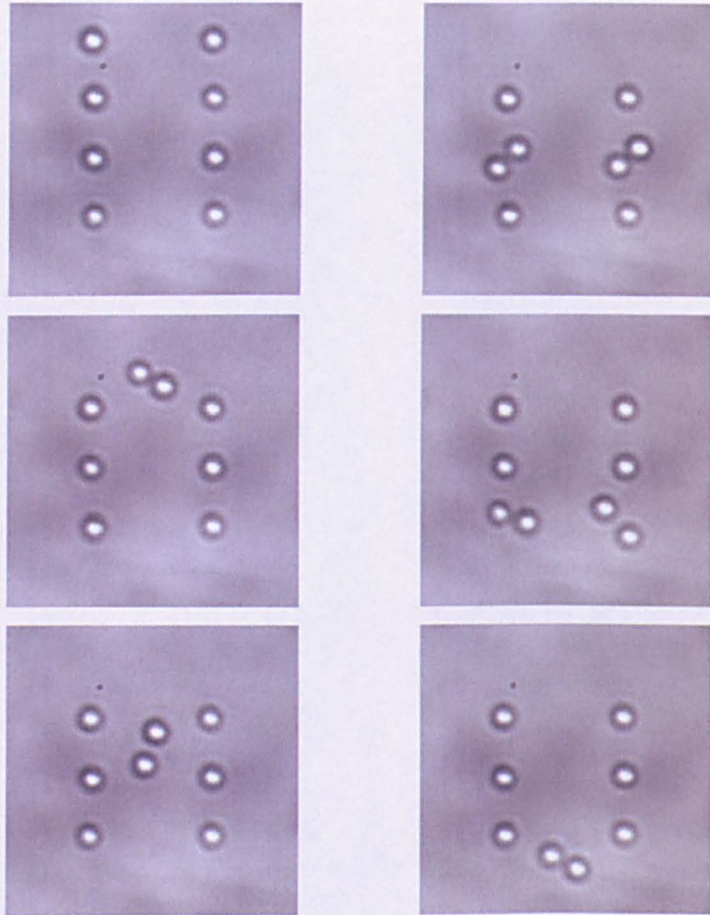


Figure 5.9: A sequence of frames showing eight $2\ \mu\text{m}$ diameter silica spheres being manipulated to represent a Strip-the-Willow dance.

The Strip-the-Willow sequence displayed over 900 holograms at a rate of 3 per second, taking about 5 minutes to complete one loop of the whole sequence. After initially filling each trap in the initial trap geometry, the user has no interaction with the control of the manipulation process and just hits the go key on the computer, leaving the LabVIEW interface to control the trap positions. Although the Strip-the-Willow manipulation sequence has no specific application in mind, it does show the manipulation a greater number of particles and more complex manipulation trajectories.

5.3.3 Three Dimensional Manipulation

The final section of results presents three dimensional morphing of trapped particles. Most of these results were obtained with the modified GS algorithm LabVIEW interface, with a spreadsheet specifying the positions of the optical traps as x, y and z coordinates. The rest of the results were obtained from pre-calculated hologram sequences, generated by Dr. Lazcik, using his DBS algorithm. All these experimental results were obtained by myself.

Initial three dimensional manipulation of six $2\ \mu\text{m}$ diameter silica particles was carried out using pre-calculated sequences of 120 holograms generated using the modified GS algorithm (Figure 5.10). The whole morphing sequence was completed in around 24 seconds.



Figure 5.10: A sequence of frames showing six $2\ \mu\text{m}$ diameter silica spheres being manipulated from two lines of three in a single plane to two triangles in separate planes.

The next two results are shown in Figures 5.11 and 5.12, produced from the automated manipulation of trapped $1\ \mu\text{m}$ diameter silica spheres. The positions of the initial trap geometry, intermediate positions and final trap positions were specified in a spreadsheet

file similar to that shown in figure 5.3.

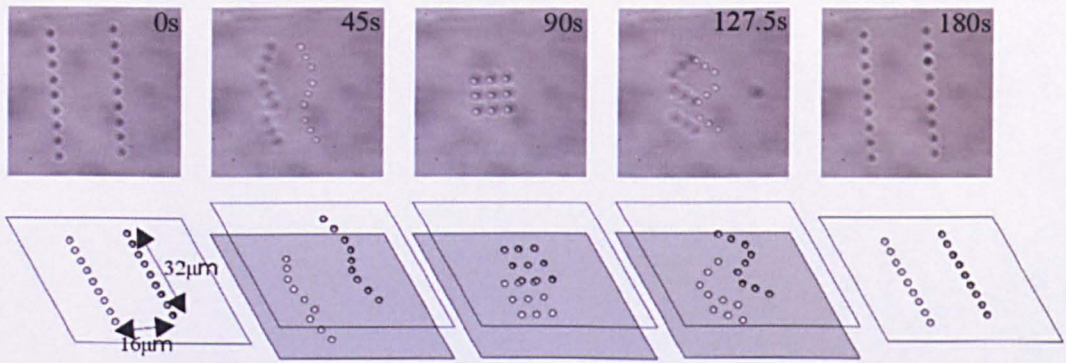


Figure 5.11: A sequence of frames showing eighteen $1\ \mu\text{m}$ diameter silica spheres morphed in real-time to form two layers separated by $8\ \mu\text{m}$. The spheres in each layer form a square $8\ \mu\text{m}$ by $8\ \mu\text{m}$. The times shown in the top left hand corners of the frames, indicate the length of the sequence.

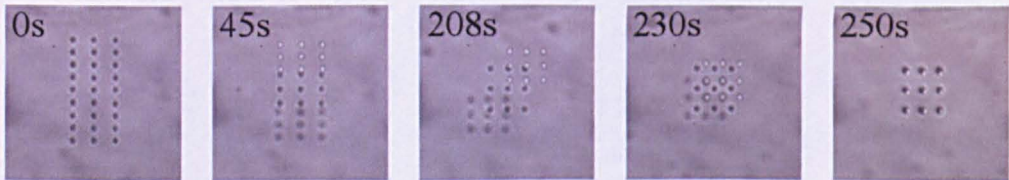


Figure 5.12: A sequence of frames showing twenty-seven $1\ \mu\text{m}$ diameter silica spheres morphed in real-time to form an extended cubic structure. Spacing between two adjacent layers is $8\ \mu\text{m}$ and the spheres in each layer form a square $8\ \mu\text{m}$ by $8\ \mu\text{m}$. The times shown in the top left hand corners of the frames, indicate the length of the sequence.

Similar to the Strip-the-Willow result (Figure 5.9), the holograms are calculated and displayed at a rate of three per second. These two sequences trap larger numbers of particles and also demonstrate that multiple traps can be positioned above each other in a line. They also represent extensions of the cubic unit cell shown in Figure 5.6.

The final two results in this chapter are a diamond unit cell and zinblende unit cell are shown in Figures 5.13 and 5.14. Both results were produced from the same sequence of holograms, designed using the DBS algorithm. Similar to the hologram sequences designed using the modified GS algorithm, the starting positions of the trapped spheres is a simple geometry in a single plane. The number of hologram sequences used to morph the

diamond and zinblende unit cells was 1500 individual holograms. The diamond structure was morphed from start to finish over a period of 9 minutes, a hologram display rate of 3 holograms a second. The hologram display rate for the zinblende unit cells was initially 5 per second up to the start of rotation of the trapped structure and then reduced to 2 per second for the rotation of the structure.

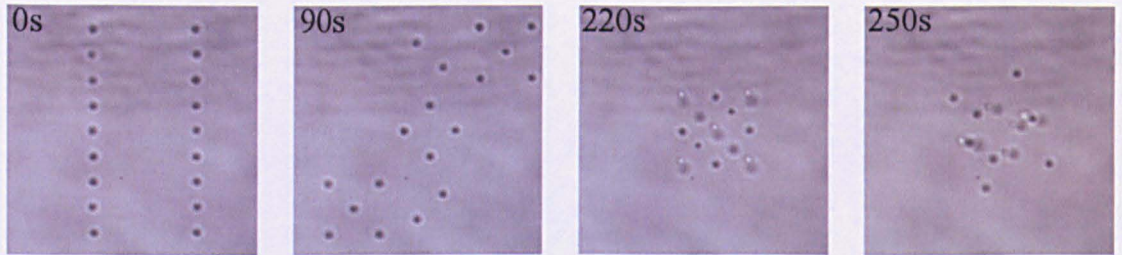


Figure 5.13: A pre-generated hologram sequence designed with the DBS algorithm used to trap eighteen $1\ \mu\text{m}$ diameter silica spheres morphed to form a $15\ \mu\text{m}$ diamond unit cell. The times shown in the top left hand corners of the frames, indicate the length of the sequences. Each sequence started and ended with the trapped spheres in the same position.

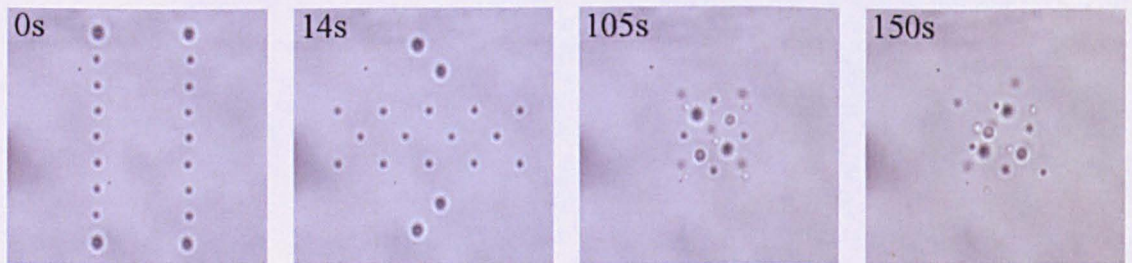


Figure 5.14: A pre-generated hologram sequence designed with the DBS algorithm used to trap fourteen $1\ \mu\text{m}$ diameter silica spheres and four $2\ \mu\text{m}$ diameter silica spheres morphed to form $15\ \mu\text{m}$ zinblende unit cell. The times shown in the top left hand corners of the frames, indicate the length of the sequences. Each sequence started and ended with the trapped spheres in the same position.

As the diamond and zinblende unit cells are rotated, an increased number of trapping planes is created, reaching a maximum of 18 planes containing a single trapped sphere. The rotation shows the structure is indeed fully three dimensional and by returning all the trapped spheres to their original starting positions, they are shown to be independent of each other.

5.4 Discussion

It was shown that both symmetrical and arbitrary patterns of trapped objects were realized. These patterns were trapped from static holograms and using automated manipulation of trapped particles. The use of static holograms and sequences of holograms to automate the manipulation of trapped particles are discussed here.

5.4.1 Crystal-Like Structures

In the case of the cube, the structure could be rotated and scaled in size. The ability to change the size of the cube has some advantages, it allows the structure to be trapped in an initial small unit cell size and then expanded to a larger size. This alleviates the problem of filling traps within a limited sample cell volume. Also, aberrations introduced by the objective lens in the axial trapping plane and the spatial limitations of the SLM in the lateral trapping plane, making filling of traps far apart problematic because they are weakened by the fall-off in diffraction efficiency of the SLM.

In both examples, there are specific moments when two of the traps were placed in the same lateral position, but at different axial positions. One might expect this to be difficult to achieve since one trap is in the shadow of the other. However, the high numerical aperture of the objective lens allows beams to be tightly focussed in this way. Additionally, the DBS algorithm corrects for some aberrations in the optical arrangement during the hologram design, allowing light to be more efficiently placed into the trapping orders, giving some control of contrast.

The DBS algorithm cannot calculate holograms as fast as the anti-blazing hologram design method, but is still fast compared to other algorithms that can calculate three dimensional holograms [82]. The DBS algorithm completes over 500 000 iterations in a few minutes for a typical 265 by 256 pixel, 16 phase level hologram, for example the hologram used to trap the diamond unit cell. The main advantage the DBS algorithm has over the anti-blazing design method, is that it can specify arbitrary patterns of optical traps in the target plane. This makes the DBS algorithm more suited to designing all types of crystal

unit cells.

The initial cube unit cell and the diamond unit cell holograms were static holograms. Filling the traps in these structures is problematic because they have optical traps stacked on top of each other, in the axial plane. The diamond structure is more challenging because it has five layers in its structure.

5.4.2 Automated Manipulation

The automated manipulation of particles involves several areas that influence the process of trapping; maintaining trap integrity and the speed of trap movement were the two most important in my research. These will be discussed separately because each has a different set of parameters.

5.4.2.1 Speed of Manipulation and Hologram Design

The different techniques used to automate the manipulation of trapped particles can be compared using several parameters, speed of hologram design, complexity of the trapped pattern of particles, degrees of freedom in manipulation and speed of manipulation. Of these parameters, the speed of hologram design and speed of particle manipulation are of highest importance.

Of the techniques used, pre-generating holograms with the modified GS algorithm is slow, but using the DBS algorithm is slowest. Pre-generating holograms with the modified GS algorithm may be slow, but it allows the user to specify the exact position of each trap throughout the manipulation trajectory. Through this process it was found that moving a particle more than half its diameter from frame to frame, the particle movement become jerky and it was easily lost from the trap.

Although the DBS algorithm cannot be used to design holograms in real-time, it produces hologram sequences that allow rotation of trapped structures, an extra degree of freedom in manipulation compared to the modified GS algorithm. Rotation is possible because

the DBS calculates the pattern of optical traps in a fully three dimensional hologram.

The modified GS algorithm used to design holograms in real-time was the fastest method used to automate the manipulation of trapped particles. However, rotation using the modified GS algorithm is difficult because the holograms are not fully three dimensional, but are actually comprised of many layers. As a greater number of trapping planes are introduced into a structure (e.g. rotating a structure can increase the number of trapping planes), the algorithm slows and would no longer be able to design holograms in real-time. The speed at which a particle is manipulated is controlled by three parameters, the number of holograms to be displayed a second, the time delay between displaying the holograms and the distance a particles has to travel.

5.4.2.2 Trap Integrity

When designing a hologram sequence for manipulating trapped particles in HOTs, the user does not necessarily want to be able to trap as many particles as possible. In my research, the aim was to move trapped particles from simple patterns into complex patterns and not to fill as many traps as possible. Although trapping of hundreds of particles is possible using HOTs [1], there is a space problem (the field of view of the CCD camera and objective in the experimental arrangement) and it is not always possible to place a single particle in each trap. Also, with so many optical traps present, traps adjacent to each other can have an influence on each other. This can influence the integrity of the optical traps in a set pattern and is discussed below.

In all the results presented in this chapter, no two trapped particles were positioned closer than 2 microns to each other. The spacing between particles was kept at this distance or larger because as traps become close, particles are attracted from the weaker trap to the stronger trap. In the case of the DBS algorithm, the intensity in each trap is calculated to be equal and any imbalance in trap strength is due to the trapped structure being displaced in the lateral plane from the zeroth order. If the modified GS algorithm is to calculate hologram sequences that produce traps with equal intensities, it would not be able to calculate them in real-time. Control of the trap intensities could be achieved by

pre-generated holograms using the modified GS algorithm, but it would be an extremely time consuming process.

Even with good control of the intensity in each trap, there are other problems to overcome. So called ghost orders or unwanted orders occur and even though they may not be strong enough to trap a particle, they can still influence traps enough to make trapped particles to be lost from them. Ghost orders can be reduced by optimizing the blazing of the hologram, thus maximizing as much of the light into the +1st diffraction order. The diameter of the trap is important, controlled by the trapping laser's wavelength and the numerical aperture of the objective lens. The trap's diameter can be reduced by increasing the NA of the objective or by reducing the trapping laser wavelength. As two traps are moved closer to each other, interference between the two traps occurs due to the superposition of light waves. The trap strength will be weakened when destructive interference dominates. The superposition occurs when the trap diameters are so large, they overlap with adjacent traps. Due to the tight focus of the trapping beams, this effect is less of a problem for traps more than a few microns apart, but becomes more significant as the traps are positioned closer together.

5.5 Conclusions

Static holograms were used to trap two different crystal-like structures containing particles in different planes, but in the same lateral positions, using holographic optical tweezers. A symmetrical cubic structure was scaled in size and rotated around its three principle axes. The anti-blazing hologram design method is limited to generating symmetrical patterns of optical traps. The DBS algorithm, although slower at designing holograms, can generate both symmetrical and arbitrary patterns of optical traps. The individual layers of the diamond unit cell were imaged by introducing an axial offset into the structure.

The automated manipulation of trapped particles in HOTs was realised. Automated manipulation of multiple trapped particles was achieved using both pre-generated hologram sequences designed with the DBS and modified GS algorithms and using real-time hologram design using the modified GS algorithm. Automated manipulation was used to

create both two and three dimensional patterns of trapped particles. Rotation of three dimensional patterns of trapped particles was achieved using the DBS algorithm, but was unsuccessful using the modified GS algorithm. It is envisaged the manipulation techniques devised will be applied to biological and photonic crystal research in the future (see chapter 9).

Chapter 6

Optical Trap Quality

6.1 Introduction

The previous chapter described complex arrangements of trapped particles and the stacking of particles on top of each other. In all these experiments assembling two and three dimensional patterns of trapped particles, no two particles were brought to within $2\ \mu\text{m}$ of each other. Although the distance between particles trapped in these complex arrangements was not crucial, the distance trapped particles are spaced could be important in areas such as crystal seeding. Therefore, trapping of particles very close to each other is worth pursuing and would show that holographic optical tweezers (HOTs) can be applied to sub-micron control of particle manipulation.

In the work presented in this chapter, controlling the position of trapped particles adjacent to and above each other with a high precision is the primary aim. The ability to trap particles close to each other is attained by controlling the intensity of the light in the optical traps. By controlling the intensities of the traps and their integrities, particles held by the traps can be moved very close to each other. It is also shown that trapped particles can be positioned very closely for prolonged periods of time without loss of trap integrity.

6.2 Experimental Arrangement and Procedure

The experimental arrangement is similar to that described in chapter 3. A single $2\ \mu\text{m}$ diameter silica sphere and pairs of these spheres were manipulated back and forth over a distance of $10\ \mu\text{m}$ using pre-calculated computer generated holograms for the pairs of spheres and holograms calculated on-the-fly for the single sphere (Figure 6.1). For the sequences of pairs of traps, the holograms were displayed at a rate of 6 per second. In all cases, the particles were lifted about $3\ \mu\text{m}$ from the surface of the sample cell. The pairs of particles were passed over each other, separated axially from 0 to $5\ \mu\text{m}$ at $0.5\ \mu\text{m}$ increments and the laser power reduced until either of the particles was lost from its trap. Two different sequences of holograms were run for each axial spacing; a) zero intensity specified between the traps and b) no zero intensity specified between the traps. In addition to the experiments with pairs of particles, a single particle was manipulated back and forth at increasing speed until released from the trap, with the power in the trapping beam set to the power at which the pairs of spheres were released from their traps. All holograms were displaced by $10\ \mu\text{m}$ above the zeroth diffraction order along the y-axis to prevent the zeroth diffraction order from interfering with the optical traps (Figure 6.1).

6.3 Hologram Design

The computer generated holograms used in the experiments were designed using two different hologram design algorithms. The single trap sequences were generated using a blazed grating to offset the trapping order [54]. The pre-generated hologram sequences for the two-trap experiment were designed using a direct binary search algorithm [66]. For the first set of sequences, three target positions were specified. Two of these positions correspond to the two traps, the third position to a point halfway between the two trap positions. The error function for the direct binary search optimization was specified to maximize the intensity at the trap positions, but keep the intensity close to zero at the halfway point between the traps. The optimization runs were then repeated with a modified error function, to only maximize the trap peak intensities and ignore the intensity

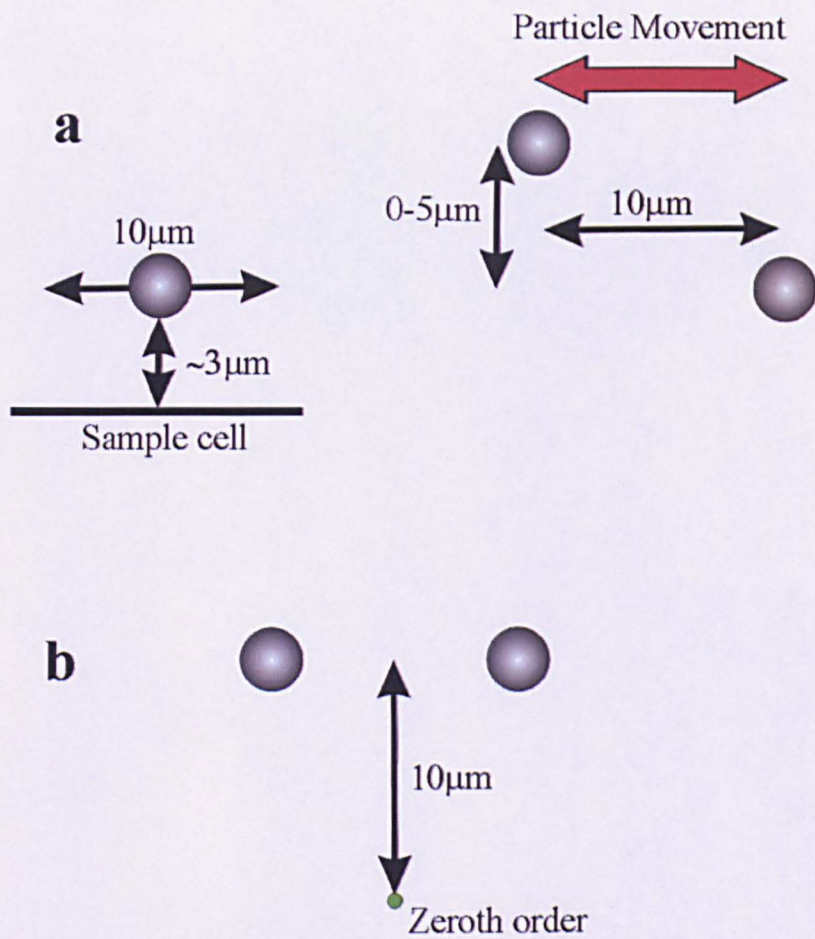


Figure 6.1: Schematic representation of a) the position of the trapped spheres, indicating the 10 μm distance of manipulation and an example of a pair of trapped spheres, b) the offset of traps from the zeroth order.

values at the halfway point. Examples of these direct binary search algorithm holograms are shown in Figure 6.2.

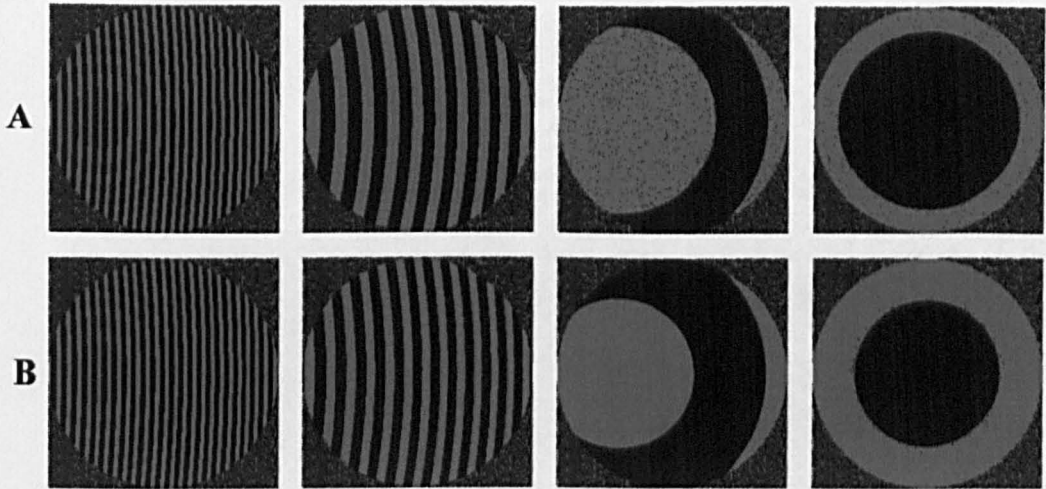


Figure 6.2: *Examples of frames (showing the phase represented as bitmaps where black is π and grey is 0π) from the hologram sequences used in the two-trap experiments; designs with zero intensity specified between the two traps are shown in the bottom row, and designs with no zero intensity specified are shown in the the top row. In the images grayscale corresponds to hologram phase.*

6.4 Results

Four sets of results are shown as sequences of video frames (Figures 6.3 - 6.6). Figure 6.3 shows a set of frames from the sequence in which zero intensity was specified between the traps. At the point of trap failure the power in each of the individual traps was 0.375 mW, with the laser emitting 5.2 mW of power. For the corresponding sequence of holograms with no zero intensity specified between the traps, failure occurred at 0.375 mW in each trap and the laser was emitting 4.5 mW of power. The difference in laser output indicates a difference in diffraction efficiency of the different holograms.

At the point of the particles being released by their traps in Figure 6.3, the particles are positioned next to each other and not along the z-axis. To indicate that these positions are not a weakness in the hologram sequences, particles were positioned close to each

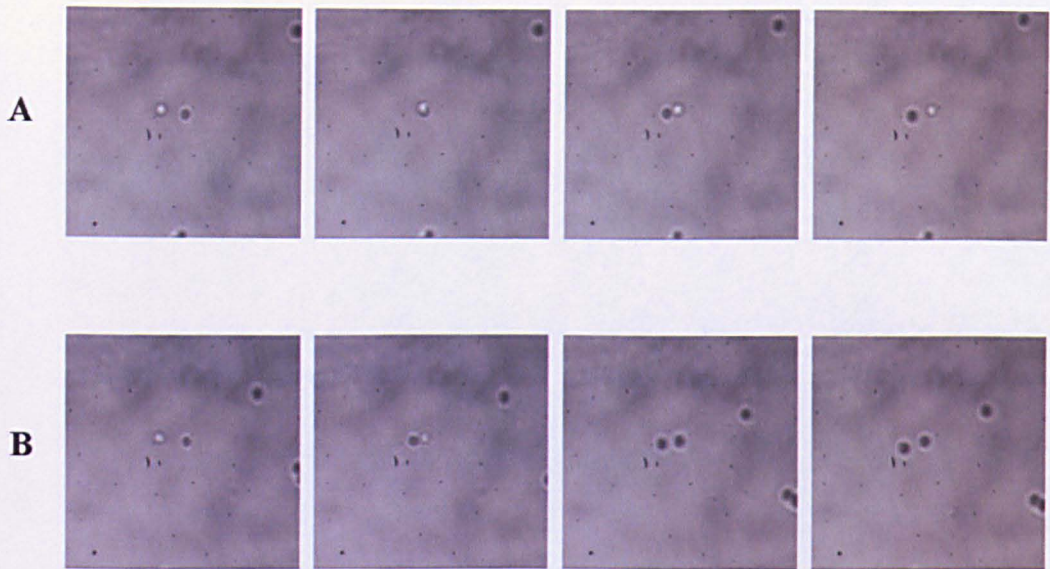


Figure 6.3: *Two sequences of frames showing two 2 μm diameter silica spheres separated by 5 μm (Sequence A) in the z-axis being moved over each other and when the axial distance is closed to 2 μm (Sequence B), the particles are lost from the optical traps.*

other and them moved apart (Figure 6.4). This was achieved for all hologram sequences; 0 - 5 μm spacing between trapped particles. The next set of results shown in figure 6.5 were carried out to determine if particles could be trapped directly above each other for prolonged periods of time. Each sequence of holograms was run with particles held in position for at least 1 minute and then the particles were returned to their original positions. However, particles can be held for over 2 minutes, probably more than enough for any practical applications of HOTs.

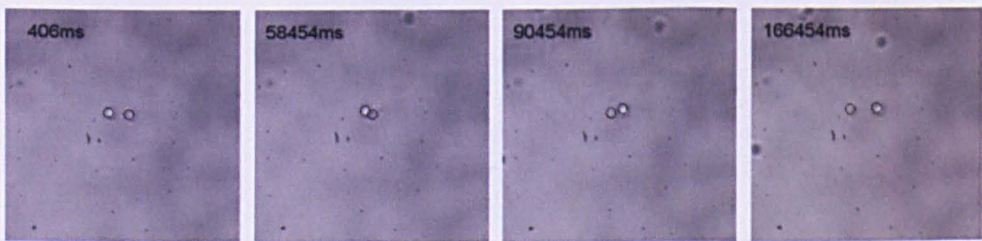


Figure 6.4: *Frames showing particles two traps separated by 2 μm , being held adjacent to each other for around a minute and the trap integrity is not affected. The numbers indicate the times at which each frame was recorded.*

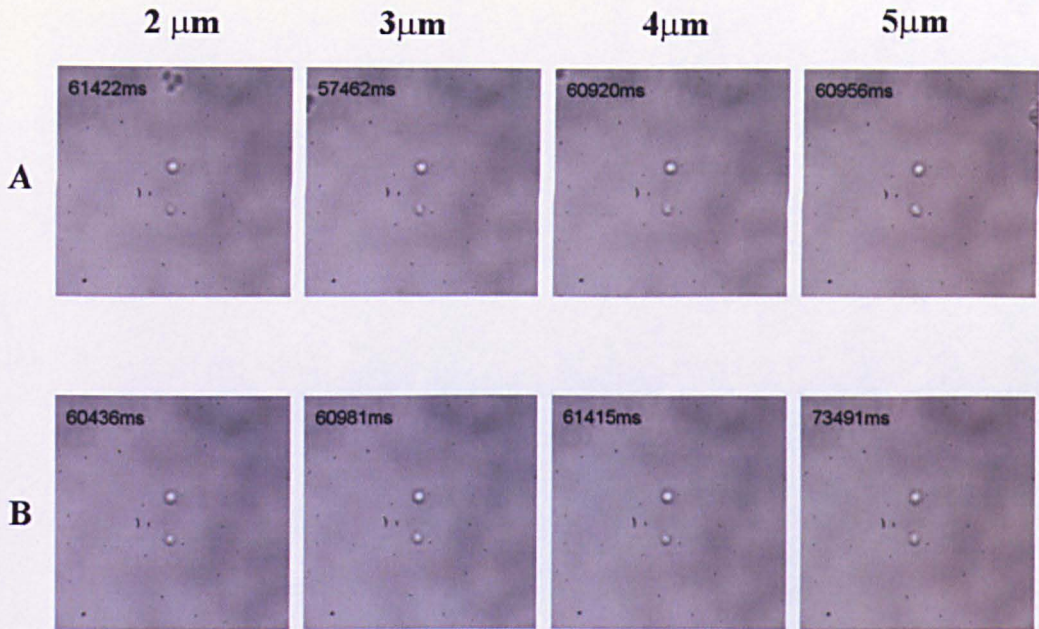


Figure 6.5: *Frames showing two particles stacked in the axial plane, held for over a minute before being separated. The frames in A are for holograms with an area of zero intensity specified between the traps and the frames in B have no area of zero intensity specified between the traps. The lower sphere is held by the zeroth order trap and the numbers indicate the length of time the particles were held in position.*

Finally, a single particle was held with 0.375 mW of laser power (from a laser emitting 2.2 mW of power) and moved from side-to-side at increasing speed until the particle was released from the trap (Figure 6.6). The particle was released from the trap when displaying holograms at 11 per second.

6.5 Discussion

Previously, other workers have produced complex arrangements of trapped particles (e.g. [56, 1]). In these studies and others, there are no reports of objects being positioned directly next to each other. Although, positioning particles very close to each other and maintaining control of their position may appear an academic exercise, it could well become useful in applications of optical tweezers in the future and is therefore worth

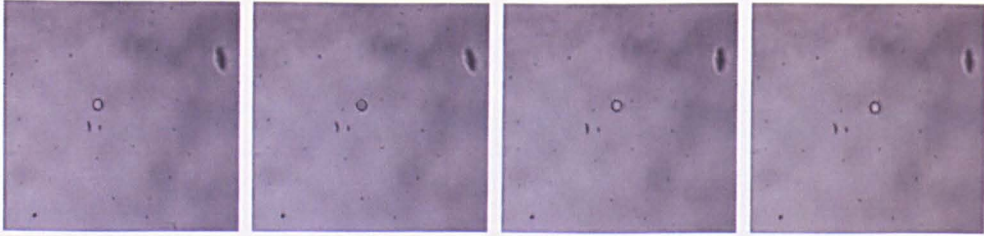


Figure 6.6: *A sequence of frames showing a single particle being moved 10 μm from left to right in the lateral plane.*

investigating.

To allow trapped particles to be manipulated close to each other without one trap interfering with adjacent traps using holographic optical tweezers, the holograms must be designed to allow traps to have equal intensities. In our experiments we have successfully manipulated 2 μm diameter trapped particles and maintained trap integrity, even when the particles were touching. This shows that holographic optical tweezers can be used to trap and manipulate particles adjacent to each other. We explored the possibility of specifying a zero intensity region between traps in order to improve trap quality, and to prevent the collapse of two traps, or to prevent the loss of the trapped object from one of the traps. The experimental results indicate that, at least for the two-trap case, specifying a zero intensity position between the two traps did not improve the integrity of the traps. In fact, there seemed to be very little difference in trapping behavior between the two cases, and the overall diffraction efficiency of the hologram designs with the zero intensity specified was slightly lower. The lower diffraction efficiency is due to the weighting of the DBS algorithm, which also influences the intensity of the specified traps. The intensity of the optical traps is decreased by increasing the weighting on the region of zero intensity because it produces a decrease in light everywhere.

In this work, the diameter of the trapped particle (2 μm) was larger than the wavelength of the trapping laser (532 nm). Many workers use particles of a smaller size in their experiments, ranging from 10's nm to 1 μm in diameter. The trapping of particles increases in difficulty as the particle size decreases and usually requires a greater power in the trapping laser. The increased trapping power accentuates the imbalance in the optical traps and

particles will be lost to the stronger trap. Additionally, as the particle size decreases the beam waist and particle size ratio decreases, making the trap less stable.

6.6 Conclusions

This work has shown that trapped particles can be manipulated until touching each other with HOTs and that the particles do not stick to each other. Specifying an area of zero intensity between the traps can reduce interference effects due to unwanted light around each trap. When an area of zero intensity is specified between the traps, a reduction in diffraction efficiency is produced, thus compromising the integrity of the optical traps. Particles can be held above other particles for several minutes. The ability to manipulate particles and hold them in position is of interest in many applications of optical tweezers, such as photonic crystal fabrication and seeding of crystal/biological tissue growth. The next challenge is to adapt these manipulation techniques for particles a few hundreds of nanometers in size.

Chapter 7

Optical Tweezers Systems

7.1 Introduction

Over the last 2 - 3 years I have been involved in several collaborations with researchers at the University of Strathclyde and the Department of Electrical Engineering, University of Glasgow were instigated and will continue in the future. As part of these collaborations, my role was to build several optical tweezers systems. In each collaboration the optical tweezers were built and tested in the optics lab before being installed in the respective collaborator's lab. Details of the optical tweezers systems and their applications are given below.

7.2 Optical Tweezers and SERRS

Over the last 2 years the optics group has been involved in a collaboration with Prof. Ewen Smith of the Department of Pure and Applied Chemistry at the University of Strathclyde and Prof. Jon Cooper of the Department of Electrical Engineering at the University of Glasgow. The collaboration was concerned with developing a new analytical microscale tool, mainly for detecting surface enhanced resonant Raman scattering (SERRS) from partially silver-coated silica spheres. The motivation behind this work is to develop the

ability to probe small volumes of sample, with the potential of multiplexing using SERRS to look at several molecular species simultaneously and to use a lower costing analytical technique with a similar sensitivity to existing technologies (e.g. fluorescence). The use of SERRS sensitive microprobes could allow micron scale features to be probed; for example cell membrane surfaces and chemical reactions within cells.

SERRS experiments are carried out using a conventional microscope attached to a Raman Spectrometer and in many experimental arrangements, the sample is not visualised while measuring the Raman signal. The sample can be visualised by using a beamsplitter to divert an image to a camera, but this could lead to a reduced Raman signal. By combining SERRS with optical tweezers, not only can the sample be visualized, but the SERRS signal can be seen at the same time and the optical tweezers permits spatial resolution of the microprobes.

Initial work as part of the collaboration was carried out on the optics group's optical tweezers [33] to develop optical tweezers as a tool to enable SERRS measurements to be performed while manipulating micron-sized objects. The capability to manipulate objects of this scale was developed to allow the probing of small volumes, surfaces and objects. To enable more applied studies to be carried out, optical tweezers were constructed around an Olympus BH-2 microscope in the optics lab and then attached it to a Renishaw 2000 Ramascope Microprobe at Prof. Smith's lab at the University of Strathclyde (Figure 7.1). The details of the optical arrangement are shown in Figure 7.2.

This section gives details of Raman scattering, SERRS, sample preparation and a summary of some of the experimental work carried out at Glasgow University with members of Prof. Ewen Smith's group. My role in this research was mainly to set-up the optical arrangements and operate the optical tweezers during the experiments, as well as to commission optical tweezers in Prof. Smith's laboratory.

7.2.1 Raman Scattering

Raman scattering was discovered by Sir C. V. Raman and K. S. Krishnan in 1928. Raman scattering measures a change in vibrational energy at the molecular level. The energy

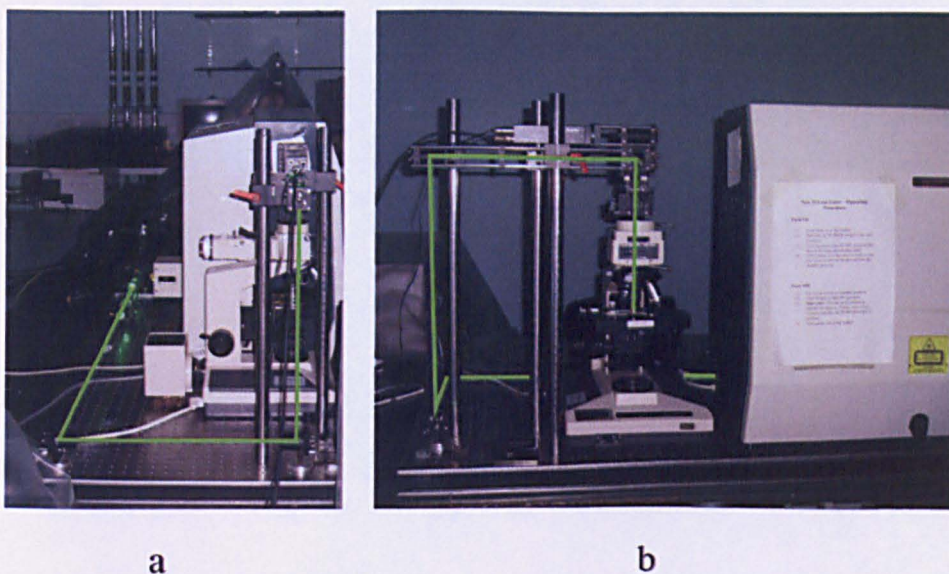


Figure 7.1: *Photos showing the optical tweezers installed in the Department of Pure and Applied Chemistry, University of Strathclyde: a) shows a side view and path of laser beam (green line) from the laser head, through the beam-expander to beam-steering mirror and b) shows the beam path from beam-steering mirror to the Renishaw 2000 Ramascope Microprobe. The green line shows the path of the trapping laser beam.*

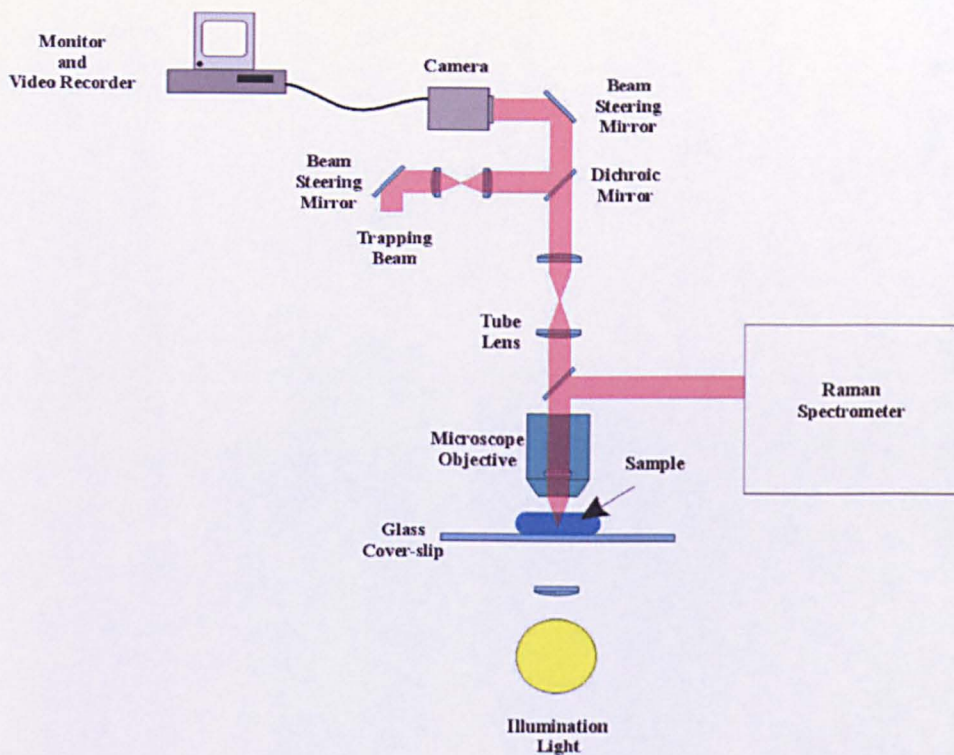


Figure 7.2: Schematic diagram of the experimental set-up of an optical tweezers combined with Raman spectrometer.

required to excite the vibration of molecules is less than that required to excite electrons (e.g. rotational < vibrational < electronic). As such, if the molecule is Raman active, it can be used to identify the molecule of interest. Raman scattering is an inelastic effect, with the incident light mainly having a higher frequency than the scattered light, thus the light is frequency shifted [83]. Raman scattering uses a monochromatic excitation light source tightly focused and passed through a Raman active sample. Typically the excitation light source is a laser, but can be a white light source if appropriate filters are used to give monochromatic light. Most of the light passes at the same frequency through Rayleigh scattering, but about every 1 in a million photons is inelastically scattered and emitted at a different frequency. The frequency shift is highly dependent on the molecular structure of the molecule of interest, allowing unknown molecules to be identified. This change in frequency is termed a Stokes shift, but arises from a different mechanism than fluorescence. Raman scattering occurs when a photon is absorbed, excites an electron into a virtual state, and is emitted again with a shift in frequency (Figure 7.3). The

difference in energy between the incident and scattered light is the Raman shift expressed as wavenumbers (cm^{-1})

$$\Delta\nu = \frac{1}{\lambda_{\text{incident}}} - \frac{1}{\lambda_{\text{scattered}}}. \quad (7.1)$$

In crystalline phases, the light scattered is often of a specific wavelength because only specific photons are allowed in to the crystal structure.

Stokes Raman scattering (Figure 7.3a) occurs when the electron is in the ground state and is excited to a virtual state before returning to the final state. In a resonant molecule, some electrons will be in an excited (final) state, move to the virtual state and return to the initial state. This is called anti-Stokes Raman scattering (Figure 7.3b). This anti-Stokes Raman scattering (Figure 7.4) is always weaker than the Stokes Raman scattering [84].

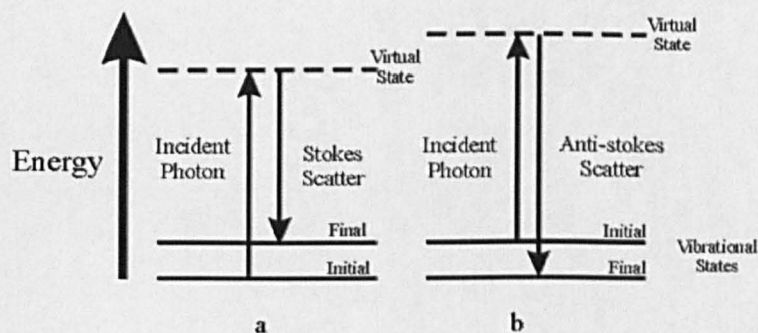


Figure 7.3: Energy level diagram for Raman scattering showing the two forms of inelastic scattering of photons; (a) Stokes Raman scattering (b) anti-Stokes Raman scattering.

7.2.2 SERRS Theory

Raman scattering is a weak effect, affecting 1 in every million scattered photons. To overcome this, enhancement of the Raman signal can be achieved by employing two techniques; resonance Raman scattering and surface enhanced Raman scattering (SERS) or a combination of both to give SERRS. SERS and SERRS occur from two different mechanisms. SERS is an enhanced Raman signal produced by the interaction of the

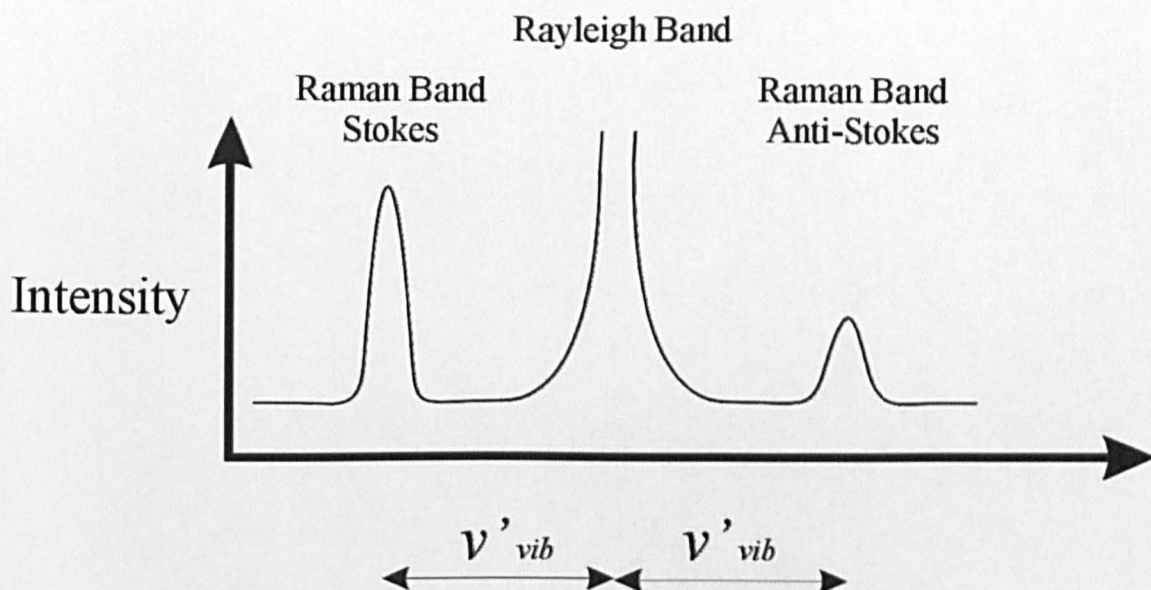


Figure 7.4: Intensity of the Stokes and anti-Stokes bands compared to the Rayleigh band.

excitation light source and the plasmon on the metallic surface area of the sample. SERS uses a laser to induce an electric field, called a surface plasmon around the particle; in our case silver coated silica spheres. Other metals used to coat the substrate are gold and copper, but they do not produce as large a Raman enhancement as silver. The metallic coating produces a roughened surface, increasing the number of points of high field strength, which in turn produces a point of high intensity. The molecules in proximity to the surface experience an exceptionally large electromagnetic field and vibrations normal to the surface are strongly enhanced, up to 10^6 stronger in comparison to a typical normal Raman signal [84].

SERRS is a Raman spectrometry technique using both resonant Raman scattering and SERS to give a further enhanced signal. In SERRS the resonant Raman scattered wavelength occurs at the same wavelength as the SERS wavelength. The overall SERRS signal can be up to 10^{14} times stronger than a conventional Raman signal. The SERRS mechanism of enhancement is due to an electronic excitation (i.e. the molecules require a chromophore near the excitation wavelength). The electronic transitions of many charge transfer complexes are in the visible, so that resonance enhancement occurs. The roughened surface provides a larger surface area for the chromophore to adhere to and provides

a strong plasmon at the surface. Having the plasmon at the surface is beneficial because it decays exponentially with respect to distance [84].

7.2.3 Sample Preparation

Silver coated silica spheres were used in the SERRS experiments (Figure 7.5b). Although the spheres were coated with silver to give a roughened surface, not all of the surface was covered in silver (Figure 7.5b) and the spheres still behaved as dielectric particles when the coating was less than 25 percent, allowing them to be trapped with optical tweezers [33]. The process of coating the silica spheres is detailed below.

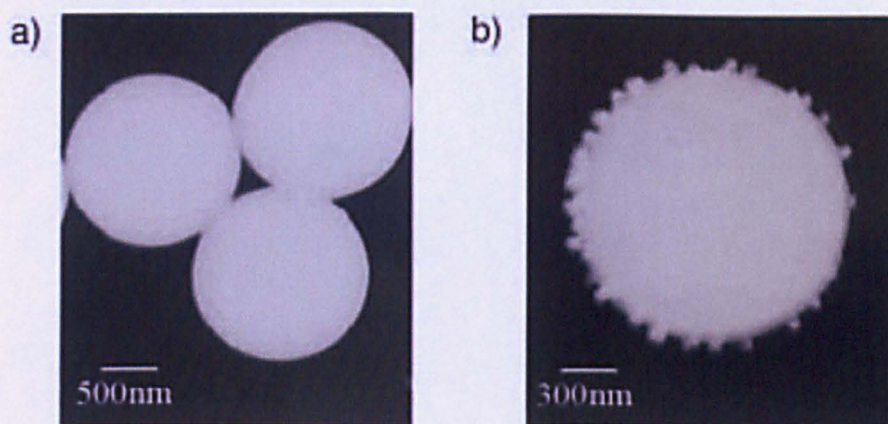


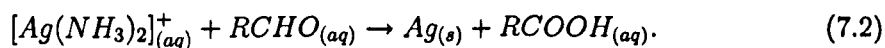
Figure 7.5: *Transmission electron micrographs of a) plain 1.5 μm diameter silica microparticles and b) a partially silver-coated 1.5 μm diameter silica microparticle.*

Samples of 1.5 μm diameter silica particles were coated in silver (Figure 7.5), onto which a dye (chromophore) was absorbed. The spheres were prepared by Graeme McNay at the Department of Pure and Applied Chemistry, University of Strathclyde. The silver coating method was carried out using a Tollen's reagent [85]. This method is explained in detail in this section.

Firstly, Tollen's reagent $[\text{Ag}(\text{NH}_3)_2]^+$ is prepared by adding 10 drops of 0.4 M sodium hydroxide (NaOH) to 0.1 M silver nitrate (AgNO_3), giving a brown suspension of silver (I) oxide (Ag_2O) and the excess solution is poured off. Drops of ammonia (NH_3) are added to the silver (I) oxide suspension until the brown colour disappears to give the

Tollen's reagent.

The final step in coating the silica spheres involved adding 1 g of spheres and 0.5 g of glucose to the solution of Tollen's reagent. The glucose reacts with the Tollen's reagent to deposit silver on to the surface of the silica spheres. The reaction is summarised below [86]



After the silver was deposited onto the silica spheres, a SERRS active dye (chromophore) was absorbed on to the silver (e.g 10-4M 3, 5-dimethoxy-4-(6-azobenzotriazolyl)-phenylamine). This dye has an absorption maxima at 532 nm, the excitation frequency of the surface plasmon resonance of the silver, allowing a SERRS signal to be generated.

7.2.4 Summary of SERRS Experiments

Several experiments were carried out by the collaborators and the optics group. These experiments were carried out using the optical tweezers at the Department of Physics and Astronomy, University of Glasgow. The optical arrangement is shown in figure 7.6. My input to the work has been setting-up the experimental arrangements and assisting with the part of the experiments using the optical tweezers. The SERRS experiments were carried out by myself, Pamela Jordan and Graeme McNay. A more comprehensive report of this work is covered in Pamela's doctoral theses [87]. Below is a brief summary of this work.

Two SERRS experiments were carried out with the optical tweezers in the optics group's lab. The first experiments showed partially silver-coated silica spheres could be trapped using optical tweezers and a SERRS signal could be obtained from the trapped spheres. By trapping a single partially silver-coated silica sphere with an optical trap and letting another sphere collide with the trapped particle, a SERRS signal was observed (Figure 7.7). The radiation pressure of the trap pulls others particles towards the trapped particle, creating the collision. Another technique used was to manipulate a trapped partially

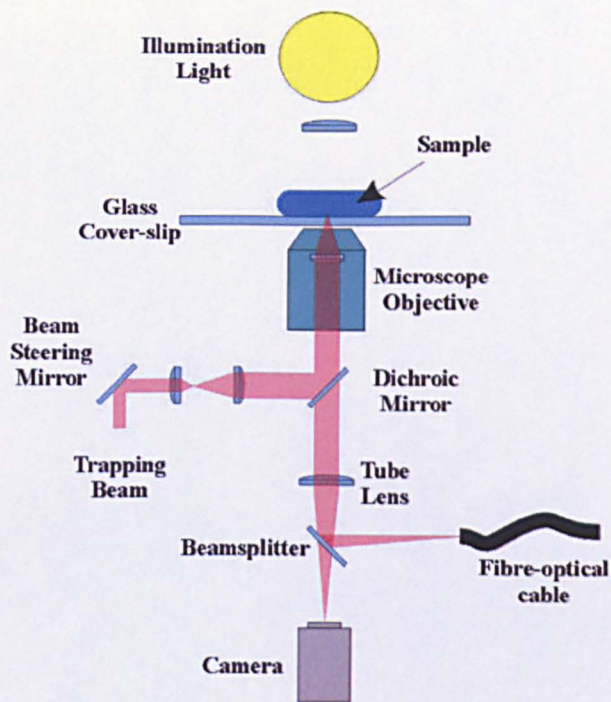


Figure 7.6: A schematic representation of the optical tweezers used for the SERRS experiments. The fibre-optical cable was attached to a PC mounted spectrometer.

silver-coated silica sphere to positions beside either a single sphere or clumps of spheres to induce a SERRS signal. By positioning two SERRS active spheres adjacent to each other a high field point is generated and a SERRS signal in the form of a flash of light is produced. An example of a SERRS signal is shown in Figure 7.8. This first experiment successfully showed that SERRS from single microspheres and optical tweezers could be combined.

These early results were collected from spheres trapped with a 532 nm laser, which photobleached the samples in a few seconds due to the high power of the laser. The second experiment used an infrared wavelength laser (1064 nm). The infrared laser prevents the sample being photobleached, but does not excite the sphere to produce a SERRS signal. To allow a SERRS signal to be collected from trapped spheres, a frequency doubling KTPiOPO_4 (KTP) crystal was positioned at an intermediate beam-waist and produced a few microwatts of 532 nm light, enough to generate a SERRS signal (Figure 7.9). The advantage of using the KTP crystal in an infrared laser beam, is the functionalised sphere

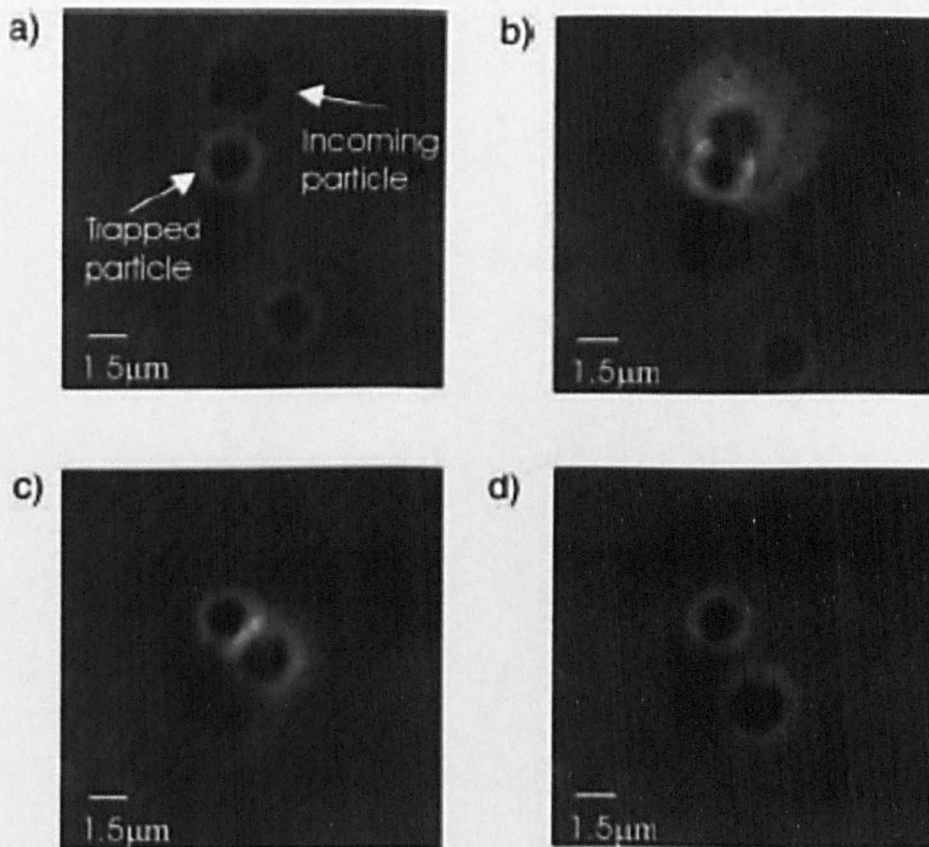


Figure 7.7: A sequence of frames showing a) a dye coated particle moving towards the trapped particle, b) a SERRS emission as the particles touch and the particle moving away in c) and d) from the trapped particle.

can be trapped, released and retrapped, without significant loss of the SERRS signal.

7.3 Optical Tweezers For Trapping Functionalised Particles

As part of the optics groups collaborations, we have been carrying out work with Dr Norbert Klauke, a member of Prof. Jon Cooper's group from the Department of Electrical Engineering at the University of Glasgow. My part in this collaboration was to build

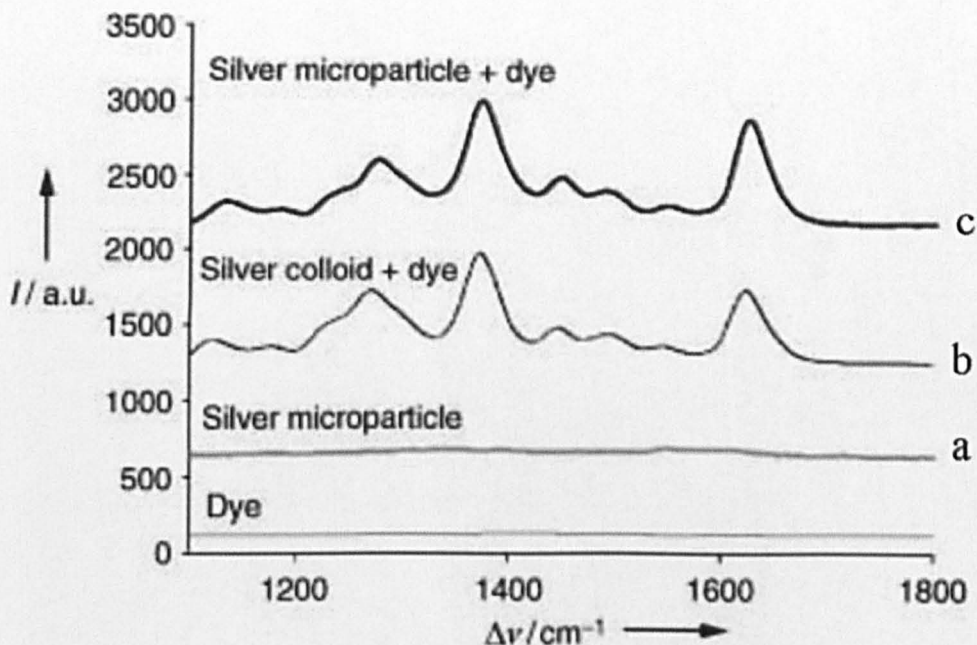


Figure 7.8: Three Raman spectra from; a) plain silver-coated microparticles b) SERRS spectra from the dye adsorbed on aggregated silver colloid and c) dye adsorbed on the silver-coated microparticles. The back ground spectra of the azo dye is also shown. I =intensity, arbitrary units.

optical tweezers (Figure 7.10) to carry out experiments on biological samples. More information about these experiments will be given in chapter 8.

These optical tweezers were built around a commercially available Zeiss Axiovert 200 inverted microscope, as shown in figure 7.11. Several different optical paths are available to bring the trapping laser beam into an Axiovert 200 microscope. At the time of moving the optical tweezers to Dr Klauke's lab, he did not have access to an infrared laser, so the trapping beam (532nm) was coupled through the microscope's base port (Figure 7.12). The optics supplied in the microscope by the manufacturer do not allow an infrared laser to be coupled through the base port, but the microscope was adapted by fitting an infrared beamsplitter to allow an infrared laser beam to be coupled through the base port. These photos show the versatility of using an off-the-shelf research inverted microscope to build optical tweezers.

The use of the Axiovert 200 inverted microscope was selected because it is familiar to

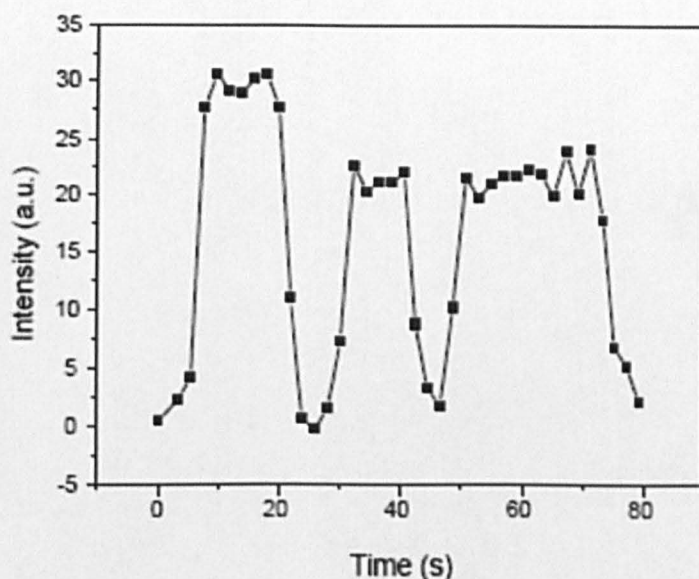


Figure 7.9: *The SERRS signal recorded from a bead that was trapped, released and re-trapped. The SERRS signal was produced from the 532 nm light generated from the KTP crystal and was only recorded when the bead was trapped.*

members of Prof. Cooper's group. Therefore, experimental equipment developed for current research could be attached to it.

An added advantage to building a set of tweezers around an Axiovert 200 inverted microscope was that it allowed the optics group to gain experience in the use of such a microscope with optical tweezers. This has allowed me to design new optical tweezers around custom-built Axiovert 200 microscopes for the optics group. By building both an optical tweezers and holographical optical tweezers arrangements around Axiovert 200 microscopes, better visualization of the sample cell (Figure 7.13) is obtained compared to that of the older optical tweezers, built from Linos components and the ports on the microscope allow easy attachment of cameras and other specialist equipment.

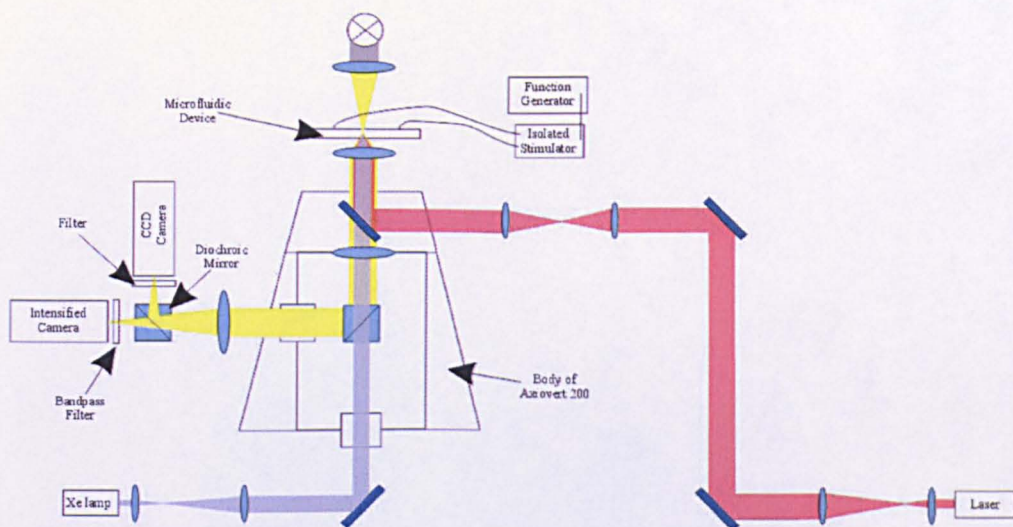


Figure 7.10: Schematic diagram of the optical tweezers built for Dr Norbert Klauke.

7.4 Abraham-Minkowski Experiment

The interactions of electromagnetic radiation with dielectric media has been of interest to scientists for over 100 years. There are two competing theories regarding the interaction between electromagnetic radiation and dielectric media, proposed by Abraham and Minkowski [88]. The first optical tweezers system I built was for an experiment to be carried out at the University of Strathclyde to investigate these interactions. This work was carried out in collaboration with Dr John Girkin and Dr Gail McConnell of the Centre for Biophotonics, University of Strathclyde. The collaboration brought together expertise in optical trapping from Glasgow University and femtosecond-pulse laser facilities at Strathclyde University.

It was proposed that by combining optical trapping with a femtosecond-pulse laser of near infrared wavelength (800 nm), only one photon can be passed through a dielectric particle at a time. The influence of the angular momentum carried by the photon as it passes through a dielectric particle of refractive index n would either produce rotation of the particle (Abraham formulation) or not (Minkowski formulation).

The Minkowski formulation suggests the linear momentum (p) and the orbital angular momentum (L) of a photon inside a dielectric are



Figure 7.11: *Photo showing the optical tweezers built around an Axiovert 200 inverted microscope, prior to being moved to Dr Klauke's lab.*

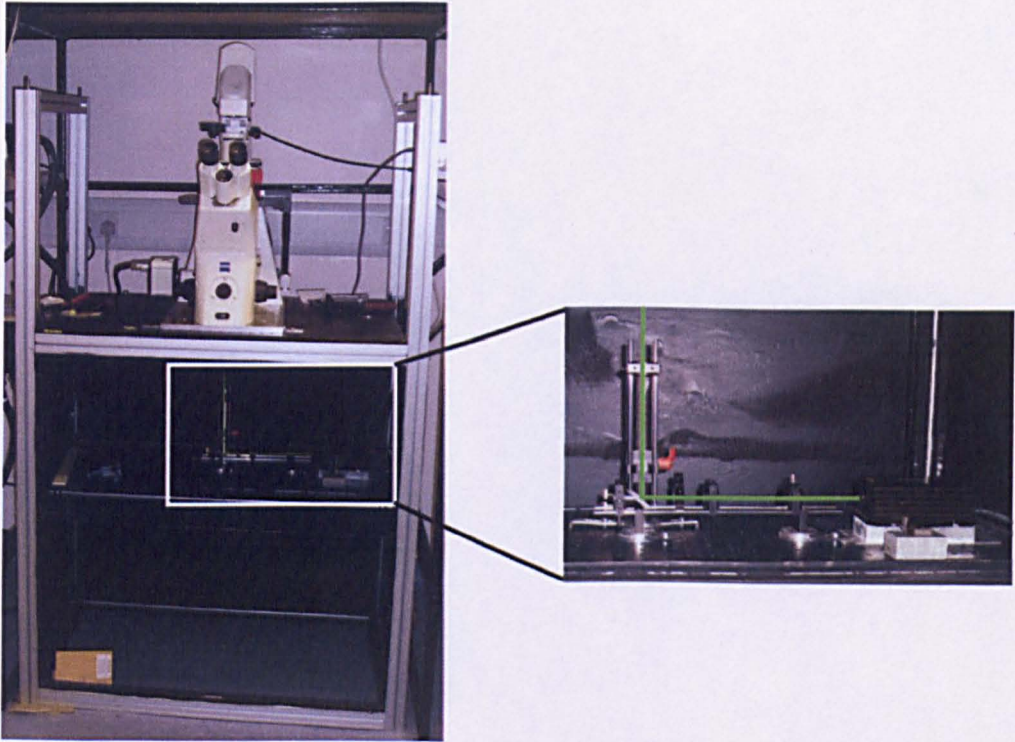


Figure 7.12: *Photo showing the optical tweezers built around an Axiovert 200 inverted microscope in Dr Klauke's lab. The detailed photo shows the trapping laser beam is expanded through a simple relay system below the base.*

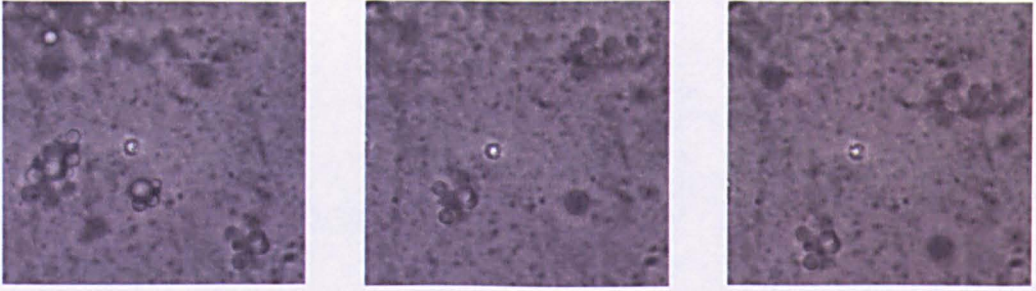


Figure 7.13: *Three frames showing a 1 micron silica sphere trapped in optical tweezers built for Dr. Klauke.*

$$p = n\hbar k_o \quad (7.3)$$

$$L = \hbar \quad (7.4)$$

where \hbar is the reduced Planck constant and k_o is the wavevector component in the direction of propagation.

According to the Abraham formulation

$$p = \frac{\hbar k_o}{n} \quad (7.5)$$

$$L = \frac{\hbar}{n^2} \quad (7.6)$$

and both quantities scale with $\frac{1}{n^2}$ compared to the Minkowski formulation.

To allow continuous rotation of a particle to be observed, the dielectric particle must be small enough to permit a pulse to pass through it and exit before the next pulse has entered the particle. As a photon enters the dielectric particle of refractive index n from a suspension solution of refractive index n_o , its angular momentum changes by

$$\Delta L = \frac{\hbar}{n^2} - \frac{\hbar}{n_o^2} \quad (7.7)$$

according to the Abraham formulation. The change in angular momentum is zero according to the Minkowski formulation (angular momentum is conserved). The direction of the rotation is controlled by the angular momentum of the light beam (i.e. left or right circularly polarized).

In the case of our experiment, several different types (e.g. glasses with n of 1.54 and 1.58, diamond) and sizes (mainly 2-3 μm in diameter) of particles were used. Diamond particles ground to near spherical shape were suspended in a deionized water solution, were used because they had the highest refractive index ($n = 2.42$) available at the time of the experiment. The Abraham interpretation predicted a 1 μm diameter diamond particle would complete 1 full rotation over a period of 30 hours.

The experimental arrangement is shown schematically in figure 7.14 and in the photo in figure 7.15. Rotation of a trapped particle is brought about by controlling the angular momentum in the trapping laser beam using a quarter wave plate. The speed of rotation is proportional to the power of the trapping laser beam and the difference in refractive index of the trapped particle and the liquid of suspension.

Although initial results were promising, we were unable to detect any certain rotation as predicted by the Abraham formulation. However, these initial experiments were encouraging enough to prompt the submission of a successful application to EPSRC, for a research grant to carry out a more detailed experiment with particles of higher refractive index than diamond, with an air-damped optical tweezers system.

7.5 Summary

Three different experimental arrangements have been described. Although each optical tweezers functions on the same principles of physics, their applications are varied. The optical tweezers built for the Abraham-Minkowski experiment were applied to investigate

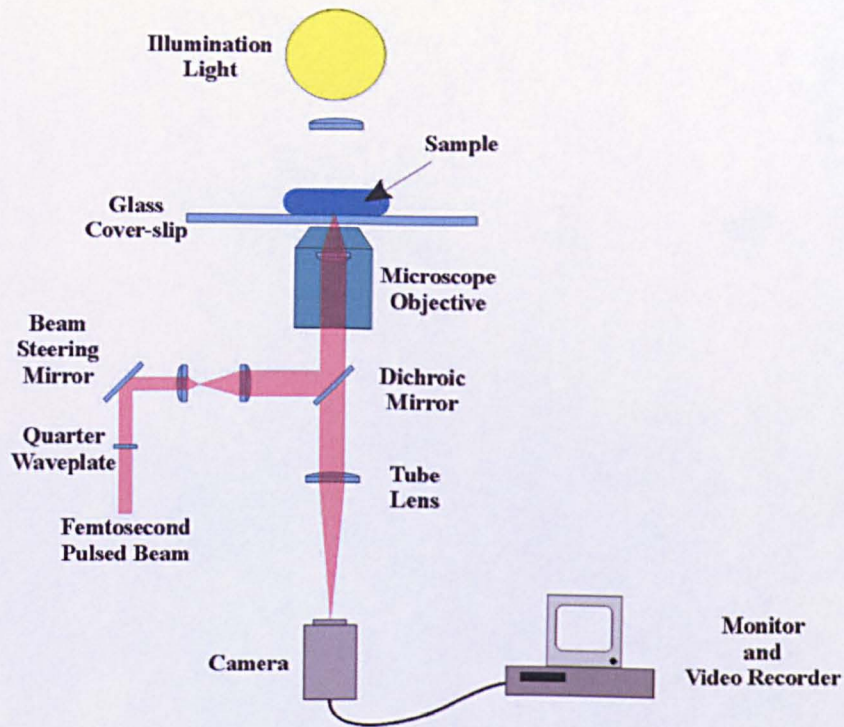


Figure 7.14: *Schematic diagram of the experimental set-up for the Abraham-Minkowski experiment.*

fundamental aspects of light's behavior. The optical tweezers built for Prof. Smith give him an extra tool to compliment existing Raman spectroscopy equipment in his lab. The tweezers supplied to Prof. Cooper give an extra degree of freedom to manipulate and position either functionalised particles or biological specimens. However, common to all three optical tweezers arrangements, they were built to the users specifications and require minimal knowledge of optical physics to operate.

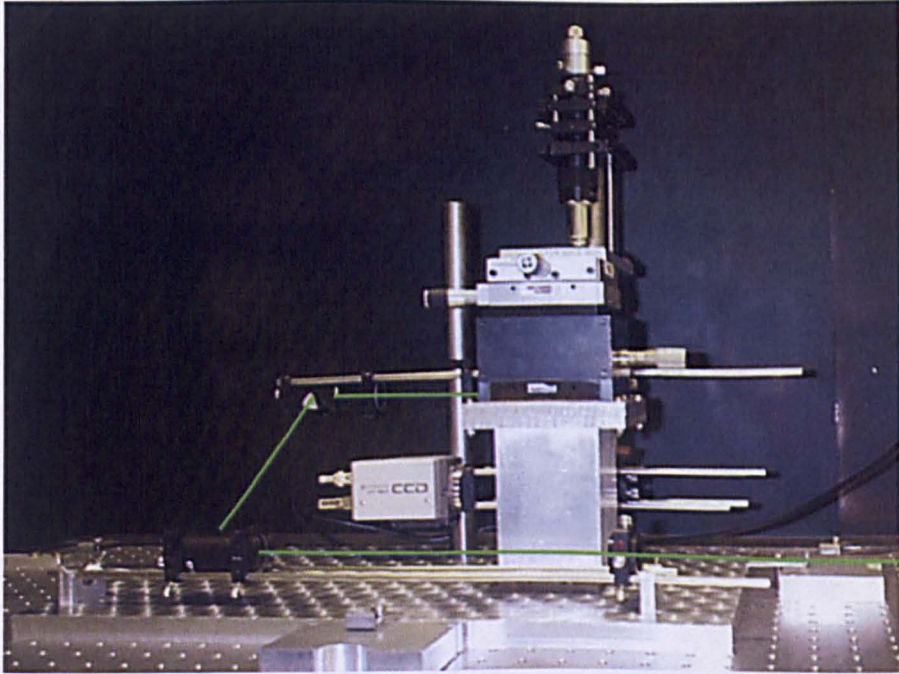


Figure 7.15: *Photograph of the optical tweezers built for the Abraham-Minkowski experiment. The green line shows the path of the trapping laser beam.*

Chapter 8

pH Microprobe Calibration

8.1 Introduction

Optical tweezers [4] have been in use for nearly 30 years and are used to trap and manipulate nano- to micron-sized particles [19]. These particles are usually dielectric; e.g. glass spheres, latex spheres, polystyrene spheres or biological cells. Optical tweezers are being used increasingly in biological research and this is the biggest area of optical tweezers research at present. For studies in the biological sciences, dielectric spheres are often coated with a fluorescent indicator (such as a dye), to detect changes in either physical or chemical properties of biological samples [5]. The use of fluorescence in optical trapping was first reported for polymer microparticles in water [27]. Three dimensional pH microprobes have also been created from fluorescent particles and used to study water/glass interfaces [89]. The combination of optical trapping and fluorescence still continues, for example, in the measurements of patch clamped cells [90]. Another technique for studying pH changes in biological systems is the use of fluorescent dyes in lab-on-a-chip devices (often termed microfluidic devices) and one such device is used in the research presented in this chapter. Many microfluidic devices rely on the flow of fluids and suspended particles through micro-channels, with little or no control over the positions of particles [91]. In our work, we are maintaining control of particle positions with optical tweezers.

In recent years optical tweezers have been combined with microfluidic devices for novel and

new applications [47]. These studies include cell sorting [51, 52], micro-pumps and micro-valves [48]. In our work we are using optical tweezers to control a pH probe, enabling us to spatially map the pH profile between two electrodes within a microfluidic system.

8.2 Sample Preparation

Samples of 3 μm diameter amine-coated latex microspheres (2.5 percent solids, Polysciences, Inc.) were functionalized with seminaphthorhodafluors (SNARF-1) carboxylic acid acetate (Figure 8.1). The emission spectrum of carboxy SNARF-1 undergoes a pH-dependent wavelength shift, thus allowing the ratio of the fluorescence intensities from the dye at two emission wavelengths to be used for more accurate determinations of pH. The SNARF-1 molecules were immobilized on to the latex spheres through its succinimidyl ester group coupling via the amine groups.

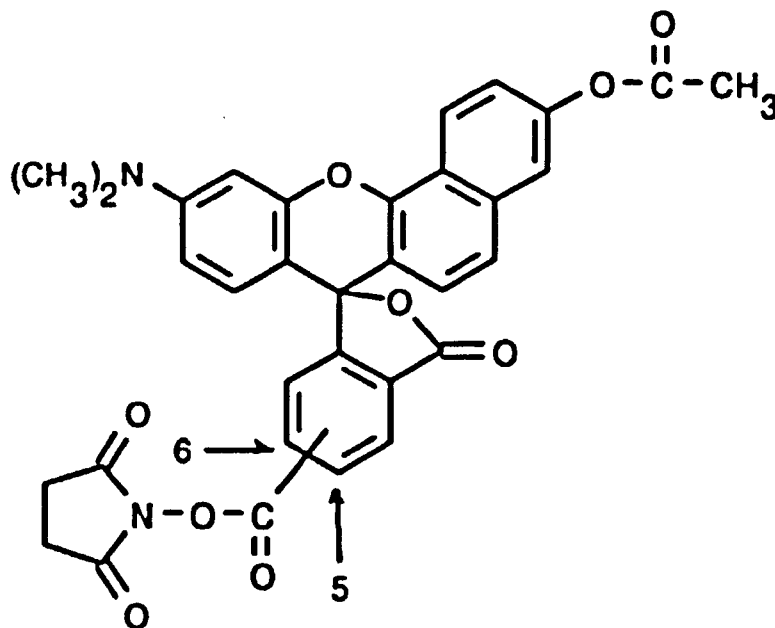


Figure 8.1: A diagram showing the molecular structure of a SNARF-1 molecule, formula $C_{33}H_{24}N_2O_9$.

After the sphere's surface was functionalised with the SNARF-1, they were suspended in

a buffer solution of 1mM HEPES and 50mM sodium perchlorate electrolyte (NaClO_4), at a pH of 7.4. This buffer solution was selected because it is an electrolyte without chloride ions, thus does not dissolve gold microelectrodes during passage of a transient current. The amount of electrolysis is governed by the faradic current during the electrical pulses passed through the microelectrodes in the microfluidic device. When excited at 488nm and 515nm, the SNARF-1 dye fluoresces at the two wavelength 580nm and 640nm. Monitoring the fluorescence intensity at 580nm which decreases with increasing pH [92], forms the basis of our pH microprobe system.

8.3 Microfluidic Device Fabrication and Operation

Microdevices were fabricated using a chrome-coated mask made by Dr. Norbert Klauke (Department of Electrical Engineering, University of Glasgow). The mask was fabricated using a Philips electron beam writer (Philips Electronics UK). The microdevices were designed for experiments carried out on heart cells [93] and the fabrication process described below summarised from this paper.

The microdevices consist of an array of five channels fabricated on a 25 mm wide glass microscope cover-slip. Pairs of gold microelectrodes, 20 μm wide were positioned at a regular spacing of 500 μm along the lengths of each channel (Figure 8.2). Glass cover-slips were chosen because they are a good substrate for oil and water immersion objective lenses with high numerical apertures.

The electrodes we fabricated using a lift-off process. The first stage in the fabrication process was deposition of the gold microelectrodes on to a glass cover-slip. This cover-slip was then spin-coated with thin layer of positive photoresist (S1818) at 4000 rpm, baked at 90°C for 30 minutes with an intermediate 15 minute chlorobenzene soak and exposed to UV through the photomask. The gold microelectrode array was laid by sequential electron beam assisted deposition of an adhesive under-layer of 10nm of titanium and a 100nm electrochemically stable gold overlayer. The microelectrode array was realised by lift-off of the unwanted metal by resist solvation. The second stage of the fabrication is forming the channels in silicon rubber by replica molding against a straight-line pattern. This

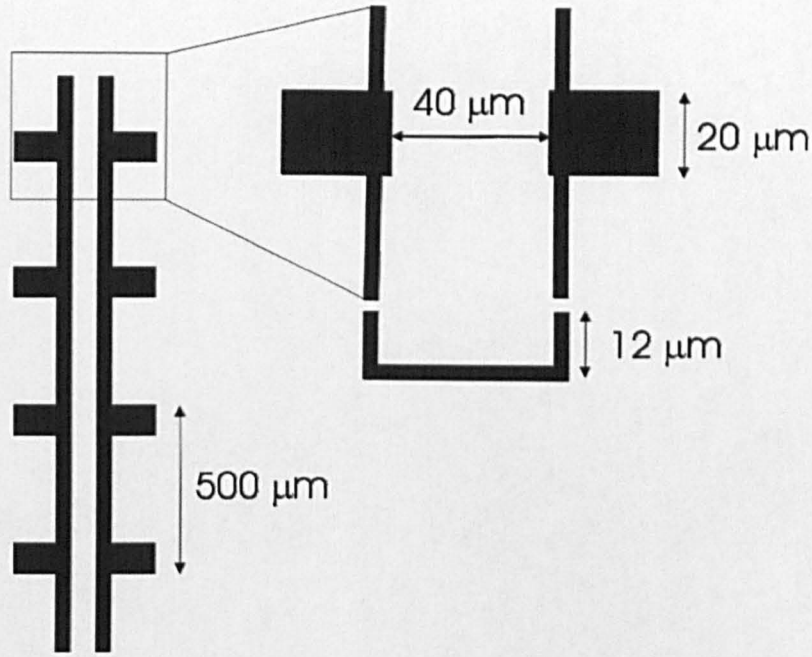


Figure 8.2: A schematic representation of a microelectrode array and micrograph showing a close-up of a pair of microelectrodes.

pattern is formed by spin-coating the microelectrode array with a $10\ \mu\text{m}$ layer of thick photoresist at 1300 rpm and baked at 90°C for 30 minutes. Photoresist is removed after placing a photomask over the photoresist, by exposing it with UV light and transferring the desired pattern to the photoresist. The remaining photoresist is spin-coated with elastomer at 10 000 rpm with a 1:4 dilution of polymethylsiloxene (PDMS) in toluene and cured by baking it at 120°C for 2 minutes. The residual photoresist was removed by an acetone wash to leave the microelectrodes protruding approximately $2\ \mu\text{m}$ into the channels, ensuring they will be in contact with the electrolyte, used to fill the channels. This reduces the effective width of the microchannel from $45\ \mu\text{m}$ to $40\ \mu\text{m}$ and allows a suspension of the latex spheres to be placed in direct contact with the microelectrodes. This fabrication process is summarized in figure 8.3.

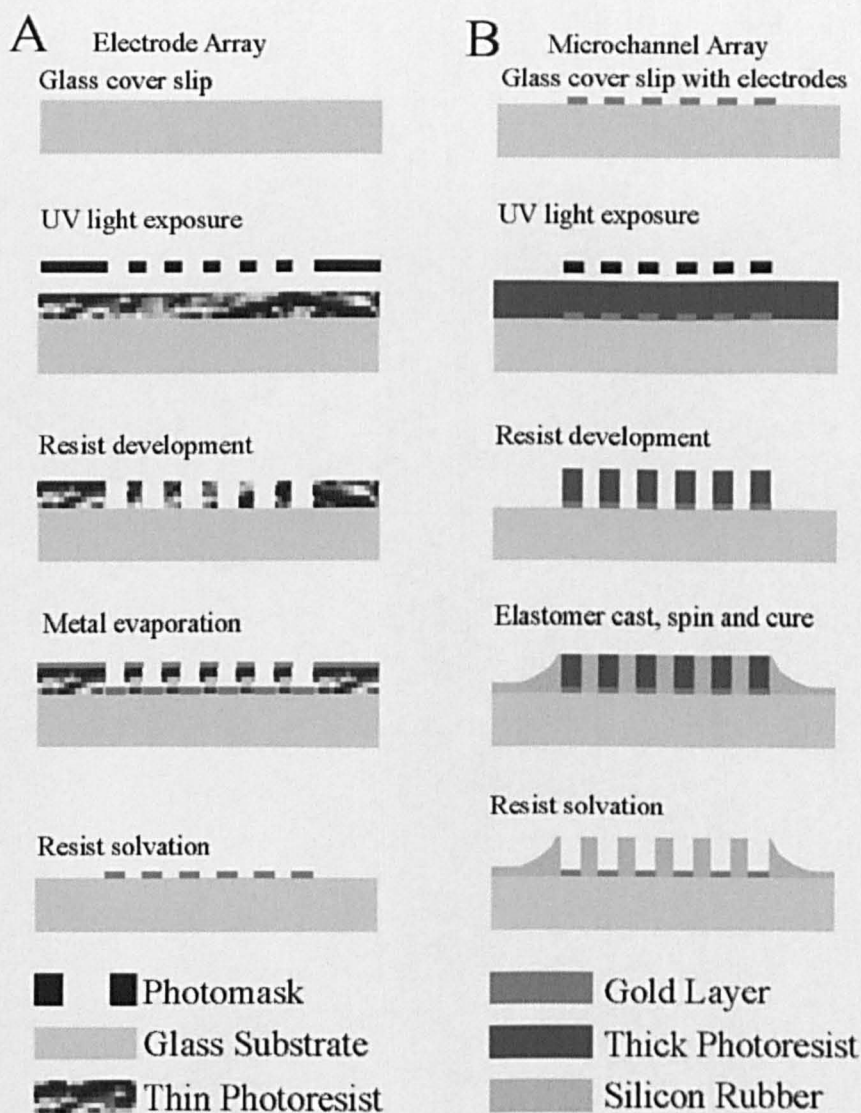


Figure 8.3: Schematic diagram of the microfluidic fabrication processes; (A) microelectrode fabrication and (B) channel fabrication.

8.4 Experimental Procedure

The optical tweezers is based on a Zeiss Axiovert 200 microscope (Figure 8.4). The trapping beam (50 mW of 1064 nm light) enters through a 100, 1.45 NA, Aqua-Plan Fluor objective lens, bypassing the internal optics of the microscope. The use of an infra-red trapping beam reduces background fluorescence and associated photo-bleaching of the dye. The fluorescence excitation source was a 75W Xe arc lamp, filtered using a monochromator to give 515 nm, coupled through the base port of the microscope and focused through the objective lens, to overlap the position of the trapping laser beam. A CCD camera and intensified camera were attached to a dual port adapter, allowing both a normal, white-light, and a highly sensitive fluorescence image to be obtained. A 1064 nm blocking filter and a 580 ± 10 nm bandpass filter were placed in front of the intensified camera such that its image corresponded to the 580 nm fluorescence emission of the functionalized sphere. Images from both cameras were recorded directly on to a desktop computer via frame grabber cards. Using the computer software (IonOptix), regions of interest could be defined in the fluorescence image captured on the intensified camera, from which the summed intensity was measured and recorded as a function of time. Typically, the software records the difference in intensity between the bead fluorescence and a neighboring background region as a function of time. The video frame-rate corresponds to a temporal resolution of 60 milliseconds.

A thin film of mineral oil was placed over the microfluidic channels to prevent evaporation of the electrolyte. The suspension of 3 μm diameter latex spheres was micropipetted into a microchannel, through a 10 μm capillary connected to a syringe pump and inserted through the mineral oil to form a pocket (approximately 100pL) of suspension around a pair of microelectrodes (Figure 8.5).

The gold microelectrodes in the microfluidic device were connected to a stimulator, that applied rectangular 6 volt electrical pulses lasting 20 microseconds. The stimulator controlled the voltage amplitude, polarity, shape and duration of the electrical pulses and the 0.2Hz frequency of the pulses was set with a signal generator. The effect of the electric pulse on the electrolyte solution, is to produce a change in charge (H^+ concentration), thus a pH gradient is created around each microelectrode.

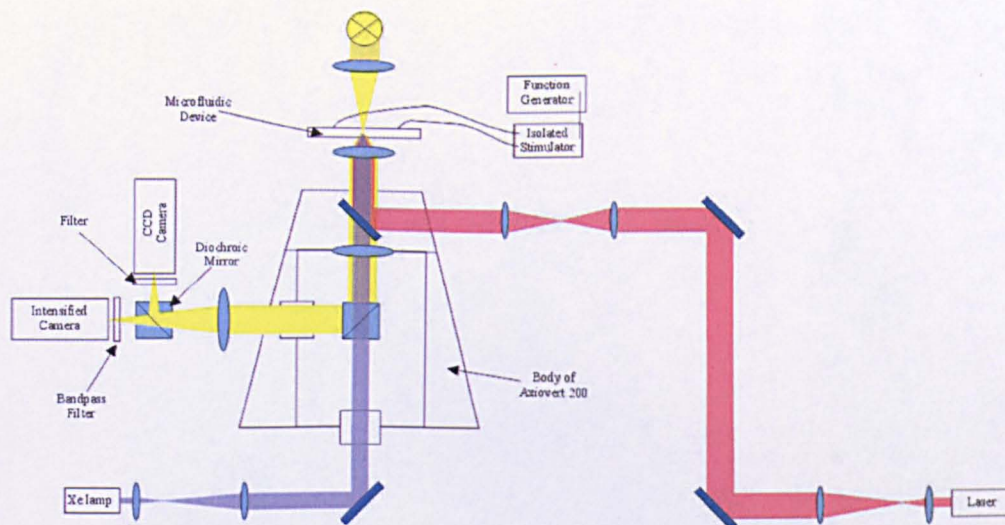


Figure 8.4: *Schematic representation of the experimental apparatus.*

8.5 Results

When an electrical pulse was applied to the electrode a corresponding change in the fluorescence intensity was observed. Visually, the fluorescence of the beads is seen as a bright flash or a decrease in fluorescence depending on the polarity of the electrical pulse (Figure 8.6). Although in this work we have not yet calibrated the fluorescence change to absolute pH values, the SNARF-1 dye shows variations in changes of fluorescence for the pH ranges of 9.0 and 6.8 to that of the electrolyte at 7.4, and it is anticipated that these observations cover this range.

The magnitude of the fluorescence change decreases with both exposure to the excitation light and the number of pulses applied to the microelectrodes. The later effect being a result of the limited buffering capacity of the pL volume of electrolyte. To enable these fluorescent latex spheres to be used to probe an area of sample, we had to ensure that they remain photostable for a period of time sufficient to perform a series of measurements. Hence, to minimize the photo bleaching, the excitation wavelength was blocked between each electrical pulse. The fluorescence was monitored over a period of several minutes and continuous pulses applied to determine degradation of fluorescence signal. It can be seen from figure 8.7, that for a latex sphere in a fixed position (close to the cathode),

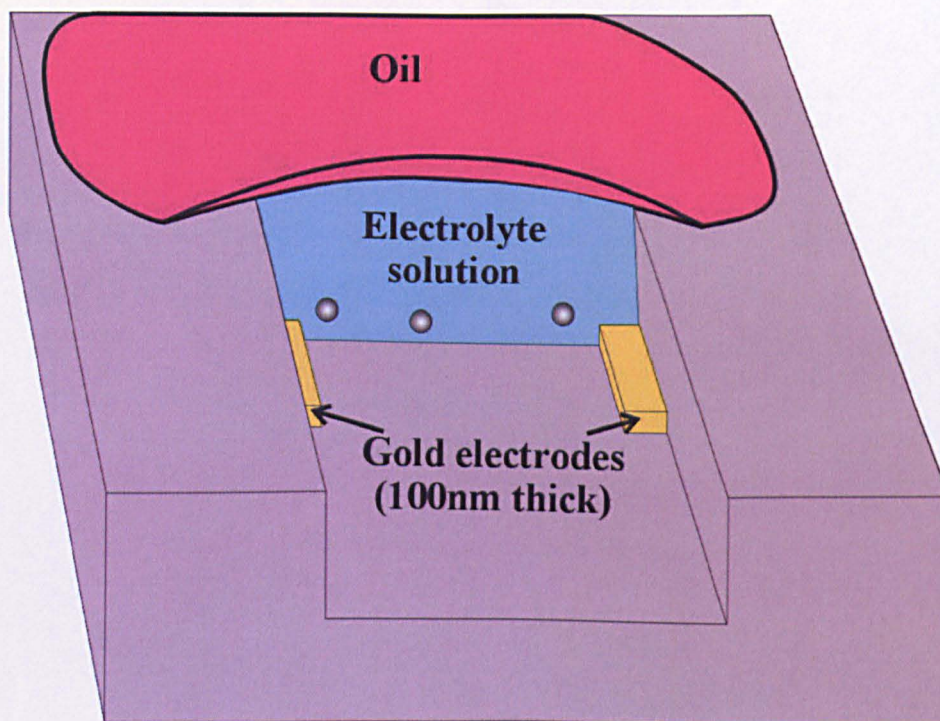


Figure 8.5: *Schematic representation of a channel filled with a solution of electrolyte with suspended functionalised spheres and the film of mineral oil. Note the small area of electrode in contact with the electrolyte solution.*

both the background fluorescence and the pulse induced change in fluorescence do indeed decrease but a sufficient signal for useful measurement is observed for many minutes.

To demonstrate the utility of our technique, we chose to map the pH change in the vicinity of the cathode. The change in fluorescence of trapped latex spheres was measured along two axes, defining an area $20\ \mu\text{m}$ (x-axis) by $30\ \mu\text{m}$ (y-axis). Several sets of measurements were taken with different spheres and the means square error calculated. In both directions, the fluorescence change decreased as the latex sphere was moved away from the edge of the microelectrode (Figure 8.8). This agrees with the anticipated pH profile, which decays to the pH of the electrolyte at a distance of approximately $20\ \mu\text{m}$ from the edge of the microelectrode, indicating the extent of diffusion of H^+ ions in addition to the buffering. These results indicate a functionalized $3\ \mu\text{m}$ diameter latex sphere can be used as a pH probe within an area up to $40\ \mu\text{m}$ by $60\ \mu\text{m}$ around a pair of exposed electrodes and for pH changes within the limits of the SNARF-1 dye coating the

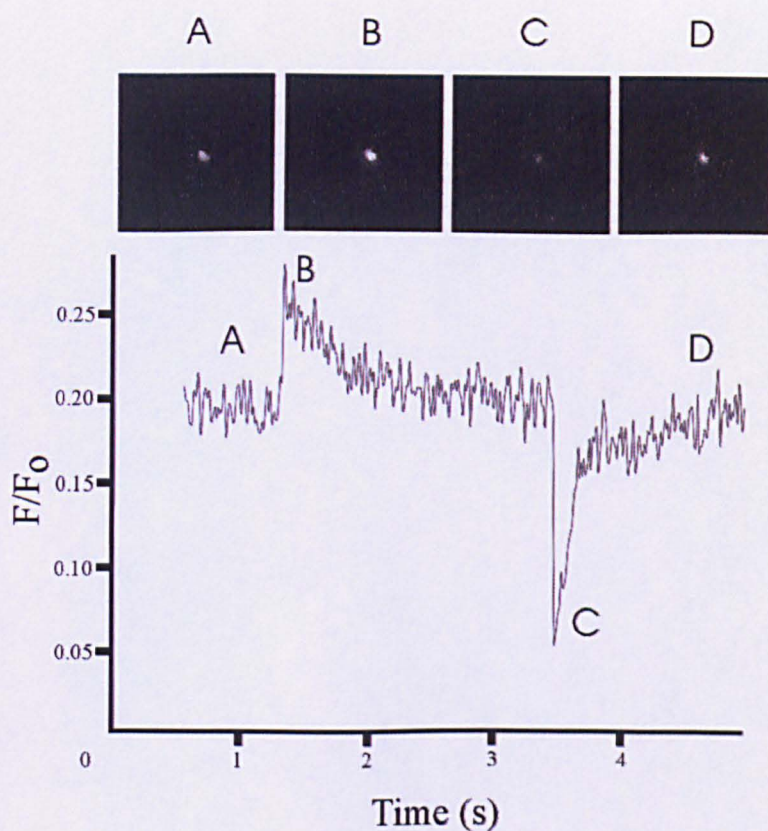


Figure 8.6: Selected video frames showing the fluorescence signal from a $3\ \mu\text{m}$ diameter latex sphere trapped close to the cathode. Two pulses of opposite polarity are applied to the microelectrodes with the corresponding change in fluorescence intensity plotted below (F_0 is the fluorescence intensity observed when the sphere is held in a solution with pH of 7.4). The increase in fluorescence shown in frame B indicates a maximum change in pH from 7.4 to 6.8 and decrease in fluorescence shown in frame C indicates a maximum change in pH from 7.4 to 9.0

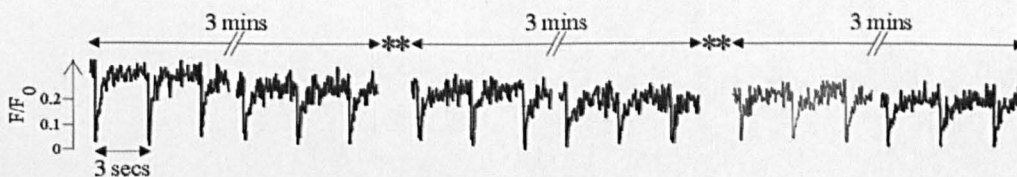


Figure 8.7: A plot of fluorescence emitted from a trapped $3\ \mu\text{m}$ diameter latex sphere as a function of time. Breaks (**) in the plot represent 2 minute periods and the pulses were generated every 2 seconds

latex spheres. The fluorescent signal could be increased by using larger diameter latex spheres, however, the depth of our microchannels ($12\ \mu\text{m}$) would then limit their mobility.

8.6 Conclusions

We have shown that optical tweezers can be combined with functionalized latex spheres to produce a pH microprobe which can be used to probe the environment within a microfluidic device. The manipulation capability of optical tweezers allows the probe to be positioned accurately within a microfluidic channel. Also, by making simultaneous fluorescence measurements at 580 nm and 640 nm it should be possible for us to calibrate the change in intensities to the absolute value of pH. It is envisaged this technique can be used to measure pH changes in biological cells and solutions, allowing a greater understanding of chemical reactions occurring within biological processes and systems.

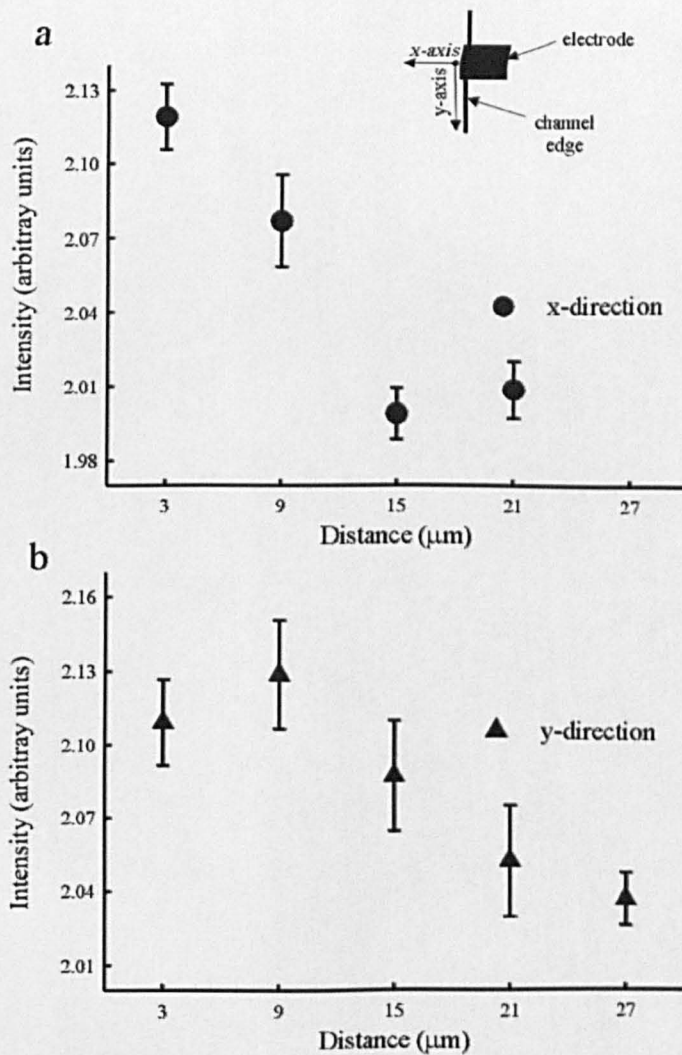


Figure 8.8: Plots of intensity versus position of latex sphere in microfluidic channel: a) at distance from the microelectrode towards the channel centre (x -axis) and b) at distances from the centre of the microelectrode and perpendicular to the channel length (y -axis). The error bars indicate the standard errors of measurements performed with six different spheres.

Chapter 9

Conclusions and Future Work

9.1 Introduction

This chapter will summarise the main conclusions of my work over the last 3 years. Although much of this work has pioneered trapping particles in three dimensional patterns, it is by no means the end of the development of three dimensional trapping techniques. It is followed by a section on future work which could take the trapping techniques I have helped to develop to either apply them to new research or improve the trapping process further.

9.2 Conclusions

The first experiment I carried out was defining the trapping limits of our Hamamatsu spatial light modulator (SLM). This experiment showed the displacement of an optical trap was of the scale of $20 \mu\text{m}$ either side of the zeroth diffraction order and $25 \mu\text{m}$ above and below the zeroth diffraction order. These parameters increase with higher laser powers, but the overall efficiency (Q value) of the trap is unchanged. The lateral displacement is limited by the spatial resolution of the SLM and the axial displacement by the objective lens performance. However, the SLM can be used to compensate for

some of the aberrations introduced by the objective lens.

Most of my work concerned the trapping of simple and complex patterns of objects using both static holograms and sequences of holograms. The trapped objects formed two dimensional and three dimensional patterns, often resembling crystal-like structures. The sequences of holograms allowed automated manipulation of particles from simple initial patterns to their final positions in the more complex patterns. The holograms were designed using various algorithms, of which a modified Gerchberg-Saxton algorithm was the fastest. A direct-binary search algorithm was used to make fully three dimensional holograms, that were rotated around arbitrary axes. In addition to manipulating particles into complex particles, the direct-binary search algorithm was used to manipulate pairs of particles to touch each other for several minutes and then move the particles to separate them.

Optical tweezers were developed to allow the measurement of surface-enhanced resonant Raman scattering (SERRS) from partially silver coated silica spheres. The ability to trap these spheres allowed SERRS signals to be observed while the spheres were trapped and such particles to be manipulated to give spatial resolution. These improvements offer a SERRS measurement system with improved visualization of both the SERRS signal and the sample, compared to a conventional Raman system.

Optical tweezers were also used to trap functionalised silica spheres to develop a pH microprobe. These microprobes can be used to measure pH changes over periods of several minutes and can detect pH changes induced by electrodes in microfluidic devices.

9.3 Future Work

Although I have been involved in developing trapping techniques with holographic optical tweezers (HOTs), there are some areas that are of interest for further research and development.

- Fully automated trapping could be envisaged by adding particle recognition software

to the current suite of LabVIEW interfaces.

- The application of HOTs could be extended to trapping nanoscale particles, allowing photonic crystal devices to be built with HOTs and nano-sized particles to be trapped in microfluidic devices.
- The trapping of functionalised particles is of great interest and should be extended to trapping of different types of particles, allowing multiple measurements to be made at the same time. The trapping of functionalised particles could also be applied to pharmaceutical research.
- To date the use of HOTs in biological research is in its infancy and the use of HOTs should be extended further in this area of research.
- The mechanical properties of materials (including biological substances) could be investigated using HOTs. The control of trap positions offered by HOTs could well be advantageous.

I have listed five areas for future work. This list could be extended as the applications are many and the list will continue to grow as HOTs are used more in biological research.

9.3.1 Update on Current Research

At the time of my oral examination, I had already left the optics group. In the months since my departure from the group several experiments and improvements to the HOTs have been completed. These are listed below.

- An optical hand that uses several trapped spheres to hold and manipulate other particles has been developed with the HOTs. A joystick has been added to the LabVIEW interface to control the optical hand.
- Further work involving optical tweezers and microfluidic devices has developed an optical pump [94] and a flow line for measuring the velocity of fluids [95].

- Work has commenced on a grant awarded to carry out the Abraham-Minkowski experiment.
- An aberration correction experiment has been successful carried out in HOTs [96].

References

- [1] J. E. Curtis, B. A. Koss, and D. G. Grier. Dynamic holographic optical tweezers. *Opt. Commun.*, 207:169–175, 2002.
- [2] D. G. Grier. A revolution in optical manipulation. *Nature*, 424:810–816, 2003.
- [3] A. Ashkin. Acceleration and trapping of particles by radiation pressure. *Phys. Rev. Lett.*, 24:156–159, 1970.
- [4] A. Ashkin, J. M. Dziedzic, J. E. Bjorkholm, and S. Chu. Observation of a single-beam gradient force optical trap for dielectric particles. *Opt. Lett.*, 11:288–290, 1986.
- [5] N. Kitamura and F. Kitagawa. Optical trapping–chemical analysis of single microparticles in solution. *J. Photochem. Photobio. C: Photochem. Rev.*, 4:227–247, 2003.
- [6] A. Ashkin and J. M. Dziedzic. Optical levitation by radiation pressure. *Appl. Phys. Lett.*, 19:283–285, 1971.
- [7] A. Ashkin and J. M. Dziedzic. Observation of light scattering from nanospherical particles using optical levitation. *Appl. Opt.*, 19:660–668, 1980.
- [8] N. Kitamura, M. Hayashi, H. B. Kim, and K. Nakatani. Photometric analyses of optically-trapped single microparticles in solution. *Analyt. Sci.*, 12:49–54, 1996.
- [9] S. Chu, J. E. Bjorkholm, A. Cable, and A. Ashkin. Experimental observation of optically trapped atoms. *Phys. Rev. Lett.*, 57:314–317, 1986.
- [10] Y. L. Sun, Z. P. Luob, A. Fertilac, and K. N. Ana. Direct quantification of the flexibility of type I collagen monomer. *Biochem. Biophys. Res. Commun.*, 295:382–386, 2002.

- [11] R. Omori, T. Kobayashi, and A. Suzuki. Observation of a single-beam gradient-force optical trap for dielectric particles in air. *Opt. Lett.*, 22:816–818, 1997.
- [12] K. T. Gahagan and Jr. G. A. Swartzlander. Optical vortex trapping of particles. *Opt. Lett.*, 21:827–829, 1996.
- [13] S. M. Block. *Non-invasive Techniques in Cell Biology, Chapter 15*. Wiley-Liss, New York, 1990.
- [14] A. Ashkin, J. M. Dziedzic, and T. Yamane. Optical trapping and manipulation of single cells using infrared-laser beams. *Nature*, 330:769–771, 1987.
- [15] H.M. Haruff, J. Munakata-Marr, and D.W.M. Marr. Directed bacterial surface attachment via optical trapping. *Colloids and Surfaces B: Biointerfaces*, 27:189–195, 2002.
- [16] A. Ashkin and J. M. Dziedzic. Optical trapping and manipulation of viruses and bacteria. *Science*, 235:1517–1520, 1987.
- [17] G. Leitz, K. O. Greulich, and E. Schnepf. Displacement and return movement of chloroplasts in the marine dinophyte pyrocystis-noctiluca-experiments with optical tweezers. *Botanica Acta*, 107:90–94, 1994.
- [18] S. M. Block, D. F. Blair, and H. C. Berg. Compliance of bacterial flagella measured with optical tweezers. *Nature*, 338:514–518, 1989.
- [19] J. E. Molloy and M. J. Padgett. Lights, action: optical tweezers. *Contemp. Phys.*, 43:241–258, 2002.
- [20] A. Ashkin, K. Schutze, , J. M. Dziedzic, U. Euteneuer, and M. T. Schliwa. Force generation of organelle transport measured invivo by an infrared-laser trap. *Nature*, 348:346–348, 1990.
- [21] M. D. Wang, H. Yin, R. Landick, J. Gelles, and S. M. Block. Stretching DNA with optical tweezers. *Biophys. J*, 72:1335–1346, 1997.
- [22] S. B. Smith, Y. J. Cui, and C. Bustamante. Overstretching B-DNA: The elastic response of individual double-stranded and single-stranded DNA molecules. *Science*, 271:795–799, 1996.

- [23] J. T. Finer, R. M. Simmons, and J. A. Spudich. Single myosin molecule mechanics: piconewton forces and nanometre steps. *Nature*, 368:113, 1994.
- [24] H. Liang, W. H. Wright, S. Cheng, W. He, and M. W. Berns. Micromanipulation of chromosomes in PTK2 in cell using laser microsurgery (optical scalpel) in combination with laser-induced optical force (optical tweezers). *Exp. Cell. Res.*, 204:110–120, 1993.
- [25] H. Liang, W. H. Wright, C. L. Rieder, E. D. Salmon, G. Profeta, J. Andrews, Y. Liu, G. J. Sonek, and M. W. Berns. Direct movement of chromosome arms and fragments in mitotic newt lung cells using optical scissors and optical tweezers. *Exp. Cell. Res.*, 213:308–312, 1994.
- [26] D. T. Chiu, C. F. Wilson, F. Ryttsén, A. Strömberg, C. Farre, A. Karlsson, S. Nordholm, A. Gaggar, B. P. Modi, A. Moscho, R. A. Garza-Lopez, O. Orwar, and R. N. Zare. Chemical transformations in individual ultrasmall biomimetic containers. *Science*, 283:1892–1895, 1987.
- [27] H. Misawa, M. Koshoika, K. Sasaki, N. Kitamura, and H. A. Masuhara. Laser trapping, spectroscopy, and ablation of a single latex particle in water. *Chem. Lett.*, 8:1479–1482, 1990.
- [28] M. Mammen, K. Helmerson, R. Kishore, S. K. Choi, W. D. Phillips, and G. M. Whitesides. Optically controlled collisions of biological objects to evaluate potent polyvalent inhibitors of virus-cell adhesion. *Chem. and Bio.*, 3:757–763, 1996.
- [29] T. T. Perkins, S. R. Quake, D. E. Smith, and S. Chu. Relaxation of a single DNA molecule observed by optical microscopy. *Science*, 264:822–826, 1994.
- [30] Y. Liu, D. K. Cheng, G. J. Sonek, M. W. Berns, C. F. Chapman, and B. J. Tromberg. Evidence for localized cell heating induced by infrared optical tweezers. *Biophys. J.*, 68:2137–2144, 1995.
- [31] Y. Liu, G. J. Sonek, M. W. Berns, K. Konig, and B. J. Tromberg. Two-photon fluorescence excitation in continuous-wave infrared optical tweezers. *Opt. Lett.*, 20:2246–2248, 1995.

- [32] K. Schaschek, J. Popp, and W. Kiefer. Observation of morphology-dependent input and output resonances in time-dependent raman-spectra of optically levitated microdroplets. *J. Raman Spectrosc.*, 24:69–75, 1993.
- [33] G. McNay, F. T. Docherty, D. Graham, W. E. Smith, P. Jordan, M. Padgett, J. Leach, G. Sinclair, P. B. Monaghan, and J. Cooper. Visual observations of SERRS from single silver-coated silica microparticles within optical tweezers. *Angew. Chem. Int. Ed.*, 43:2512–2514, 2004.
- [34] K. Visscher, G. J. Brakenhoff, and J. J. Kroll. Micromanipulation by multiple optical traps created by a single fast scanning trap integrated with the bilateral confocal scanning laser microscope. *Cytometry*, 14:105–114, 1993.
- [35] J. E. Molloy, J. E. Burns, J. C. Sparrow, R. T. Tregear, J. Kendrick-Jones, and D. C. S. White. Single-molecule mechanics of heavy-meromyosin and S1 interacting with rabbit or drosophila actins using optical tweezers. *Biophys. J.*, 68:S298–S305, 1995.
- [36] K. Sasaki, M. Koshoika, H. Misawa, N. Kitamura, and H. A. Masuhara. Pattern formation and flow control of fine particles by laser-scanning micromanipulation. *Opt. Lett.*, 16:1463, 1991.
- [37] H. M. Warrick, R. M. Simmons, J. T. Finer, T. Q. P. Uyeda, S. Chu, and J. A. Spuddich. In-vitro methods for measuring force and velocity of the actin-myosin interaction using purified proteins. *Meth. Cell. Biol.*, 39:1–21, 1993.
- [38] K. Visscher, S. P. Gross, and S. M. Block. Construction of multiple-beam optical traps with nanometer-resolution position sensing. *IEEE J. Selected Topics Quantum Electr.*, 2:1066–1076, 1996.
- [39] A. L. Birkbeck, R. A. Flynn, M. Ozkan, D. Q. Song, M. Gross, and S. C. Esener. VCSEL arrays as micromanipulators in chip-based biosystems. *Biomed. Dev.*, 5:47–49, 2003.
- [40] M. Edidin, S. C. Kuo, and P. Sheetz. Lateral movements of membrane glycoproteins restricted to dynamic cytoplasmic barriers. *Science*, 254:1379–1382, 1991.

- [41] K. Sasaki, M. Koshoika, H. Misawa, N. Kitamura, and H. A. Masuhara. Optical trapping of a metal-particle and a water droplet by a scanning laser-beam. *Appl. Phys. Lett.*, 60:807–809, 1992.
- [42] H. He, M. E. J. Friese, N. R. Heckenberg, and H. Rubinsztein-Dunlop. Direct observation of transfer of angular momentum to absorptive particles from a laser beam with a phase singularity. *Phys. Rev. Lett.*, 75:826–829, 1995.
- [43] S. Sato, M. Ishigure, and H. Inaba. Optical trapping and rotational manipulation of microscopic particles and biological cells using higher-order mode Nd:YAG laser beams. *Electron. Lett.*, 27:1831–1832, 1991.
- [44] M. E. J. Friese, T. A. Nieminen, N. R. Heckenberg, and H. Rubinsztein-Dunlop. Optical alignment and spinning of laser-trapped microscopic particles. *Nature*, 394:348–350, 1998.
- [45] A. T. O’Neil and M. J. Padgett. Three-dimensional optical confinement of micron-sized metal particles and the de-coupling of the spin and orbital angular momentum within an optical spanner. *Opt. Commun.*, 185:139–143, 2000.
- [46] K. Ladavac and D. G. Grier. Microoptomechanical pumps assembled and driven by holographic optical vortex arrays. *Optics Express*, 12:1144–1149, 2004.
- [47] P. Galajda and P. Ormos. Complex micromachines produced and driven by light. *Appl. Phys. Lett.*, 78:249–251, 2001.
- [48] A. Terray, J. Oakey, and D. W. M. Marr. Microfluidic control using colloidal devices. *Science*, 296:1841–1844, 2002.
- [49] J. Dapprich and N. Nicklaus. DNA attachment to optically trapped beads in microstructures monitored by bead displacement. *Bioimaging*, 6:25–32, 1998.
- [50] M. Ozkan, M. Wang, C. Ozkan, R. Flynn, A. Birkbeck, and S. Esener. Optical manipulation of objects and biological cells in microfluidic devices. *Biomed. Microdev.*, 5:61–67, 2003.

- [51] R. W. Applegate Jr., J. Squier, T. Vestad, J. Oakey, and D. W. M. Marr. Optical trapping, manipulation, and sorting of cells and colloids in microfluidic systems with diode laser bars. *Optics Express*, 12:4390–4398, 2004.
- [52] M. P. MacDonald, G. C. Spalding, and K. Dholakia. Microfluidic sorting in an optical lattice. *Nature*, 425:421–424, 2003.
- [53] M. Reicherter, T. Haist, E. U. Wagemann, and H. J. Tiziani. Optical particle trapping with computer-generated holograms written on a liquid-crystal display. *Opt. Lett.*, 24:608–610, 1999.
- [54] J. Liesener, M. Reicherter, T. Haist, and H. J. Tiziani. Multi-functional optical tweezers using computer-generated holograms. *Opt. Commun.*, 185:77–82, 2000.
- [55] R. W. Gerchberg and W. O. Saxton. A practical algorithm for the determination of the phase from image and diffraction plane pictures. *Optik*, 35:237–246, 1972.
- [56] J. Glückstad. Phase contrast image synthesis. *Opt. Commun.*, 130:225–230, 1996.
- [57] W. J. Hossack, E. Theofanidou, and J. Crain. High-speed holographic optical tweezers using a ferroelectric liquid crystal microdisplay. *Opt. Exp.*, 11:2053–2059, 2003.
- [58] P. A. Bancel, V. B. Cajipe, F. Rodier, and J. Witz. Laser seeding for biomolecular crystallization. *J. Crystal Growth*, 191:537544, 1998.
- [59] J. P. Hoogenboom, D. L. J. Vossen, C. Faivre-Moskalenko, M. Dogterom, and A. van Blaaderen. Patterning surfaces with colloidal particles using optical tweezers. *Appl. Phys. Lett.*, 80:4828–4830, 2002.
- [60] P. T. Korda and D. G. Grier. Annealing thin colloidal crystals with optical gradient forces. *J. Chem. Phys.*, 114:7570–7573, 2001.
- [61] A. Moroz. Metallo-dielectric diamond and zinc-blende photonic crystals. *Phys. Rev. B*, 66:115109, 2002.
- [62] G. Zhou, M. J. Ventura, M. R. Vanner, and M. Gu. Use of ultrafast-laser-driven microexplosion for fabricating three-dimensional void-based diamond-lattice photonic crystals in a solid polymer material. *Opt. Lett.*, 29:2240–2242, 2004.

- [63] T. Ota, S. Kawata, T. Sugiura, M. J. Booth, M. A. A. Neil, R. Juškaitis, and T. Wilson. Dynamic axial-position control of a laser-trapped particle by wave-front modification. *Opt. Lett.*, 28:465–467, 2003.
- [64] M. A. Seldowitz, J. P. Allebach, and D. W. Sweeney. Synthesis of digital holograms by direct binary search. *Appl. Opt.*, 26:2788–2798, 1987.
- [65] G. Sinclair, J. L., P. Jordan, G. Gibson, E. Yao, Z. J. Laczik, M. J. Padgett, and J. Courtial. Interactive application in holographic optical tweezers of a multi-plane Gerchberg-Saxton algorithm for three-dimensional light shaping. *Opt. Express*, 12:1665–1670, 2004.
- [66] Z. J. Laczik. 3D beam shaping using diffractive optical elements. *Proc. SPIE*, 4770:104–111, 2002.
- [67] T. Haist, M. Schönleber, and H. J. Tiziani. Computer-generated holograms from 3D-objects written on twisted-nematic liquid crystal displays. *Opt. Commun.*, 140:299–308, 1997.
- [68] G. Shabtay. Three-dimensional beam forming and Ewald’s surfaces. *Opt. Commun.*, 226:33–37, 2003.
- [69] G. Whyte and J. Courtial. Experimental demonstration of holographic three-dimensional light shaping using a Gerchberg–Saxton algorithm. *New. J. Phys.*, 7:117, 2005.
- [70] V. Soifer, V. Kotlyar, and L. Doskolovich. *Iterative Methods for Diffractive Optical Elements Computation*. Taylor & Francis Ltd, London, 1997.
- [71] J. W. Goodman. *Introduction To Fourier Optics*. McGraw–Hill International Editions, Singapore, 1996.
- [72] E. Z. G. Yao. *Characterisation of spatio-temporal disorder in liquid crystal light valves with feedback*. PhD Thesis, University of Strathclyde, 1997.
- [73] P. J. Rodrigo, R. L. Eriksen, V. R. Daria, and J. Glueckstad. Interactive light-driven and parallel manipulation of inhomogeneous particles. *Opt. Exp.*, 26:1550 – 1556, 2002.

- [74] V. Garcés-Chávez, K. Dholakia, and G. C. Spalding. Extended-area optically induced organization of microparticles on a surface. *Appl. Phys. Lett.*, 80:031106, 2005.
- [75] H. Felgner, O. Mller, and M. Schliwa. Calibration of light forces in optical tweezers. *Appl. Opt.*, 34:977–982, 1995.
- [76] A. T. O’Neil and M. J. Padgett. Axial and lateral trapping efficiency of Laguerre–Gaussian modes in inverted optical tweezers. *Opt. Commun.*, 193:45–50, 2001.
- [77] N. Malagnino, G. Pescea, A. Sassoa, and E. Arimondo. Measurements of trapping efficiency and stiffness in optical tweezers. *Opt. Commun.*, 214:15–24, 2002.
- [78] G. Spalding. Personal communication. 2003.
- [79] E. Theofanidou, L. Wilson, W. Hossack, and J. Arlt. Spherical aberration correction for optical tweezers. *Opt. Commun.*, 236:145–150, 2004.
- [80] D. Leseberg and C. Frre. Computer-generated holograms of 3-D objects composed of tilted planar segments. *Appl. Opt.*, 27:3020–3024, 1988.
- [81] J. Leach, M. R. Dennis, J. Courtial, and M. J. Padgett. Vortex knots in light. *New J. Phys.*, 7:art. no. 55, 2005.
- [82] J. Leach, G. Sinclair, P. Jordan, J. Courtial, and M. Padgett. 3D manipulation of particles in to crystal structures using holographic optical tweezers. *Opt. Exp.*, 12:220–226, 2004.
- [83] Kaiser Optical Systems Inc. <http://www.kosi.com/raman/resources/tutorial/index.html>, 2005.
- [84] E. Smith and G. Dent. *Modern Raman Spectroscopy: A Practical Aproach*. Wiley, 2005.
- [85] Y. Saito, J. J. Wang, D. A. Smith, and D. N. Batchelor. A simple chemical method for the preparation of silica surfaces for efficient SERS. *Langmuir*, 18:2959–2961, 2002.
- [86] Y. Yin, Z-Y. Li, Z. Zhong, B. Gates, Y. Xia, and S. Venkateswaran. Synthesis and characterization of stable aqueous dispersions of silver nanoparticles through the Tollens process. *J.Mater.Chem.*, 12:522–527, 2002.

- [87] P. A. Jordan. *Optical tweezers for signal detection and micromanipulation*. PhD Thesis, University of Glasgow, 2005.
- [88] M. Padgett, S. M. Barnett, and R. Loudon. The angular momentum of light inside a dielectric. *J. Mod. Opt.*, 50:1555–1562, 2003.
- [89] H. Misawa, Z. Y. Shi, R. Kopelman, and H. Masuhara. Three-dimensional pH microprobing with an optically-manipulated fluorescent particle. *Chem. Lett.*, 2:141–142, 1996.
- [90] F. Qian, S. Ermilov, D. Murdock, W. E. Brownell, and B. Anvar. Combining optical tweezers and patch clamp for studies of cell membrane electromechanics. *Rev. Sci. Instr.*, 75:2937–2942, 2004.
- [91] K. Huikko, R. Kostianen, and T. Kotiaho. Introduction to micro-analytical systems: bioanalytical and pharmaceutical applications. *Eur. J. Pharma. Sci.*, 20:149–171, 2003.
- [92] R. P. Haugland. *Handbook of Fluorescent Probes and Research Biochemicals*. Molecular Probes, 2004.
- [93] N. Klauke, G. L. Smith, and J. Cooper. Stimulation of single isolated adult ventricular myocytes within a low volume using a planar microelectrode array. *Biophys. J.*, 85:1766–1774, 2003.
- [94] J. Leach, H. Mushfique, R. Di Leonardo, M. J. Padgett, and J. M. Cooper. An optically driven pump for microfluidics. *Lab on a Chip*, 6:735–739, 2006.
- [95] R. Di Leonardo, J. Leach, H. Mushfique, J. M. Cooper, G. Ruocco, and M. J. Padgett. Multipoint holographic optical velocimetry in microfluidic systems. *Phys. Rev. Lett.*, 96:134502, 2006.
- [96] K. D. Wulff, D. G. Cole, R. L. Clark, R. Di Leonardo, J. Leach, J. M. Cooper, G. Gibson, and M. J. Padgett. Aberration correction in holographic optical tweezers. *Opt. Exp.*, 14:4170–4175, 2006.

